UNICAMP

UNIVERSIDADE ESTADUAL DE CAMPINAS
Faculdade de Engenharia Mecânica

ERICK CRISTIAN DA SILVA LOPES

Above-ground gas pipes leakage monitoring through fiber optic sensing

Monitoramento de vazamentos em tubulações aéreas de gás natural através de sensores de fibra óptica

Campinas

2024

ERICK CRISTIAN DA SILVA LOPES

Above-ground gas pipes leakage monitoring through fiber optic sensing

Monitoramento de vazamentos em tubulações aéreas de gás natural através de sensores de fibra óptica

Dissertation presented to the School of Mechanical Engineering of the University of Campinas in partial fulfillment of the requirements for the degree of Master in Mechanical Engineering, in the area of Mechatronics.

Dissertação apresentada à Faculdade de Engenharia Mecânica da Universidade Estadual de Campinas como parte dos requisitos exigidos para a obtenção do título de Mestre em Engenharia Mecânica, na área de Mecatrônica.

Orientador: Prof. Dr. Rodrigo Moreira Bacurau

Coorientador: Prof. Dr. Alex Dante

ESTE TRABALHO CORRESPONDE À VERSÃO FINAL DA DISSERTAÇÃO DEFENDIDA PELO ALUNO ERICK CRISTIAN DA SILVA LOPES, E ORIENTADA PELO PROF. DR. RODRIGO MOREIRA BACURAU E PELO PROF. DR. ALEX DANTE.

Campinas

2024

Ficha catalográfica
Universidade Estadual de Campinas (UNICAMP)
Biblioteca da Área de Engenharia e Arquitetura
Rose Meire da Silva - CRB 8/5974

L881a Lopes, Erick Cristian da Silva, 1996-
Above-ground gas pipes leakage monitoring through fiber optic sensing / Erick Cristian da Silva Lopes. – Campinas, SP : [s.n.], 2024.

Orientador(es): Rodrigo Moreira Bacurau.
Coorientador(es): Alex Dante.
Dissertação (mestrado) – Universidade Estadual de Campinas (UNICAMP), Faculdade de Engenharia Mecânica.

1. Vazamento de gás. 2. Monitoramento. 3. Sensores de fibra óptica. 4. Tubulações de gás. I. Bacurau, Rodrigo Moreira, 1988-. II. Dante, Alex, 1979-. III. Universidade Estadual de Campinas (UNICAMP). Faculdade de Engenharia Mecânica. IV. Título.

Informações complementares

Título em outro idioma: Monitoramento de vazamentos em tubulações aéreas de gás natural através de sensores de fibra óptica
Palavras-chave em inglês:
Gas leakage
Monitoring
Fiber optic sensors
Gas piper
Área de concentração: Mecatrônica
Titulação: Mestre em Engenharia Mecânica
Banca examinadora:
Rodrigo Moreira Bacurau [Orientador]
Niederauer Mastelari
Anderson Wedderhoff Spengler
Data de defesa: 25-10-2024
Programa de Pós-Graduação: Engenharia Mecânica

Identificação e informações acadêmicas do(a) aluno(a)
- ORCID do autor: https://orcid.org/0009-0004-0418-8335
- Currículo Lattes do autor: https://lattes.cnpq.br/302200691392304

UNIVERSIDADE ESTADUAL DE CAMPINAS
FACULDADE DE ENGENHARIA MECÂNICA

DISSERTAÇÃO DE MESTRADO ACADÊMICO

Above-ground gas pipes leakage monitoring through fiber optic sensing

Monitoramento de vazamentos em tubulações aéreas de gás natural através de sensores de fibra óptica

Autor: Erick Cristian da Silva Lopes

Orientador: Prof. Dr. Rodrigo Moreira Bacurau
Coorientador: Prof. Dr. Alex Dante

A Banca Examinadora composta pelos membros abaixo aprovou esta Dissertação:

Prof. Dr. Rodrigo Moreira Bacurau, Presidente
DMC/FEM/UNICAMP

Prof. Dr. Niederauer Mastelari
DMC/FEM/UNICAMP

Prof. Dr. Anderson Wedderhoff Spengler
DEM/CTJ/UFSC

A Ata de Defesa com as respectivas assinaturas dos membros encontra-se no SIGA/Sistema de Fluxo de Dissertação/Tese e na Secretaria do Programa da Unidade.

Campinas, 25 de Outubro de 2024

This task was appointed to you. And if you do not find a way, no one will.

Galadriel, The Fellowship of the Ring

ACKNOWLEDGEMENTS

After overcoming these great challenges, I can only thank those who were responsible for getting me this far.

To my parents, who have supported me from afar and provided me with courage and support. They encouraged me from an early age to face challenges, and through love built all that I am today.

To Professor Rodrigo, who opened the doors to this opportunity and has accompanied me throughout the past years, always helpful, attentive, and supportive.

To my mother, father and brother for encouraging and supporting me to follow my path.

My kitten Tina for being my faithful companion.

To all my old friends who continued with me on this adventure, helping to maintain my morale and sanity.

And to all the new friends I made along this journey, and that I intend to take with me along with this much other journeys.

Thank you all very much.

This study was financed in part by the Coordenação de Aperfeiçoamento de Pessoal de Nível Superior – Brasil (CAPES) – Finance Code 001 and by the Companhia de Gás de São Paulo (Comgás) and the Agência Reguladora de Serviços Públicos do Estado de São Paulo (Arsesp).

RESUMO

A demanda por segurança e preservação das tubulações de gás têm impulsionado o surgimento de soluções baseadas em sensores de fibra óptica para o monitoramento de possíveis vazamentos. Tais vazamentos, podem ser detectados ao monitorar temperatura e/ou vibração ao longo dos dutos, utilizando sensores distribuídos com tecnologia de espalhamento Brillouin, Ramam, Rayleigh e/ou interferometria; ou através de sensores de medição pontuais que usam Fiber Bragg Gratings (FBGs) ou filtros Fabry Perot. Apesar de tecnologias de sensores de fibra óptica já serem empregadas em alguns sistemas de monitoramento piloto, há incertezas quanto à melhor escolha de técnicas e sensores para o monitoramento de linhas de baixa pressão (<10 bar). Portanto, este estudo propõe a investigação experimental do potencial, desempenho, custo e restrições de algumas das principais tecnologias ópticas para o monitoramento de vazamentos em tubulações de gás, tais como os interrogadores DAS (*Distributed Acoustic Sensing*) e DTS (*Distributed Temperature Sensing*), além de *strain gauges* baseados em FBG e acelerômetros ópticos baseados em filtros Fabry Perot. Este projeto, financiado por uma das maiores empresas de gás do Brasil, foca na análise em linhas de gás aéreas, de polietileno (PE), de baixa pressão (até 4 bar), em cenário urbano. Devido aos desafios e riscos, o projeto propõe o estudo de vazamentos em ambiente laboratorial, através da criação de uma bancada experimental. Utilizado ar comprimido ao invés de gás natural e, com a ajuda de modelos teóricos, foi possível prever o comportamento de vazamentos com gás natural. A bancada permite simular diversas condições da linha de gás com facilidade, repetibilidade e segurança, além de permitir a coleta de dados de referência da linha de gás durante o experimento com os sensores de fibra óptica. Experimentos foram realizados para investigar vazamentos em furos de 2 mm de diâmetro em tubulações pressurizadas a 0,35, 1, 2 e 4 bar. Foram empregados os sensores distribuídos DAS e DTS, além dos sensores pontuais FBG, *strain gauge* baseado em FBGs e acelerômetro óptico baseado em filtros Fabry Perot. Os resultados indicam que o DTS é capas de identificar vazamentos efetivamente quando a tubulação está sob pressão mínima de 1 bar e coberta por material (tecido ou conduíte), para gás natural, a pressão mínima na qual será possível identificar vazamentos é estimada em 0,5 bar. Não foram observaram quedas de temperatura significativas em tubulações aéreas descobertas. O DAS identificou as vibrações no início do vazamento (transiente) para pressões acima de 1 bar, embora não tenha se mostrado capaz de obter vibrações contínuas com os vazamentos em estado estacionário. Em relação aos sensores pontuais, as FBGs nuas e os *strain gauges* não conseguiram identificar as vibrações causadas por vazamentos em nenhuma das pressões testadas. Por outro lado, os acelerômetros baseados em filtros Fabry Perot conseguiram detectar vazamentos quando a tubulação esta pressurizada com pelo menos 2 bar. Esses sensores podem ser utilizados para encontrar a região de vazamento usando os dados de vibração para estimar a distância do vazamento em relação aos sensores próximos em conjunto com multilateração. Nenhuma das técnicas foi capaz de identificar vazamentos em tubulações pressurizadas com 350 mbar. Este trabalho permitiu, através da análise comparativa, a identificação do potencial e limitações de várias técnicas e sensores de fibra óptica para identificação de vazamentos em linhas de gás. Em pesquisas futuras, será avaliado o desempenho desses sensores em campo. Além disso, serão desenvolvidas técnicas de processamento de sinais e de fusão sensorial para aumentar a robustez do sistema a falsos positivos e negativos devido às interferências externas.

Palavras–chave: vazamento de gás, monitoramento, sensores de fibra óptica, tubulações de gás.

ABSTRACT

The demand for safety and preservation of gas pipes has driven the emergence of solutions based on fiber optic sensors for monitoring possible leaks. Such leaks can be detected by monitoring temperature and/or vibration along the pipelines, using distributed sensors with Brillouin, Ramam, Rayleigh scattering technology and/or interferometry; or through point measurement sensors that use Fiber Bragg Gratings (FBGs) or Fabry Perot filters. Although fiber optic sensor technologies are already used in some pilot monitoring systems, there are uncertainties regarding the best choice of techniques and sensors for monitoring low-pressure lines (<10 bar). Therefore, this study proposes the experimental investigation of the potential, performance, cost and restrictions of some of the main optical technologies for monitoring leaks in gas pipes, such as DAS (*Distributed Acoustic Sensing*) and DTS (*Distributed Temperature Sensing*), as well as *strain gauges* based on FBG and optical accelerometers based on Fabry Perot filters. This project, financed by one of the largest gas companies in Brazil, focuses on the analysis of overhead gas lines, made of polyethylene (PE), of low pressure (up to 4 bar), in an urban scenario. Due to the challenges and risks, the project proposes the study of leaks in a laboratory environment, through the creation of an experimental bench. Compressed air was used instead of natural gas and, with the help of theoretical models, it was possible to predict the behavior of natural gas leaks. The bench allows for the simulation to simulate different conditions in the gas line with ease, repeatability and safety, in addition to allowing the collection of reference data from the gas line during the experiment with fiber optic sensors. Experiments were carried out to investigate leaks in 2 mm diameter holes in pressurized pipes at 0.35, 1, 2 and 4 bar. The DAS and DTS distributed sensors were used, in addition to the FBG point sensors, *strain gauge* based on FBGs and an optical accelerometer based on Fabry Perot filters. The results indicate that the DTS is capable of effectively identifying leaks when the piping is under a minimum pressure of 1 bar and covered by material (fabric or conduit). For natural gas, the minimum pressure at which it will be possible to identify leaks is estimated at 0.5 bar. No significant temperature drops were observed in uncovered overhead pipes. DAS identified vibrations at the beginning of the leak (transient) for pressures above 1 bar, although it was not capable of obtaining continuous vibrations with steady-state leaks. Regarding point sensors, bare FBGs and *strain gauges* were unable to identify vibrations caused by leaks at any of the pressures tested. On the other hand, accelerometers based on Fabry Perot filters were able to detect leaks when the piping was pressurized to at least 2 bar. They can be used to find the

leak region using vibration data to estimate the distance of the leak from the near sensor sensors together with multilateration. None of the techniques were able to identify leaks in pressurized pipes at 350 mbar. Through comparative analysis, this work allowed the identification of the potential and limitations of various fiber optic techniques and sensors for identifying leaks in gas lines. In future research, the performance of these sensors in the field will be evaluated. Furthermore, signal processing and sensory fusion techniques will be developed to increase the system's robustness to false positives and negatives due to external interference.
Keywords: gas leakage, monitoring, fiber optic sensors, gas pipes.

LIST OF FIGURES

LIST OF TABLES

CONTENTS

1 INTRODUCTION

This chapter presents a motivation for the study on the detection of leaks in gas lines, highlighting the serious consequences of this type of accident and the importance of an effective monitoring systems. It also presents the research objectives as well as outline the structure of subsequent chapters.

1.1 Motivation

Leaks in gas lines can have consequences for industry, people and the environment. A notorious example occurred in San Bruno, California, in 2010, when a pipeline managed by the *Pacific Gas and Electric Company* exploded, resulting in eight fatalities, the destruction of residential property, and substantial environmental damage (PHMSA, 2017). This traumatic incident was triggered by a failed weld on a high-pressure gas pipeline built in 1956, which was subject to weathering. Unfortunately, the company has received mixed criticism for its maintenance and neglect of necessary inspections. This disaster could have been avoided if there had been a more effective system for monitoring leaks in the gas lines.

Recently, distributed fiber optic sensors have emerged as a potential solution for the continuous detection and monitoring of leaks in gas lines. The company *OptaSense* has successfully implemented a project of a line of 1,850 km, which runs from Azerbaijan to Europe, using this technology (Optasense, 2021). Fiber optic sensors installed along this long pipeline have proven capable of accurately detecting a gas leak and providing real-time monitoring under conditions that allow for the detection of any leaks or unwanted variations. This technology has proven to be effective in preventing leaks, facing the risks associated with transporting gas in large transmission lines, but there is still much to be discovered and tested, especially in smaller and low-pressure distribution lines, which is the focus of this work.

The main advantage of fiber optic sensors compared to electronic sensors is their ability to monitor a larger area. With fiber optics, whether in a distributed sensor or point sensors, it is possible to monitor, in real-time, tens or hundreds of kilometers of pipes using a single acquisition equipment. This ensures a quick response to leaks or other emergencies. Furthermore, these sensors are immune to electromagnetic interference as they use light and not electricity. This also makes them safe for explosive environments as they do not generate sparks, a critical factor in flammable gas lines.

It is noteworthy that the use of distributed fiber optic sensors not only increases the safety and integrity of gas lines but also has substantive economic effects. According to the *US PIRG Education Fund*, between 2010 and October 2021, gas leaks reported to the US government resulted in the lost of 26.6 billion cubic feet of methane gas (PIRG, 2022). In addition, these leaks represent a threat to the environment, as the gases released can pollute the air, contribute to the greenhouse effect, and pose risks to human health. Early and accurate detection of leaks using fiber optic sensors helps reduce these economical and environmental impacts.

As the technology advances, we anticipate an increase in the adoption of fiber optic sensors in the oil and gas industry. These sensors offer solutions that are particularly suited to the monitoring of gas lines, as exemplified by their continuous monitoring capability, their effectiveness in explosive environments and their extensive range. Although fiber optic sensors are already being used in some pilot monitoring systems, it is still not clear which techniques and types of sensors are the most appropriate for this purpose. Considering the monitoring of leaks in gas lines, and the unique characteristics of fiber optic sensors in detecting these leaks, this dissertation proposes an investigation into the potential and performance of existing technologies for the detection of gas leaks in above ground distribution lines. In addition, the research also focuses on technical and scientific issues that are still pending, such as the smallest leak detectable under conditions of low pressure of aerial polyethylene (PE) pipes. Thus, the objective of this research is to fill an existing gap in the study of the use of fiber optic sensors in gas lines, exploring its potential and addressing technical and scientific issues still unresolved.

1.2 Objectives

This work aimed to experimentally investigate the suitability of various fiber optic sensor techniques and technologies for monitoring natural gas leakes in low-pressure (up to 4 bar), polyethylene (PE) pipes, above ground, gas distribution lines in urban environments. This research aim to evaluate the potential, performance and restrictions of some of the main optical technologies for monitoring leaks in gas pipes, such as DAS (Distributed Acoustic Sensing) and DTS (Distributed Temperature Sensing) interrogators, as well as FBG-based strain gauges and optical accelerometers based on Fabry Perot filters. The following specific objectives were established:

- Building an experimental bench to provide a controlled and safe environment where leaks could be simulated with compressed air in a variety of conditions. This bench made it possible to test the effectiveness of the sensors in conditions close to the real and helped establish the precision and reliability of the systems/technologies;
- Develop software to control, monitor, and record experimental bench data;
- Identify methods to detect leaks in above ground gas distribution lines using a distributed temperature sensor, as well as assessing the minimum identifiable leak;
- Investigate the frequencies at which vibrations generated by gas leaks occur;
- Analyze the ability of a distributed fiber optic vibration sensor to detect vibrations caused by a gas line leak;
- Check whether point sensors based on Bragg gratings (FBGs) or Fabry Perot filters are suitable for identifying leaks by monitoring vibrations;
- Identify the frequency spectrum of the vibrations generate by leaks;
- Identify which techniques and fiber optic sensors are most suitable for monitoring leaks in above ground low pressure gas distribution lines.

1.3 Structure

This work is organized as follows: In Chapter 2, Related Works are discussed, where distributed optical fiber sensors and their applications in pipeline monitoring are explored, as well as recent advances in this field. In Chapter 3, the Theory Review is dealt with, which explores the operating principles of fiber optic sensors, such as DAS and DTS interrogators, and FBG reflectivity modulation, in addition to discussing the Joule-Thompson effect. In Chapter 4, the Methodology is detailed, describing the experimental setup, data acquisition and processing, as well as the analysis and interpretation of the results. In Chapter 5, Results are presented, including an analysis of temperature variations and vibration monitoring, along with challenges and considerations in implementing fiber optic monitoring. Finally, in Chapter 6, the Final Considerations are displayed, where contributions to the monitoring of gas lines, limitations and possible future improvements are discussed.

2 RELATED WORKS

In this chapter, we provide a review of the literature concerning the application of fiber-optic sensing technologies for the monitoring and detection of gas pipeline leaks. This review encompasses various studies that have investigated the use of fiber-optic distributed acoustic sensing (DAS) systems, Fiber-Optic Distributed Temperature Sensing (DTS) systems and Fiber Bragg Grating (FBG) sensors, elucidating their capabilities, methodologies, and potential in enhancing the safety and integrity of gas pipelines.

2.1 Gas pipeline leak monitoring with distributed acoustic sensing

Traditional methods of leak detection, such as pressure monitoring and visual inspections, have limitations in terms of accuracy and efficiency (Daley *et al.*, 2013). However, advancements in technology have led to the development of new and improved leak detection systems. One such technology is the Distributed Acoustic Sensing (DAS) system which utilizes the fiber cable itself as a sensor, eliminating the need for point sensors (Daley *et al.*, 2013). The system works by measuring ground motion and vibrations along the pipeline, which can be indicative of leaks or other disturbances. The DAS system has been successfully tested for subsurface seismic monitoring, demonstrating its potential for pipeline leak detection in this condition (Daley *et al.*, 2013).

Optical fiber acoustic sensing systems, including DAS, have seen rapid development in recent years. Various sensing techniques, such as Mach-Zehnder interferometry (MZI), Michelson interferometry (MI), and Sagnac interferometry (SI), have been optimized to improve the sensing performance (Wang *et al.*, 2019). These advancements have led to the application of optical fiber acoustic sensing systems in domains that include military defense, structural health monitoring, and petroleum exploration (Wang *et al.*, 2019).

Other advantage of DAS-based leak detection is its ability to provide real-time monitoring of flammable and explosive gas pipeline networks, ensuring the safety of life and property (Zuo *et al.*, 2020). By analyzing the acoustic signals using advanced signal processing techniques, the DAS system can detect and classify different types of threats to the pipeline (Tejedor *et al.*, 2017), such as the movement of machinery and workers in an excavation in the area around of the pipe or even a leak. Another advantage is its simple structure and ease of implementation. The DAS system can use the existing optical fiber infrastructure of the pipeline, eliminating the need for additional sensors or cables (Daley *et al.*, 2013). This makes it a cost-effective solution for pipeline operators. If there is no optical fiber installed alongside the pipeline, it must be installed to the DAS.

A practical application of DAS technology is exemplified in a study that introduces a method for locating abnormal pipeline conditions based on sliding window outlier analysis (Hao *et al.*, 2022). This method leverages the distributed optical fiber sensor to monitor amplitude, enabling real-time diagnosis of abnormal pipeline states under unknown conditions. By introducing sliding window technology, the study effectively analyzes amplitude data that changes in time and space. Through tests involving buried pipelines, the method successfully identified invasion events and accurately located the invasion position with an error range stable at 0.5 m, significantly reducing the false alarm rate (Hao *et al.*, 2022). This demonstrates the DAS system's capabilities.

Another study highlights the use of DAS for detecting leak-induced pipeline vibrations. While DAS systems are commonly used for detecting third-party intrusion on pipelines, they can also be utilized for leak detection with the fiber wrapped helically around the main body of a pipe segment as seen in the Figure 2.1 or installed alongside near to the pipe. By monitoring the acoustic signals along the pipeline, DAS can identify and locate leaks, providing a solution for leak detection in short- to medium-length gas pipeline systems with 25-30 bar pressurization or even 5 bar, with the vibration frequencies in this case at around 5 kHz (Stajanca *et al.*, 2018). Overall, the use of distributed optical fiber acoustic sensing systems, such as DAS, offers a solution for pipeline leak detection. These systems leverage the fiber cable itself as a sensor, providing continuous monitoring and accurate detection of leaks along the pipeline as seen in the tests on the high-pressure tubes.

Regarding distributed temperature sensors (DTS), Shuyu Zhang presented in his 2023 article (Zhang *et al.*, 2023), the indication that the multi-physics coupling process between leakage-induced stress waves and the sensor fiber is significantly influenced by the viscous resistance of the soil. Soils with greater viscous resistance, such as clay, promote better propagation of stress waves, increasing the sensitivity of the DAS system. The study showed that, in clay soil and with the pipe pressurized at 1 bar, the maximum distance between the sensor fiber and the pipeline to detect a 15 mm diameter leak is 0.9 m, reducing to 0.5 m in the case of a 2 mm leak. Therefore, for the detection of smaller leaks, this distance should not exceed

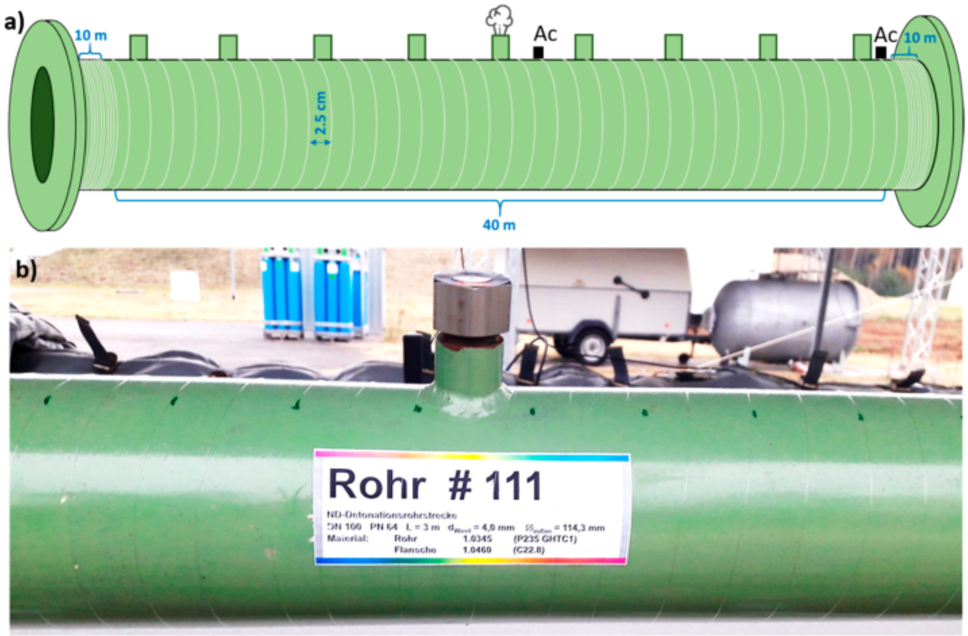

Figure 2.1 – Schematic illustration of the employed fiber application approach relying on fiber helical wrapping around the pipe segments. Position of simulated leak and reference accelerometers “Ac” (only in pipe zone 2) are indicated as well; (b) Detail photo of one of the instrumented pipe segments showing a pipe side adapter and applied fiber. Source: (Stajanca *et al.*, 2018)

0.5 m. The clay soil also showed the greatest amplitude of the deformation power spectrum and the longest duration of the deformation oscillation caused by the leak, providing a longer detection window.

2.2 Gas pipeline leak monitoring with distributed temperature sensing

Another approach is based on distributed optical fiber sensing, specifically Raman distributed optical fiber sensing. Raman scattering allows for the measurement of temperature and strain distribution along the optical fiber, for long distances (up to a few hundred kilometers) (Zuo *et al.*, 2020). This technology has been used to detect pipeline leakages and optimize oil production from wells. However, there are still challenges to overcome, such as reconciling sensing distance and spatial resolution and improving signal-to-noise ratio and measurement time (Zuo *et al.*, 2020).

In addition to leak detection, distributed temperature sensing (DTS) based on optical fiber systems can also be used for fire source localization in pipelines (Sun *et al.*, 2016). By analyzing the Raman backscattered light and using optical time-domain reflectometry, the temperature profile along the pipeline can be derived, allowing for the localization of fire sources.

This method has been experimentally validated and has been demonstrated for long sensing ranges (Sun *et al.*, 2016).

A compelling example of the practical application of optical fiber sensing is the use of a stimulated Brillouin-based Distributed Temperature Sensing (DTS) system for detecting pipeline leakage was in a 55 km pipeline in the northeast of Berlin constructed in 2002 developed by the company GESO. During the construction of underground natural gas storage caverns in a rock-salt formation. The creation of these caverns required the use of large quantities of hot water, resulting in large volumes of water saturated with salt, known as brine. Since brine is harmful to the environment, it needed to be safely transported to processing sites via pipelines. To ensure the safety of this transport, a pipeline monitoring system was necessary, and a DTS system was employed. This system was selected due to its ability to monitor the extensive pipeline with high accuracy and rapid acquisition time—achieving 1°C accuracy over the entire distance in less than 10 minutes. Over one year of operation, the system successfully detected a leakage, demonstrating the effectiveness of DTS in identifying temperature anomalies associated with leaks as seen in the Figure 2.2. The system's performance also highlighted its potential for fire detection in large structures like tunnels and chemical plants, where rapid detection of hotspots is crucial. Ongoing research is focused on extending the system's distance range beyond 100 km while maintaining high spatial resolution (Vogel *et al.*, 2001).

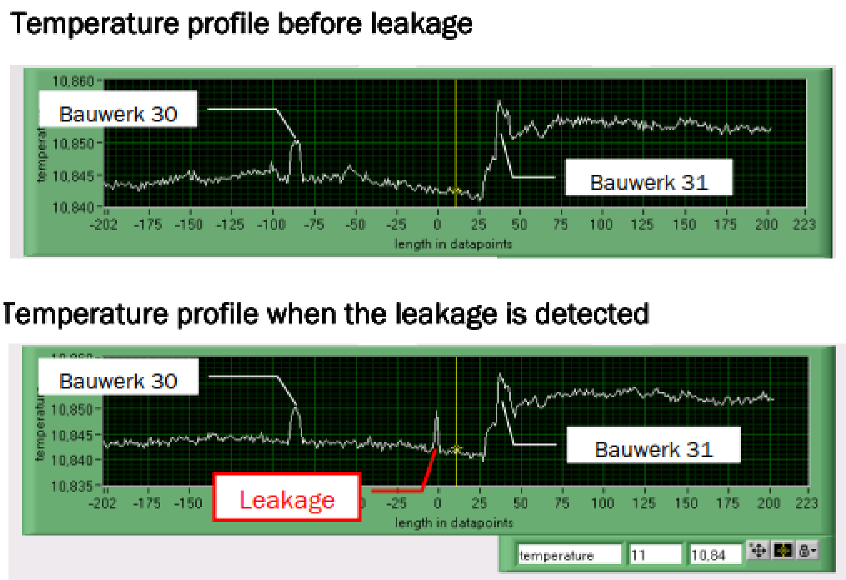

Figure 2.2 – Measured profiles before and after the leakage occurred at distance 17'970 meter from the pumping station, as displayed on the central PC in the control room. The vertical scale corresponds to raw Brillouin frequency shift given in GHz. The observed local temperature increase associated to the leakage was measured to be of around 8°C. Source: (Vogel *et al.*, 2001)

Overall, the combination of distributed optical fiber sensing technology, such as DAS and DTS, with advanced signal processing methods, such as wavelet transform and spectrum analysis, provides a promising approach for pipeline leak detection (Gigih; Ghazali, 2021). These technologies offer advantages such as high spatial resolution, long sensing distances, and immunity to electromagnetic fields. However, further research is needed to address challenges related to implementation, accuracy, and system performance.

2.3 Gas pipeline leak monitoring with Fiber-optic sensors based on Fiber Bragg Grating and Fabry-Perot accelerometer

Fiber-optic sensors, particularly those based on Fiber Bragg Grating (FBG) technology, have emerged as a promising solution for leak detection and localization (Jia *et al.*, 2018), (Jiang *et al.*, 2017), (Hou *et al.*, 2013). These sensors offer several advantages, including high sensitivity, immunity to electromagnetic interference, and the ability to monitor long-distance pipelines.

One approach involves the use of FBG hoop strain sensors installed along the pipeline to measure hoop strain variations induced by leaks or pressure drops (Jia *et al.*, 2018), (Jiang *et al.*, 2017). These sensors provide a nondestructive testing method for pipeline leakage detection and localization (Jia *et al.*, 2018). By employing a back-propagation neural network and using hoop strain variations as input neurons, it was possible to achieve pattern recognition and predict the leakage point (Jia *et al.*, 2018). The results demonstrate the feasibility and robustness of this integrated approach for leak localization (Jia *et al.*, 2018).

Another approach is the Fabry-Perot accelerometer, a sensitive and compact sensor that utilizes the photothermal effect in a hollow-core fiber Fabry-Perot interferometer (FPI) (Zhang *et al.*, 2022). In the context of pipelines, they can be used to monitor vibrations and detect potential issues such as leaks or structural damage. The high sensitivity of these accelerometers allows for the detection of even small vibrations, enabling early detection of problems and preventing further damage (Lu *et al.*, 2021). The compact structure of Fabry-Perot accelerometers makes them suitable for installation in pipelines, where space may be limited.

In addition to these approaches, FBG sensors have also been researched and developed for various applications in the oil and gas industry. For example, a research group has been focusing on nonlinear optics, photoelectronic technology, and optical fiber sensing technology, particularly in the fields of well-logging, oil and gas pipeline monitoring, and downhole seismic exploitation (Qiao *et al.*, 2017). Their work includes the inscription of in-fiber gratings into diverse fibers using femtosecond infrared and UV laser light, micromachining fibers with femtosecond lasers, and developing physical, biomedical, and chemical sensors using FBGs and interferometers. These advancements highlight the potential of FBG sensors for sensitive, non-destructive, long-term in-situ measurements in harsh environments, such as those encountered in oil and gas fields.

However, despite the significant progress and the promising applications of FBG sensors, there are still challenges that need to be addressed, such as the development of novel sensing fibers and FBGs with higher performance, improved mechanics of host material/fiber interfaces, and adequate fiber coatings and packaging designs. Furthermore, the standardization of fiber-optic sensors is crucial for their widespread adoption in the oil and gas industry, as the current lack of standards can lead to confusion and hinder industrialization efforts, (Qiao *et al.*, 2017).

Other study for oil and gas exploration, (Rong; Qiao, 2019), highlighted the use of cladding FBGs, which exhibit high sensitivity to vibrations and acceleration, making them particularly effective for seismic exploration. The study also introduced the use of these cladding FBGs as vector vibration detectors, capable of accurately locating unknown vibration sources. The ability of cladding FBGs to reference out power fluctuations induced by temperature or optical components further enhances their reliability in harsh environments. Additionally, the study reviewed several FBG-based underwater (UW) sensors, including the FBG-Fabry-Perot (FBG-FP) probe, which demonstrated significant improvements in sensitivity and frequency, crucial for enhancing spatial resolution in seismic physical modeling (SPM). Experimental results confirmed the FBG-FP's superior performance in UW detection, and physical models simulating various geological structures were successfully imaged using continuous scanning and echo data reconstruction.

Overall, the use of FBG sensors in leak monitoring of gas pipelines offers advantages, including high sensitivity and immunity to electromagnetic interference (Jiang *et al.*, 2017). Features on the accelerometers such as sensitivity, compact structure, and simple optical path make them well-suited for this application. When compared to DAS and DTS, the use of those point fiber optic sensors has the advantage of being significantly cheaper to install (in the order of a third or less of the cost of a DAS or DTS system). However, their disadvantage is the smaller segment of pipe monitored (up to a few kilometers versus several tens of kilometers), making them particularly suitable for monitoring short stretches of pipe, such as the ones used in bridges.

Table 2.1 presents a comparison of experimental results from various studies on fiber-optic sensing technologies applied to gas pipeline leak detection. It highlights the key findings, advantages, and limitations of techniques such as Distributed Acoustic Sensing (DAS), Distributed Temperature Sensing (DTS), Fiber Bragg Grating (FBG) sensors, Fabry-Perot accelerometers, and FBGs.

Table 2.1 – Comparison of Results from Related Works

Technique	Study/Authors	Key Findings	Advantages	Limitations
Distributed Acoustic Sensing (DAS)	Daley et al., 2013; Zuo et al., 2020; Hao et al., 2022; Stajanca et al., 2018	DAS technology uses fiber optics for detecting pipeline vibrations, identifying leaks, and real-time threat classification. Demonstrated potential in subsurface monitoring with accuracy up to 0.5m.	Real-time monitoring; Cost-effective using existing fiber infrastructure; High spatial resolution.	Requires fiber installation if not pre-existing; Limited effectiveness in certain soil types.
Distributed Temperature Sensing (DTS)	Sun et al., 2016; Vogel et al., 2001; Zhang et al., 2023	DTS uses Raman scattering for temperature profiling along pipelines. Achieved 1°C accuracy over a 55 km pipeline with a leakage detection capability of 8°C anomaly.	Suitable for long-distance monitoring; Useful for fire detection in structures; High accuracy.	Challenges in balancing distance and resolution; Affected by environmental conditions.
Fiber Bragg Grating (FBG) Sensors	Jia et al., 2018; Jiang et al., 2017; Hou et al., 2013	FBG sensors detect pipeline strain and vibration for leak localization using neural networks and Fabry-Perot accelerometers.	High sensitivity and immunity to electromagnetic interference; Compact for small spaces.	Limited monitoring range; Higher costs than DAS/DTS for large areas.
Fabry-Perot Accelerometers	Lu et al., 2021; Zhang et al., 2022	Detect vibrations to identify structural damages with high sensitivity, suitable for short pipelines.	Compact structure; Detects small vibrations with high sensitivity.	Effective over shorter distances; Limited by spatial constraints within pipelines.
Cladding FBGs for Seismic Monitoring	Rong & Qiao, 2019	High sensitivity to vibrations, enables location of seismic activity, effective in underwater detection.	Improved reliability in harsh environments; Suitable for detailed geological monitoring.	High cost for extended deployment; Sensitivity to environmental interferences requiring robust packaging solutions.

3 THEORY REVIEW

This chapter presents the operating principles of the fiber optic sensors used in this work. In particular, the DAS (*Distributed Acoustic Sensing*) and DTS (*Distributed Temperature Sensing*) interrogators and the sensors based on FBGs (*Fiber Bragg Gratings*) and the Fabry Perot filter. In addition, the Joule-Thompson effect is discussed.

3.1 Optical Fibers

The genesis of contemporary fiber optic sensors can be traced back to two fundamental milestones in the field of optics in the 1960s: the advent of the laser in 1960 (Schawlow; Townes, 1958) and the emergence of low-loss optical fibers in 1966 (Maurer *et al.*, 1971). Since the early 1970s, these low-loss optical fibers have had applications beyond their initial role in telecommunications, being extended to instrumentation.

Optical fibers, which consist of long flexible waveguides, stand out mainly because they are made of fused silica (amorphous silicon dioxide) (Keck *et al.*, 1973). Silica is commonly found in sand and occupies 26% of the earth's crust, in stark contrast to copper, which only occupies 0.01%. This material has properties such as transparency over a wide range of wavelengths, low absorption, and scattering losses, ease of manufacture, cleavability and fusion splicing, remarkable mechanical resistance to pulling and bending, chemical resistance, and stability. These characteristics have consolidated silica fiber as an essential basis for fiber optic sensor technology and its varied applications (Kersey *et al.*, 1997).

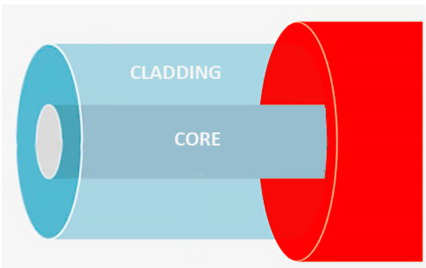

Figure 3.1 – Illustration of an optical fiber cable.

The optical fiber consists of a core, where the light travels, surrounded by cladding that guides the light, as illustrated in Figure 3.1. Typically, there is also an outer protective layer called a jacket, which provides enhanced mechanical strength and protection against external elements. The core of an optical fiber is produced through a process known as "drawing" or "pulling," where the material is melted into a liquid state to create a fine wire. The liquid material is then extruded into a thin filament, forming the core of the optical fiber. This process can be divided into two categories: single-mode and multimode. In single-mode fibers, the core is extremely thin, usually with diameters ranging from 8 to 10 micrometers, allowing only a single mode of light (a single light beam) to be guided along the fiber. Single-mode fibers are ideal for long-distance transmission and applications requiring high bandwidth (Agrawal, 2010). In multimode fibers, the core is thicker, with diameters ranging from 50 to 62.5 micrometers, enabling multiple light modes (several light beams) to propagate through the fiber. Multimode fibers are often used for shorter distances and applications that do not require high bandwidth (Agrawal, 2010). To complete the optical fiber, the core is coated with a cladding material that has a lower refractive index than the core. This difference in refractive indices allows the light to be guided within the core by the principle of total internal reflection, ensuring efficient light transmission.

3.2 Optical Fibers as distributed sensors

When a pulse of light is launched through an optical fiber, a small portion of the incident energy scatters in various directions due to local non-uniformities (Tur, 1999). However, for the phenomena used in this context, only forward and backward scattering is significant. Backscattering, in particular, is important because it travels back to the end of the original fiber where the laser light was initially introduced. Scattering phenomena arise from factors such as material impurities (Rayleigh scattering), thermally induced acoustic waves (Brillouin scattering), or atomic and molecular vibrations (Raman scattering). Distributed detection techniques rely on the analysis of the backscattered signal generated at different locations along the length of the fiber (Tur, 1999).

Rayleigh scattering, represented in Figure 3.2, is the interaction of a light pulse with material impurities. This phenomenon represents the largest of the three backscattered signals in silica fibers, maintaining the same wavelength as the incident light (Johnson, 1972). Rayleigh scattering is the physical principle behind the DAS (Distributed Acoustic Sensing) system. The reference to "acoustic" is related to the system's ability to detect and measure acoustic vibrations (sound waves - frequency less than 20 kHz) using optical fiber. Despite the name, this technology is not limited to audible sounds, it can detect a wide range of frequencies, including those beyond the range of human hearing.

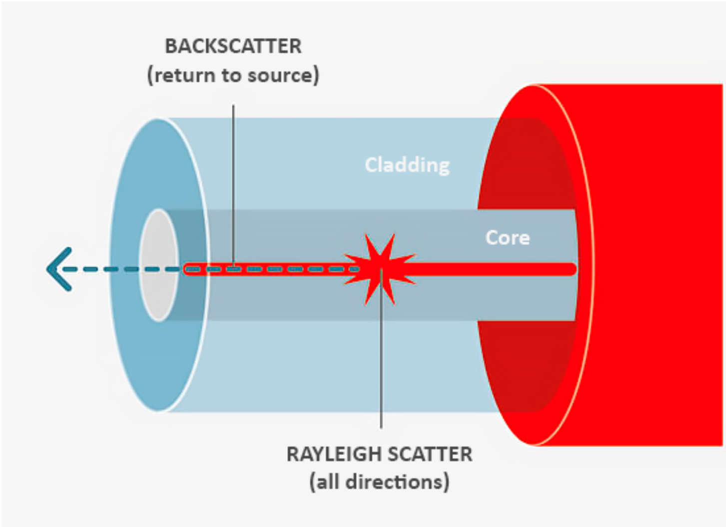

Figure 3.2 – Rayleigh backscatter. Source: (Gannon, 2018)

Rayleigh scattering is the phenomenon responsible for the blue color of the sky (Bohren; Huffman, 1983). As sunlight passes through the Earth's atmosphere, a portion of it is scattered in different directions due to Rayleigh scattering. Blue light is particularly prone to scattering because Rayleigh scattering occurs when the particles or structures involved are much smaller than the wavelength of the light interacting with them. Light, which consists of electromagnetic waves, interacts with these small particles through its electric field component (oscillation of the electric field). The extent of scattering depends on the size of the particles relative to the wavelength of the light. In the atmosphere, air molecules and tiny particles, such as dust or nitrogen and oxygen molecules, are significantly smaller than the wavelength of visible light, particularly blue light, which has a shorter wavelength compared to other colors in the spectrum. Consequently, these molecules and particles scatter blue light more effectively than colors like red or green. When we observe the sky during daylight, we see the light that has been scattered towards us by the atmosphere. A substantial portion of the blue light is scattered in multiple directions, including towards our eyes, which is why the sky appears blue to us.

In an optical fiber, when a pulse of light (at wavelengths close to the incident light) is transmitted through the fiber, a portion of this light is backscattered due to microscopic irregularities and fluctuations in the refractive index of the fiber material (Johnson, 1972). This backscattered light is detected by the interrogator, which records the time-of-flight of the laser pulse to identify the specific point along the fiber where the scattering occurred. The system then sends another pulse into the fiber a fraction of a second later, capturing data from another point along the fiber. By analyzing the interference between the incident light and the backscattered light, the Distributed Acoustic Sensing (DAS) system can accurately measure the amplitude, frequency, and location of these disturbances. By continuously repeating this process thousands of times per second, the DAS system can monitor small sections of an optical fiber cable in real-time, providing continuous and detailed sensing capabilities.

Brillouin scattering, the principle utilized by the Distributed Temperature Sensing (DTS) interrogator selected for this project, involves the interaction of a light pulse with thermally excited acoustic waves, also known as acoustic phonons (Smith, 2004). Through the elasto-optic effect, these acoustic waves induce a slight local change in the refractive index of the fiber. This change reflects a small portion of the incident light and alters its frequency (or wavelength) due to the Doppler Effect. The resulting frequency shift depends on the acoustic velocity within the fiber, while its direction is influenced by the propagation direction of the acoustic waves. As a result, Brillouin backscattering generates two frequency components around the incident light, known as the Stokes and Anti-Stokes components, as illustrated in Figure 3.3. In silica fibers, the frequency shift induced by Brillouin scattering is typically on the order of 10 GHz (equivalent to a 0.1 nm shift in the 1550 nm wavelength range) and is sensitive to both temperature and strain (Agrawal, 2010). The frequency information from the Brillouin backscattered light, specifically the shift in wavelength relative to the original laser light, can be used to measure local temperature and strain. This method is classified as a frequency-based technique since the temperature and strain data are encoded in the Brillouin frequency shift. Consequently, the frequency shift detected by most distributed sensors based on Brillouin backscattering reflects the local Brillouin shift caused by variations in environmental conditions (Motil *et al.*, 2016).

In comparison, Brillouin signals are around 15-20 dB weaker than Rayleigh signals but have an order of magnitude more intensity than Raman signals (Thévenaz *et al.*, 1996). This enables Brillouin-based sensors to achieve a higher signal-to-noise ratio, resulting in improvements in spatial resolution and sensor range.

Raman scattering is the interaction of a pulse of light with atomic particles or molecular vibrations (optical phonons), presenting the lowest intensity among the three backscattered signals (Tarcea *et al.*, 2008). Raman backscattering in the fiber core arises due to the interaction between an incident photon and a molecule, in which the backscattered photon instantly engages in two-state transitions, producing or absorbing another photon. Similar to Brillouin scattering, Raman scattering causes a frequency change of approximately 13.0 THz at 1550 nm.

Raman backscattering is sensitive to the wavelength of the laser source and strongly influenced by the deformation caused by external vibrations in the fiber (Mulugeta; S, 2021).

There are specific advantages to selecting one type of backscatter-based sensor over another, depending on the physical parameters that need to be measured. For example, with Raman scattering, the Anti-Stokes component is sensitive to temperature changes, while the Stokes component remains largely unaffected by temperature variations. In contrast, with Brillouin scattering, both the Stokes and Anti-Stokes components are influenced by temperature, shifting away from the central frequency as temperature increases. This shift provides valuable information on both temperature distribution and mechanical deformation. Rayleigh and Brillouin scattering are particularly promising for use in distributed geophysical detection systems, as they can simultaneously detect temperature and acoustic parameters. By combining Rayleigh and Brillouin scattering techniques, it is possible to perform simultaneous measurements of vibration and temperature in single-mode fibers using 1550 nm light (Miah; Potter, 2017). This combination enables more comprehensive monitoring in applications where both temperature and acoustic data are critical.

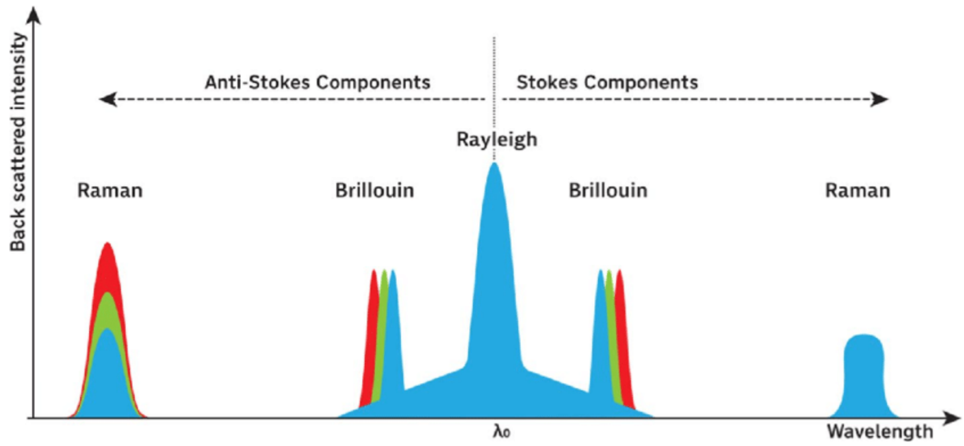

Figure 3.3 – Diagram of the Rayleigh, Raman, and Brillouin peaks in the backscattered light spectrum (Modified from (Mulugeta; S, 2021)).

3.3 FBG: Reflectivity Modulation Principle

A Fiber Bragg Grating (FBG) is an optical component that features a pattern of periodic variations in the refractive index within an optical fiber. This variation is achieved by exposing a section of the fiber to a pattern of ultraviolet light, which induces microscopic changes in the fiber's material properties. The result is a structure that functions as a band-selective mirror, reflecting specific wavelengths of incident light while allowing other wavelengths to pass through unaltered (Rao, 1999). When light encounters an FBG, the phenomenon known as "Bragg reflection" occurs. In this process, light of a particular wavelength is reflected back towards the light source, while other wavelengths continue to propagate through the fiber without alteration, as illustrated in Figure 3.4. The operation of an FBG relies on the principles of constructive and destructive interference of light (Onoufriou *et al.*, 2000). The specific wavelength that is reflected is determined by the periodicity of the refractive index variation within the FBG.

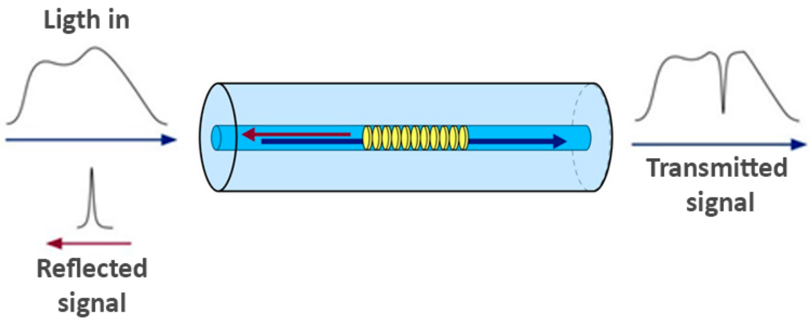

Figure 3.4 – Bragg grating - Source: (Gouveia *et al.*, 2013).

The most common method for fabricating a Fiber Bragg Grating (FBG) is through the process of photosensitization of the optical fiber. In this process, the fiber is exposed to the interference pattern created by two beams of ultraviolet (UV) light, leading to a modulation of the refractive index along the fiber (Kashyap, 1999). This modulation is caused by a phenomenon known as photo-darkening, which induces a periodic variation in the refractive index along the FBG. The spacing between these modulations determines the periodicity of the diffraction grating, which in turn defines the specific reflection wavelength of the FBG. The reflection that occurs is exclusive to a specific wavelength, which is dictated by the periodicity of the FBG, while the remaining light continues to propagate through the optical fiber. This makes FBGs effective wavelength selectors, capable of reflecting a particular spectrum of light. For instance, the sensor depicted in Figure 3.5, which was utilized in this work, operates at a wavelength of 1576 nm.

When an FBG experiences deformation or temperature variation, its refractive index changes, leading to a shift in the reflected wavelength. This shift can be precisely measured, enabling FBGs to function as sensors for various physical parameters, including stress, strain, temperature, and pressure. The Bragg wavelength (λ_B) increases if there is heating or longitudinal tension in the fiber, and it decreases if there is cooling or longitudinal compression in the fiber. The typical sensitivity of an FBG to mechanical strain is around 1.2 picometers per mi-

Figure 3.5 – FBG sensor model os1100.

crostrain (pm/ $\mu\,\varepsilon$), and its sensitivity to temperature is approximately 10 picometers per degree Celsius (pm/°C) (Albert *et al.*, 2013).

FBG-based optical sensors offer several advantages over traditional electronic sensors, such as the ability to multiplex multiple sensors along a single fiber and immunity to electromagnetic interference. This immunity is particularly crucial in environments with high electrical noise, as it stems from the dielectric nature of optical fibers, rendering them unaffected by electromagnetic fields. This makes FBG sensors a robust solution for critical applications, such as monitoring gas transmission lines, where intense electric fields may be present due to high-voltage equipment.

Another significant advantage of FBG-based sensors is their capability to operate in hostile environments. They are inherently robust and can endure adverse conditions, including high humidity, intense vibrations, and chemical corrosion, making them ideal for use in challenging settings such as industrial facilities and infrastructure monitoring (Onoufriou *et al.*, 2000).

3.3.1 Optical strain gauge sensors based on FBG

An FBG strain gauge is a type of extensometer composed of a Bragg grating, designed to measure mechanical deformations (strain). This specific application of FBG technology enables the measurement of deformations or stresses in various objects (Rao, 1999). The FBG is typically attached or bonded to the surface of the object being monitored. When the object undergoes deformation or is subjected to stress, the FBG responds by altering the wavelength of the reflected light. These sensors leverage the intrinsic reflective modulation capabilities of FBGs, where the variation in the refractive index within the optical fiber, caused by mechanical deformation, allows for precise quantification of stress levels. This is due to the periodic disturbance or change in the refractive index of the optical fiber core.

Even a small change in the fiber's structure results in a shift in the Bragg wavelength, and consequently, in the wavelength of the reflected light. FBGs are highly sensitive and can detect even the smallest deformations or stresses affecting the fiber structure, with a precision on the order of 1 microstrain. For example, the Micron Optics os3200 model, illustrated in Figure 3.6 and used in this work, has a strain measurement range of $\pm5000\ \mu\epsilon$ (microstrain) and a mechanical strain sensitivity of approximately 1.2 pm/$\mu\epsilon$. This high sensitivity makes FBG strain gauges particularly useful for applications requiring accurate monitoring of structural integrity and stress distribution.

Figure 3.6 – Optical Strain gauge based on FBG, model os3200.

FBG-based optical strain gauges offer a rapid response time, making them highly effective for real-time monitoring. The light reflected from the FBG can be instantly detected, digitized, and processed using advanced spectrometers and digital signal processing algorithms (MicronOptics, 2023b). This swift response capability ensures accurate, dynamic monitoring of stress and strain, which is crucial for applications involving sudden load changes or rapid movements. Moreover, the technology supports the multiplexing of multiple FBGs along a single optical fiber, provided that the reflected spectra of the gratings do not overlap. This feature not only simplifies the installation process by enabling the deployment of multiple sensors within a single structure—thereby reducing both time and costs—but also facilitates the simultaneous monitoring of several regions within complex structures. As a result, it provides a comprehensive overview of the stress and strain distribution across the monitored structure, enhancing the reliability and efficiency of structural health monitoring systems.

One drawback of FBG-based sensors is their sensitivity to temperature variations, which can lead to changes in the frequency of the reflected wavelength, potentially being misinterpreted as structural deformations. This occurs because temperature fluctuations can cause the optical fiber containing the FBG to undergo thermal expansion or contraction, thereby altering its refractive index and, consequently, the reflection wavelength (Rao, 1999). This temperature sensitivity poses a challenge to accurate strain measurement using FBGs. However, various strategies can be employed to mitigate this effect and enhance measurement precision.

One such strategy is the application of "Temperature Compensation" techniques, where multiple FBGs are used to measure both ambient temperature and strain, enabling the compensation of thermal variations in the readings. Another approach, known as "Dual FBG Compensation," involves placing two FBGs on opposite sides of a structure to differentiate between deformations and thermal-induced variations. Additionally, "Software Compensation" techniques can be applied, using algorithm-based corrections that consider the FBG's temperature sensitivity and the specific frequency band of the signal of interest to account for thermal variations (Yoffe *et al.*, 1995). These methods collectively contribute to improving the reliability and accuracy of FBG-based strain measurements, even in environments with fluctuating temperatures.

3.4 Optical accelerometers based on Fabry Perot filters

A Fabry-Perot filter is an optical device designed to selectively transmit a specific wavelength of light while blocking other wavelength ranges. This selective filtering is achieved through the principles of constructive and destructive interference, which occur as light waves reflect between two parallel, highly reflective surfaces known as Fabry-Perot mirrors. These mirrors are positioned a short distance apart, allowing light to bounce back and forth between them, generating an interference pattern. This pattern amplifies certain wavelengths while attenuating others, effectively acting as a "selective room" for specific wave frequencies.

The resonant wavelength that is transmitted or reflected by the Fabry-Perot filter is determined by the distance between the reflecting surfaces. This contrasts with Fiber Bragg Gratings (FBGs), which detect specific wavelength changes in an optical fiber due to variations in the refractive index. While both devices leverage the interferometric properties of light, they do so in different contexts and through different structural designs.

In optical telecommunications, Fabry-Perot filters are crucial for selecting transmission channels in fiber optic systems, typically within the 100 GHz range, corresponding to wavelengths between 0.8 nm and 1,550 nm (MicronOptics, 2023a). Additionally, these filters are employed in lasers to precisely select the wavelength needed to emit coherent light. This ability to fine-tune wavelengths makes Fabry-Perot filters essential in various high-precision optical applications.

Figure 3.7 – Optical accelerometer based on Fabry Perot, model os7510.

In optical accelerometers that utilize the Fabry-Perot principle, an applied acceleration causes the reflecting surfaces to move, thereby altering the distance between them and changing the interference pattern of the light waves. These changes in the interference pattern correspond to the detected acceleration. Such accelerometers are used in a variety of fields, including structural engineering, where they monitor vibrations in machinery and motion control systems, as well as in aerospace applications. One of the key advantages of accelerometers based on this technology is their immunity to electromagnetic interference. However, they require precise alignment of the reflective surfaces and rely on stable, high-quality light sources to function accurately.

In this work, we selected the os7510 optical accelerometer from Micron Optics, as illustrated in Figure 3.7. This accelerometer has an input range that can vary between ±2.5 g and ±10 g. For frequencies below 10 Hz, the measurement range is ±2.5 g. However, the accelerometer operates over a frequency range of 0 to 350 Hz when the full scale is ±2.5 g. With a full scale of ±10 g, the operating range is reduced to 0 to 100 Hz. It offers a sensitivity of 65 nm/g and is capable of operating in extreme temperatures, ranging from -40 to 80 °C, while also withstanding mechanical shocks up to 500 g (MicronOptics, 2023a). Figure 3.8 presents the maximum g range of the os7510 accelerometer in function of frequency. Although it is designed for a nominal operating frequency of up to 350 Hz, the accelerometer can capture vibration signals at 2 kHz, but with strong attenuation. This extended frequency response highlights the versatility of the os7510 in capturing a wide range of vibration signals, making it suitable for various demanding applications.

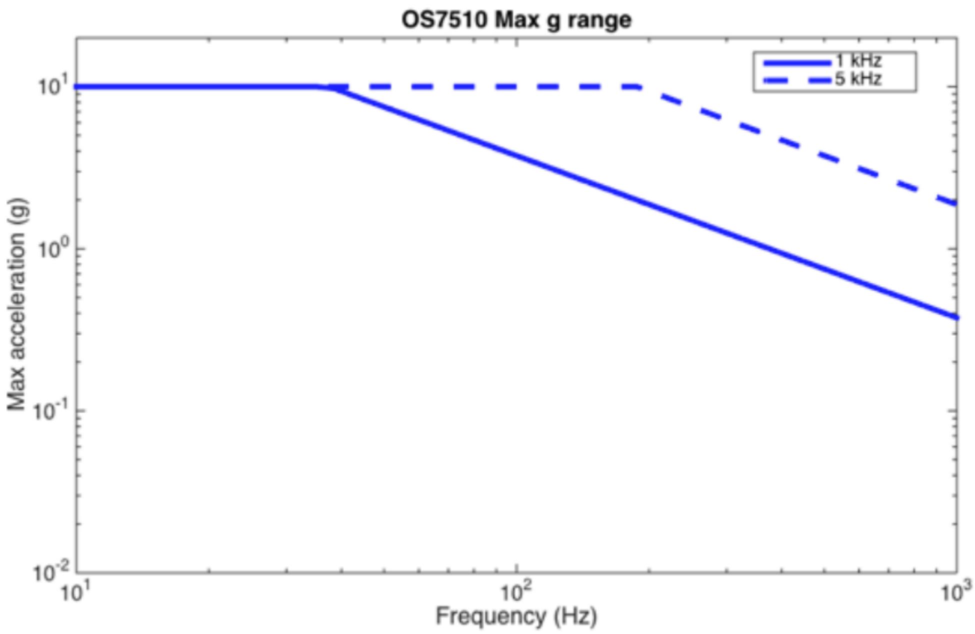

Figure 3.8 – Full scale of the os7510 accelerometer in function of frequency. Source: (MicronOptics, 2023a)

3.5 The Joule-Thomson Effect

The Joule-Thomson effect, also known as the Joule-Kelvin effect, consists of a thermodynamic phenomenon that occurs when a gas, whether ideal or real, undergoes expansion or compression in an adiabatic process - a process without heat transfer - as it passes through a valve or orifice (Zemansky; Dittman, 1981). Mathematically, the Joule-Thomson effect is defined by the Joule-Thomson coefficient (μ), which is expressed as:

$$\mu = \Delta T = \left(\frac{\partial T}{\partial P}\right)_H, \tag{3.1}$$

where $\frac{dT}{dP}$ is the variation of temperature as a function of pressure, and H denotes that the enthalpy (H) remains constant during the process. It is important to note that the Joule-Thomson coefficient (μ) depends non-linearly on the type, temperature, and pressure of the gas (Zemansky; Dittman, 1981).

The Joule-Thomson Effect is of crucial importance in refrigeration and gas liquefaction processes. An example is the everyday use of a refrigerator, where a gas is initially compressed in a compressor, heated, and then expanded utilizing a valve, leading to a reduction in temperature. This drop in temperature is then used to preserve the food inside the fridge. In the event of a gas leak in a pipeline, the cooling caused by this effect can lead to the formation of ice or condensation of moisture in the area near the leak, depending on the gas, due to the rapid cooling of the gas. Such a build-up of ice or condensation can compromise the structural integrity of the transmission line, and can even lead to an increase in the viscosity of the gas, making it difficult to flow in the transmission line and impairing the ability to deliver the gas, but this cooling is one of the key points for detecting the leak (Cengel; Boles, 2014).

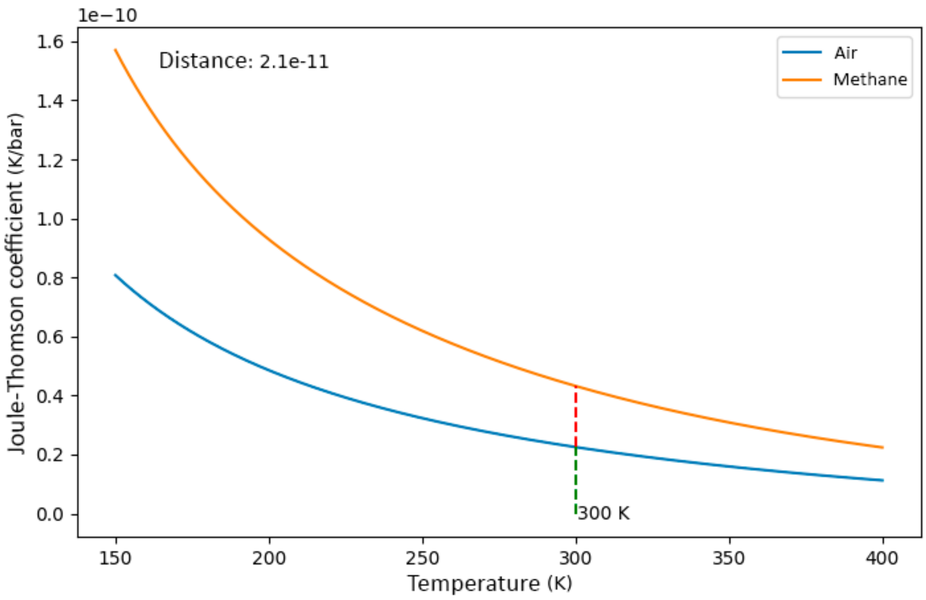

Figure 3.9 – Joule-Thomson coefficient for the temperature of atmospheric air and methane (Bell; Contributors, 2016–2024).

The magnitude of the Joule-Thomson effect depends on the intrinsic properties of the gas. Gases with a positive coefficient cool down during expansion and heat up during compression, while gases with a negative coefficient heat up during expansion and cool down during compression. Both atmospheric air and methane, the main component of natural gas, have positive coefficients. Therefore, when undergoing a Joule-Thomson expansion, the gas is subjected to a reduction in pressure and, consequently, a decrease in temperature. This phenomenon is explained by the partial conversion of the kinetic energy of the gas molecules into potential energy during expansion, which causes a reduction in thermal energy and therefore temperature. On the other hand, during a Joule-Thomson compression, the gas in question is faced with an increase in pressure and, consequently, temperature. In this case, the kinetic energy of the molecules is converted into thermal energy, a direct result of the work done by the gas during compression, which culminates in an increase in temperature (Arpaci; Smith, 2001). For atmospheric air at a temperature of 27°C (300 K), the Joule-Thomson coefficient is around 0.22 K/Bar (Roebuck, 1925), while for methane this coefficient is around 0.48 K/Bar (Sebok, 2022). This implies that, during an adiabatic expansion, methane cools the tube faster than atmospheric air. Assuming that both gases undergo the same pressure reduction at 27°C, methane will have a temperature drop 2.2 times greater than that of atmospheric air when expanded. This difference is due to the molecular properties of the gases, and behaves non-linearly, as shown in the graph in Figure 3.9. Methane, which has greater intermolecular forces and a molecular arrangement that favors a stronger Joule-Thomson effect, shows a more significant drop in the kinetic energy of the molecules during expansion, resulting in greater cooling to room temperature. In contrast, atmospheric air, despite also having a positive Joule-Thomson coefficient, has a distinct molecular structure and less vigorous intermolecular interactions, resulting in a less prominent Joule-Thomson effect (Cengel; Boles, 2014).

4 METHODOLOGY

This chapter presents the methodological procedures adopted to monitor gas lines using fiber optic sensors. Initially, the experimental setup is presented, detailing the components of the bench. This is followed by the optical equipment, preliminary tests, and the data processing methods used in the project.

4.1 Experimental bench

To test the sensors and carry out the experiments required for this work, we first need a suitable environment, and a test platform specifically designed to conduct experiments in a controlled and safe manner. With this in mind, a test bench was designed and built in the LabPetro (Experimental Laboratory of Petroleum) at UNICAMP to carry out the experimental tests. Knowing the challenges and risks associated with fire and explosion when using natural gas, compressed air was chosen as the test gas. Although, as discussed in Section 3.5, its characteristics differ from natural gas and with the help of theoretical models, it is possible to calculate and approximate the behavior of compressed air leaks to what happens with natural gas in the field. Another factor to consider about the bench is that it should allow the manipulation and monitoring of variables such as pressure inside the pipe, fluid flow at the beginning and end of the pipe, as well as the means to control this flow and pressure digitally. Non-optical sensors, such as piezoelectric accelerometers and thermometers are also essential for comparing results with data from optical sensors. Another key element is the piping itself, which was as close as possible to that used in the field, as well as its leakage conditions. Therefore, the aim of the experiment bench should be to facilitate the simulation of leak and rupture scenarios under realistic conditions, while maintaining a controlled environment to obtain consistent data with a margin for repeatability, which increases the reliability of the data collected, contributing to the validation of leak monitoring methods based on fiber optic sensors.

After considering these variables, it was necessary to choose the equipment that will fulfill the idealized proposal and the first step was to determine the equipment's control module. The CompactDAQ chassis model 9178 from National Instruments was chosen, equipped with 8 *slots* and Ethernet communication, shown in Figure 4.1. Four acquisition modules were added, one for current measurement (NI-9203) used to interrogate the pressure (gauge and differential) and flow (Coriolis) sensors; one with current output for line flow control (NI-9265); one for interrogating 4-wire temperature sensors (NI-9219); and one for measuring vibration with piezoelectric accelerometers (NI-9234). Details are given in Table 4.1.

Table 4.1 – cDAQ equipment specifications.

Equipment	Qty	Function	Specification
cDaq-9178	1	Integrate all measurement modules and provide communication with LabVIEW	CompactDAQ Ethernet chassis with 8 slots
NI - 9203	1	Interrogation of pressure sensors	Current input module, ±20 mA, 200 kS/s, 8 channels
NI - 9265	1	Proportional valve drive	C Series current output module, 100 kS/s, 8 channels
NI - 9219	1	Interrogation of 4-wire temperature sensors	C Series temperature measurement input module, 4 channels
NI - 9234	1	Interrogation of piezoelectric vibration sensors	C Series voltage input module, 50 kS/s, 4 channels

Figure 4.1 – cDaq-9178 chassis.

Two pressure sensors (gauge and differential) from Rosemount and two flow sensors (Coriolis) from Micro Motion's R Series were chosen, the details of which are shown in Table 4.2. The two Coriolis sensors used were placed at the inlet and outlet of the line, allowing the mass flow rate of the leak to be quantified. The gauge pressure sensor was used to provide pressure data during leak events and help control the internal pressure of the pipe, and the differential pressure sensor was used to quantify the pressure drop caused by the flow.

Two electronically controlled valves were used to control the line pressure and flow. A FESTO MPYE proportional flow valve is responsible for controlling the final flow of the line and a FESTO VPPM proportional pressure valve is responsible for controlling the line pressure (which is regulated by the valve itself in a closed-loop). The controller program sends only a

Table 4.2 – Characteristics of the pneumatic sensors used.

Sensors	Qty	Manufacturer	Model	Features
Coriolis	2	Micro Motion	R R050S Series	Maximum pressure: 1.450 psi/g (103 bar/g)
Differential pressure	1	Rosemount	2051	Operating range: –25 a 25 pol.H2O (–62.2 a 62.2 mbar), linear output
Absolute and gauge pressure	1	Rosemount	2088	Operating range: -1.01 a 10.3 bar (-14.7 a 150 psi), linear output

current value, from 4 to 20 mA, indicating the desired pressure and the valve itself adjusts to maintain the pressure. Details of these devices are shown in Table 4.3.

Table 4.3 – Characteristics of used pneumatic actuators.

Actuator	Qty	Manufacturer	Model	Features
Proportional flow valve	1	FESTO	MPYE-5-3/8-420-B	Operating pressure: 0-10 bar, flow rate from 100 to 200 l/min
Proportional pressure valve	1	FESTO	VPPM-6F-L-1-F-0L10H-A4N-S1	Operating pressure: 0.1-10 bar

The final arrangement of the installed pneumatic sensors and actuators is shown in Figure 4.2. The figure also shows the sequence in which the air passes from the origin until it is released, starting at 1 on the proportional pressure valve, then to the first Coriolis at 2, then to the relative pressure and differential pressure sensors, 3 and 4, respectively, and then to the pipe. On leaving the circuit, the gas returns and passes through the second Coriolis in 5 and finally passes through the proportional flow valve in 6 and escapes into the environment.

To measure the reference temperature, calibrate and validate the measurements made with the optical equipment, four PT-100 RTD (Resistance Temperature Detector) sensors were chosen. The PT-100 RTD is a type of resistance temperature sensor constructed from a platinum element that changes its electrical resistance based on temperature. The number "100" in the name refers to the sensor's nominal resistance at 0°C, which is 100 Ω. As the temperature increases, the resistance of the PT-100 RTD also increases predictably. The relationship between resistance and temperature is approximately linear. The model used has a resolution of

Figure 4.2 – Sensors installed on the gas line.

0.1°C between 0°C and 200°C, which is sufficient to detect small temperature variations over a wide range (Mikucki; Opoka, 2011).

To obtaion the pipe vibrations reference accurately, a PCB Piezotronics piezoelectric accelerometer model 352C33 was used, it has a a sensitivity of 100.2 mV/g capable of picking up vibrations up to 12,800 Hz with bandpass of 0.5 to 15,000 Hz.

To control the actuators, receive and process the data generated by the sensors and generate logs, LabVIEW was used, which is a systems development platform produced by National Instruments. The platform is renowned for its ability to create data acquisition, instrument

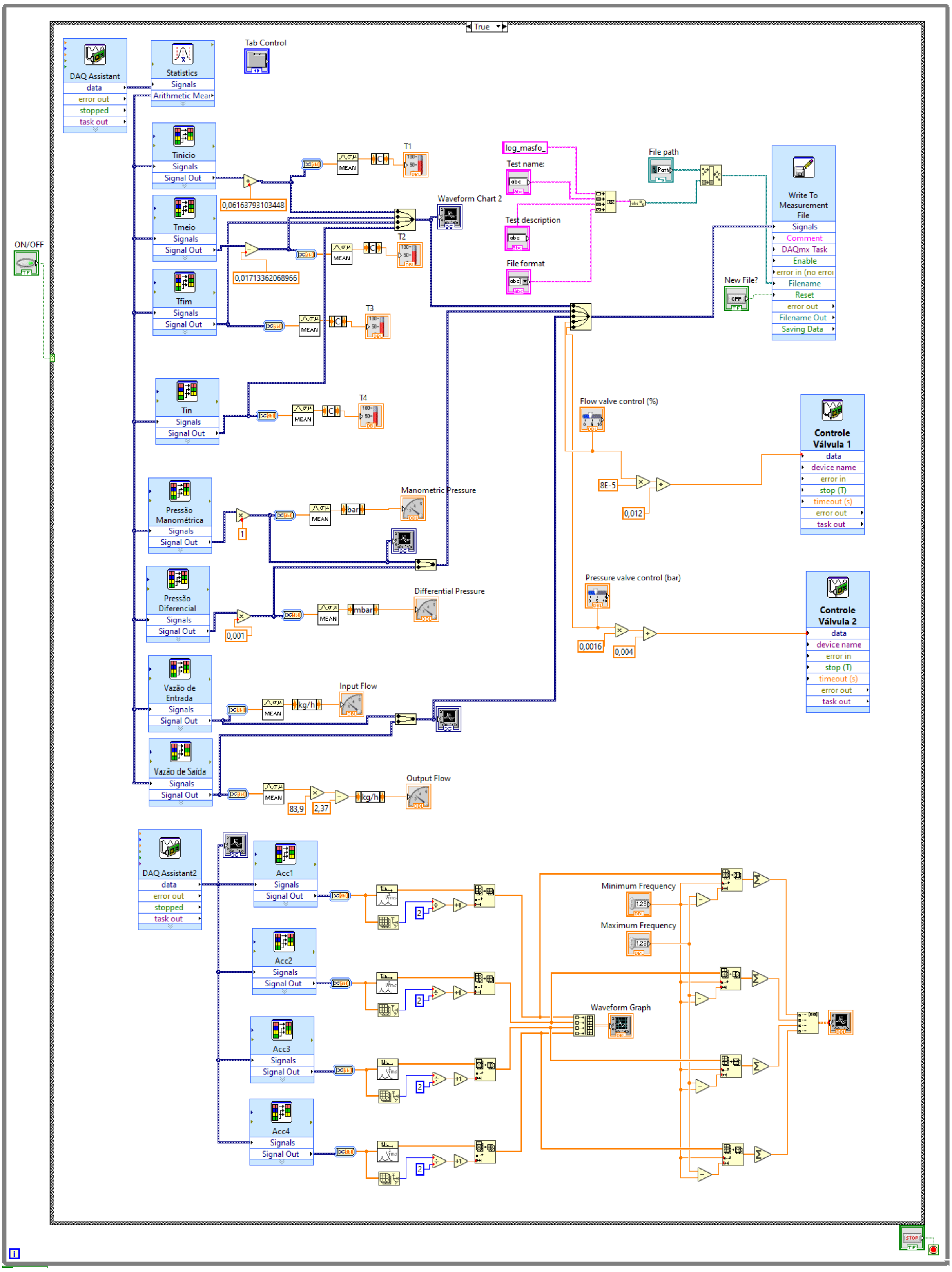

Figure 4.3 – Block diagram of the Gas Line Monitoring and Control program.

control and industrial automation systems, offering real-time data analysis and visualization capabilities, making it ideal for integrating bench instruments. LabVIEW operates based on

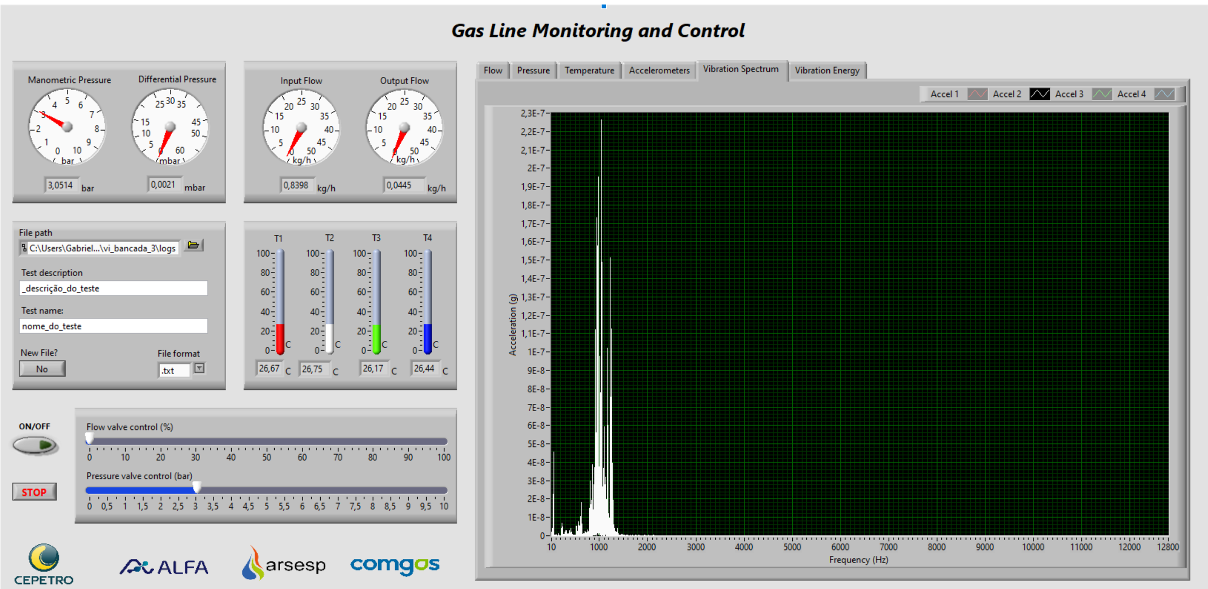

Figure 4.4 – Gas Line Monitoring and Control program interface.

graphical programming, a programming language that uses block diagrams instead of lines of text to create applications, as exemplified in the diagram in Figure 4.3, which corresponds to the VI (Virtual Instrument) developed for the control and monitoring of the experimental bench. This allows for the efficient implementation of complex control and monitoring systems more intuitively. The interface developed, shown in Figure 4.4, offers real-time control for the actuators as well as displaying the values of the measurements in real time through graphic displays in the form of *gauges*, thermometers and graphs that help the operator to know what is happening with the line in real time and to carry out experiments under specific conditions. In addition, the program developed in LabVIEW makes it possible to generate, organize and store logs of all this experimental data.

The pipe for the above ground pipeline chosen for the tests was a PE (polyethylene) pipe with a diameter of 32 mm and a wall thickness of 3 mm, manufactured by FGS Brasil SP. Horizontal sections of 30 meters were built with a ball valve in a T connection in the middle of the pipe where the first tests were carried out and an extension of the pipe was added with a hole so that the section could be isolated from the rest of the circuit.

To top it all off, a data network infrastructure was set up on the experiment bench. An 8-port switch was used to connect all the bench equipment, including two notebooks, the DTS (Distributed Temperature Sensing), the DAS (Distributed Acoustic Sensing), the FBG interrogator and the cDAQ data acquisition system. This infrastructure allows the experimental bench to be controlled and monitored remotely.

The experiment bench is completed with the piping being connected to the laboratory's compressed air system, which is capable of supplying pressures of up to 8 bar, enough for the experiments that kept their pressure values below this limit.

4.2 Optical equipment

This section presents the details of the optical equipment used in the work and its preliminary calibrations.

4.2.1 Fiber optic cables and connections

The fiber optic cabling and connector infrastructure that interconnects the system's devices is a crucial factor in the implementation of a monitoring project. The efficacy of this process relies heavily on the unique characteristics of each system being set up. Prior to planning such an application, it is imperative to evaluate the availability of suitable fiber optic cables, ascertain the requisites of the optical equipment, and assess the potential for scalability.

There are cables on the market with different types of protection, such as *loose tube* cables, which contain one or more flexible plastic tubes where the optical fibers are inserted and can move freely in a gel. Another model is the *tight buffer* cable, in which each optical fiber is individually coated for additional protection and is completely glued and bonded to the outer layers of the cable, both of which are shown in Figure 4.5. Most of these cables are dielectric, i.e. metal-free to prevent electrical conduction. In addition, the thickness of these cables also influences the internal fiber's ability to detect temperature variations (Senior, 2008).

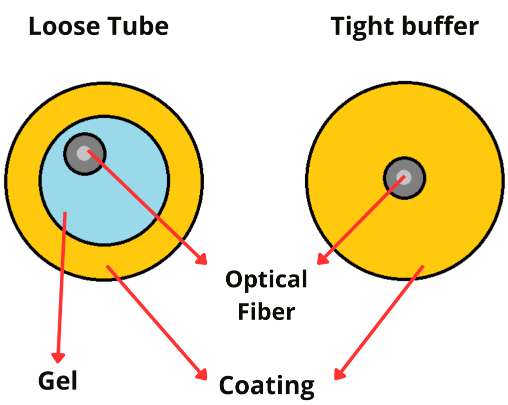

Figure 4.5 – Schematic view of the section of an optical cable *loose tube* and *tight buffer*.

Fiber optic cables need protection from damage, whether accidental or intentional.

Methods such as the use of conduit are options for preserving the infrastructure and facilitating maintenance and replacement, but this method can make measurements more difficult by adding an extra layer of insulation, a factor that this work will address. In addition, due to the greater fragility of fiber optic cables compared to copper cables, they can be more susceptible to damage during installation or handling, so care must be taken when handling fiber optic cables to avoid sharp bends (macro bends) or stresses that can affect the integrity of the cable and induce additional signal losses.

Signal loss is an important metric that indicates the reduction in light intensity as it travels through the fiber. This reduction is expressed in decibels (dB), and higher optical loss values denote a drop in the efficiency of light transmission and, consequently, in the quality of the information transmitted (Senior, 2008).

Fusing fiber optic cables is another complex task that, when poorly executed, contributes significantly to losses. Fiber optic cables require specialized techniques and equipment to avoid very large optical losses. This complexity can result in increased cost and time to install or repair fiber optic cables and is a potential contributor to significant signal losses (greater than 0.1 dB) if poorly executed. For this project, maintenance of the fiber optic infrastructure was ensured by using FSM-60S fiber optic fusion equipment and an FC-6S cleaver, as shown in Figure 4.6. Fusion is carried out by aligning the fibers and applying an electric arc to fuse the fibers. Cleaving, which is the process of cutting the fiber, must be carried out correctly and cleanly on the cables to be spliced to ensure a successful splice.

Figure 4.6 – Fiber optic welding equipment.

The fiber connectors are classified depending on the type and angle of the cut at the contact tip, as shown in Figure 4.7, and by their mating shape, as shown in Figure 4.8. Connector cut-off angles are divided into three, PC (Physical Contact) has optical losses normally around 0.5 dB. UPC connectors (*Ultra Physical Contact*) usually have optical losses of around 0.2 dB, and APC connectors (*Angled Physical Contact*), which have a cut-off angle of 8 degrees, can have optical losses of around 0.15 dB, making them the most efficient of the three and the most used in this work. The 8-degree cut-off angle in APC connectors helps to reduce reflections of light back to the source, which can lead to lower signal loss. However, in some specific situations, such as in the case of launch fiber, a PC connector was used, as this is the original connector of the product and a splice to replace it could generate losses at the individual join that add up to 0.11 dB (Soni *et al.*, 2020).

There are a variety of connector formats available on the market, but only four types were used in this work, each selected based on their suitability for the needs of the devices in use. The SC connector, with a *push-pull* locking mechanism, was used on the DAS interrogator and the launch fiber, and the typical loss of this type of connector is around 0.25 dB. The LC connector, which is smaller and has a locking mechanism similar to the SC, was used in the si155, which has an average insertion loss of 0.10 dB. The FC, with its cylindrical shape and very robust screw mechanism, was selected for harsh applications and splices, with an average insertion loss of 0.15 dB. Finally, the E2000, compact and with a retractable protective cover, was used for DTS, with an average insertion loss of 0.20 dB.

In addition to the inherent losses, dirt can compromise the quality of the connection. Each time the connectors are mated, the dirt particles around the core are dislodged, causing them to migrate and spread across the surface of the fiber. Particles larger than 5μm usually fall apart and spread after mating and can create barriers ("gaps") that prevent precise contact and promote reflection that increases optical loss, as exemplified in Figure 4.9.

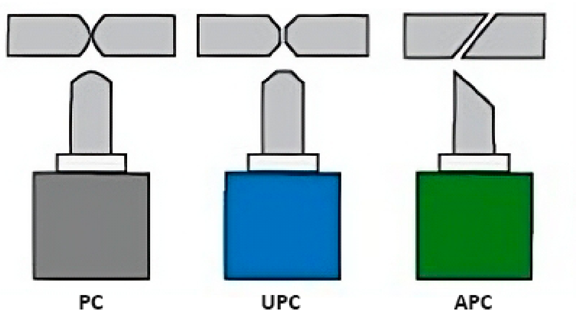

Figure 4.7 – Classification according to the cutting angle at the tip of the connector.

The quantification of optical losses in the cables generated by splices and connectors during the execution of this work is carried out using an OTDR (Optical Time-Domain

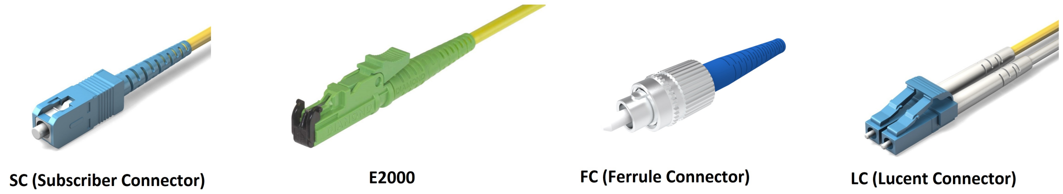

Figure 4.8 – Types of connector fitting used in this work.

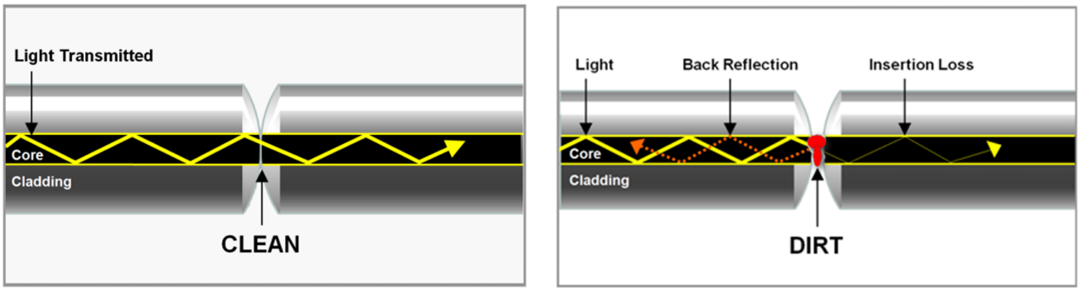

Figure 4.9 – Difference between a perfect fit (left) and one with dirt, causing optical loss (right) (Source: (Omnisens, a)).

Reflectometer) model MT9083, shown in Figure 4.6. OTDRs operate by emitting a pulse of light into the fiber and measuring the time and intensity of the light that is reflected back. The loss is then calculated based on the decrease in the intensity of the reflected light compared to the emitted light. As already discussed, in addition to the shape, proper cleaning of the connectors is necessary to optimize the connection, as improper splices or dirt can cause additional signal losses. These loss elements add up and even small losses at several points can result in a considerable loss. Despite these challenges, optical fiber is adopted due to the intrinsic advantages mentioned above. However, these limitations must be taken into account when planning and implementing a monitoring or communication system based on optical fiber.

4.2.2 DTS Interrogator - Distributed Temperature Sensing

Figure 4.10 – Rear of the DITEST-12 Interrogator.

A Distributed Temperature Sensing (DTS) system is a technology that allows continuous temperature measurement over significant lengths using a single optical fiber (Ukil *et al.*, 2012). For this work, the DITEST 12 (Figure 4.10) developed by Omnisens was used, whose specification is detailed in Table 4.4. The cost of this equipment during the period in which this work was performed was approximately $70,000.00 USD, and its operation is based on an optical interaction principle called Stimulated Brillouin Scattering (SBS). SBS is an intrinsic physical phenomenon of optical fiber materials, providing substantial information about the stress and temperature distribution in a fiber. The Omnisens DITEST systems take advantage of the low-loss characteristics of single-mode fibers and usually do not work with multimode fibers (Omnisens, b). As for the measurement method, the local peculiarities of the SBS are interrogated using a configuration called *Brillouin Optical Time Domain Analysis* (BOTDA). This approach employs a single laser source in the equipment operating at a wavelength of 1550 nm and is self-referencing, which allows periodic measurements without requiring prior calibration. It has an electro-optical signal processing module, responsible for generating the pulse and continuous probe signals, a WDM (*Wavelength DeMultiplexing*), which separates the pulse and probe signals, a photodetector that detects the intensity of the probe signal as time progresses which result in a frequency trace. The system can automatically monitor up to two detection cables with a 1x2 switching device, managing both detection channels. The operating diagram is shown in Figure 4.11.

DITEST can also be configured to operate autonomously for extended measurements. Measurement results are recorded automatically and stored in an internal database, allowing them to be retrieved for later analysis. This database can be accessed by remote computers via a LAN network, providing flexibility and convenience in analyzing and interpreting the data collected.

Spatial resolution defines the smallest extent of an event that can be accurately measured. Spatial resolution is directly associated with pulse width. Taking into account the speed of light at 1550 nm and the conversion from time to distance, a 10 ns pulse produces a spatial resolution of 1 meter according to the manufacturer's manual (Omnisens, b) Increasing the pulse width reduces the spatial resolution but increases the Brillouin gain (the energy being higher, the Brillouin interaction is increased). As a result, there is a trade-off between high spatial resolution and high precision or low uncertainty measurements. Localized temperature points or deformation events occurring at a shorter distance than the defined spatial resolution

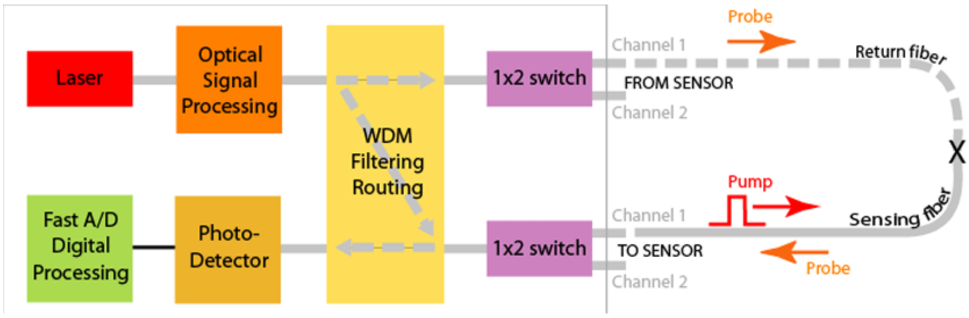

Figure 4.11 – Schematic diagram of the DITEST Interrogator showing the optical pulse and probe signals. The sensing fiber is connected to "Channel 1 - TO SENSOR" and the return fiber to "Channel 1 - FROM SENSOR". The sensing fiber and the return fiber are connected at the opposite end of the fiber using a connector or a splice - Source: (Omnisens, b).

Table 4.4 – DITEST-12 equipment specifications - Source: (Omnisens, b).

Features	**Data**
Manufacturer	Omnisens
Model	DITEST-12
Dimensions (L x P x A)	449 x 500 x 266 mm (19" rack)
Peso	21 kg
Operating temperature	0°C to 40°C
Optical connectors	E-2000 / APC
Number of channels	2 independent, selectable channels (standard) with E2000 input
Sensor fiber	Standard single-mode fibers
Range	50 km per channel
Spatial resolution	0.5 to 20 m (in 0.1 m increments) - 1 m to 20 km / 2 m to 30 km / 3 m to 50 km
Optical budget (optical loss)	Default setting: 12 dB for sensor (total loop budget 20 dB)
Acquisition time	> 1-2 minutes and 5-10 minutes for high-resolution measurements
Measurement modes	Manual or unattended automatic
Safety and laser	The product emits invisible infrared radiation in the wavelength range of 1550 nm classified as Class 1M laser products according to EN 60825-1 (2001-03)
Protection rating	IP20 (indoor use)
Pollution protection	Pollution degree 2

cannot be measured with full precision and/or may be missed. However, in leakage scenarios, temperature variation only occurs in a small region of the fiber of about 10 centimeters. Given that less than 1 meter of the fiber is exposed to temperature variation, a decrease in effective resolution is expected.

To determine the effective resolution of DTS in this context, an experiment was carried out which involved heating a 10 cm section of optical fiber in a container of water, bearing in mind that the manufacturer's resolution is the minimum of 1 m for fibers up to 20 km long. This experiment used a 50-meter coil of single-mode optical fiber of the *loose tube* type. During the experiment, two PT- 100 RTD were used to monitor the temperature conditions, one to record the ambient temperature and the other to measure the water temperature. The results indicated that the sensitivity of the DTS is approximately 2.7 times lower than that of the thermometer, i.e. the temperature in the thermometer rose almost 3 times more than that detected by the fiber. This indicates that the temperature variation captured in a 10 cm region of the optical cable is attenuated within 1 meter, requiring a greater temperature variation for it to be perceived by the interrogator in this condition. In other words, if 1 meter or more were exposed to thermal variation, the result would not suffer this attenuation. This information is essential for understanding the limits and sensitivity of the equipment in real scenarios. Thus, although the DITEST-12 equipment has an expected resolution of 0.4°C for 5-minute measurements, in fact, in a region of 10 cm from the fiber, the effective resolution is arround 1°C.

It is important to note that the resolution of the DTS DITEST-12 also depends on the length of the sensor fiber (which can be up to 50 km), as well as the time required for measurement (configurable from 1 to 10 min), as shown in Figure 4.12. In this work, sensor cables less than 500 m long and an acquisition time of 5 minutes were used.

4.2.3 Interrogator DAS - Distributed Acoustic Sensing

DAS (Distributed Acoustic Sensing) is a sensing technology that uses optical fibers to detect and measure acoustic signals along their length. In this method, the optical fiber is transformed into a continuous acoustic sensor, capable of converting sound waves into optical signals. It can be used for diagnostics to identify and locate faults that generate vibrations (He; Liu, 2021). The model used in this study is the ODAS manufactured by Omnisens (Figure 4.13).The cost of this equipment during the period in which this work was performed was approximately $90,000.00 USD. The system is based on Rayleigh scattering and uses a measurement technique called "*Chirped-phase based*" which uses a phase signal with frequency modulation, known as "*chirp*". This is used to increase the spatial resolution and sensitivity of the detection system. This technique makes it possible to distinguish signals from different locations with greater precision, improving the sensing system's ability to identify disturbances

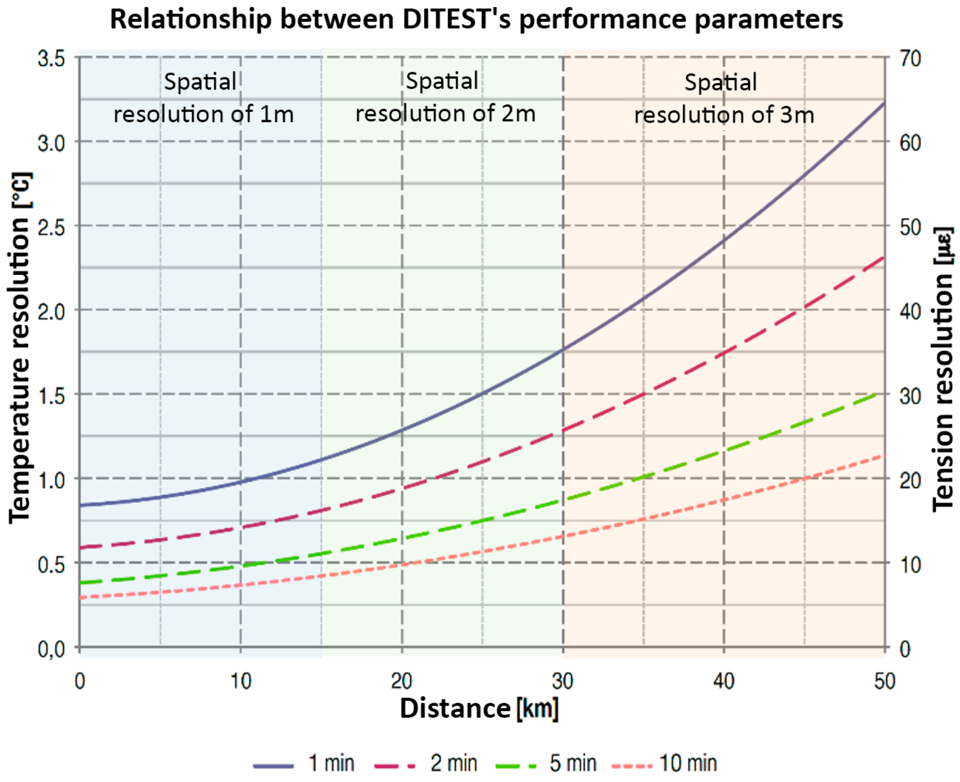

Figure 4.12 – DAS DITEST 12 resolution as a function of sensor fiber length and time (Source: (Omnisens, b)).

Figure 4.13 – Front panel of the ODAS interrogator in its transport case.

along the length of the optical fiber.

This equipment uses a single laser source at a wavelength of 1350 nm and an electro-optical signal processing module to generate signals. A schematic of how this equipment works is shown in Figure 4.14. The instrument can be configured for long-term autonomous and automatic measurements. Measurements are recorded automatically so that they can be retrieved at any time for later analysis, and are accessible from remote computers via the LAN network. Further details of the ODAS are given in Table 4.5.

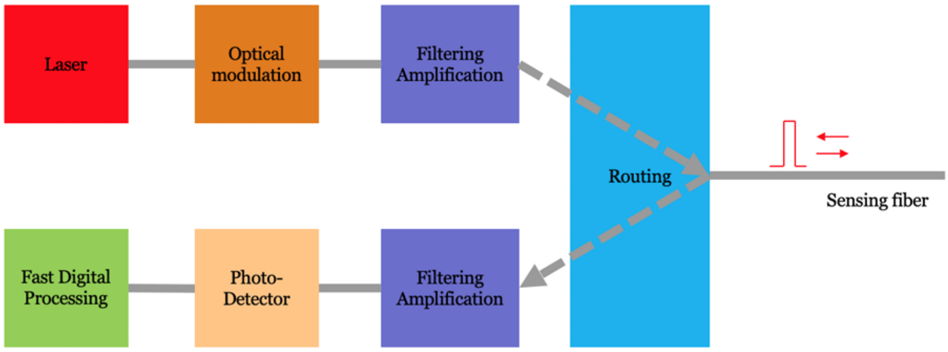

Figure 4.14 – Schematic diagram of the DAS Interrogator.

Table 4.5 – ODAS equipment specifications (source: (Omnisens, a)

Features Manufacturer	**Data** Omnisens
Model	ODAS
Operating temperature	0°C a 40°C
Optical connectors	SC/APC
Number of channels	1 channel
Sensor fiber	Standard single-mode fibers
Range	50 km per channel
Spatial resolution	1m
Vibration pickup limit	1500Hz
Optical budget (optical loss)	Less than 0.2 dB/km
Safety and laser	The product emits invisible infrared radiation in the 1350 nm wavelength range classified as Class 1M laser products (IEC 60825-1:2014)
Protection rating	IP20 (indoor use)
Pollution protection	Pollution degree 2

The *Gauge Length* defines the smallest length of an event that can be measured with total precision, it is equivalent to spatial resolution. The gauge length is directly associated with the width of the laser pulse. For example, taking into account the speed of light at 1350 nm and the conversion from time to distance, a 100 ns pulse produces a spatial resolution of 10 meters. The lowest spatial resolution according to the manufacturer (Omnisens, a) is 1 meter and events occurring over a shorter range than this cannot be measured with good precision.

To check the sensitivity and precision of the equipment, a preliminary test was carried out, consisting of stimulating a point on the fiber with a known frequency. To do this, the fiber was attached to a loudspeaker which reproduced sine waves with frequencies ranging from 100 Hz to 1,600 Hz, slightly above the interrogator's pickup limit. The signal received by the DAS control and acquisition application generated an energy map for all the data relating to the frequencies obtained, as shown in Figure 4.15, which specifically shows a 300 Hz stimulus. In the spectrum graph shown in Figure 4.16, it is also possible to see noise at other points on the line caused by disturbances during the measurement, but with less intensity in relation to the stimulus analyzed. Despite the background noise characteristic of the laboratory environment, which is full of various rotating machines, the DAS system was able to detect vibration at a specific point on the fiber.

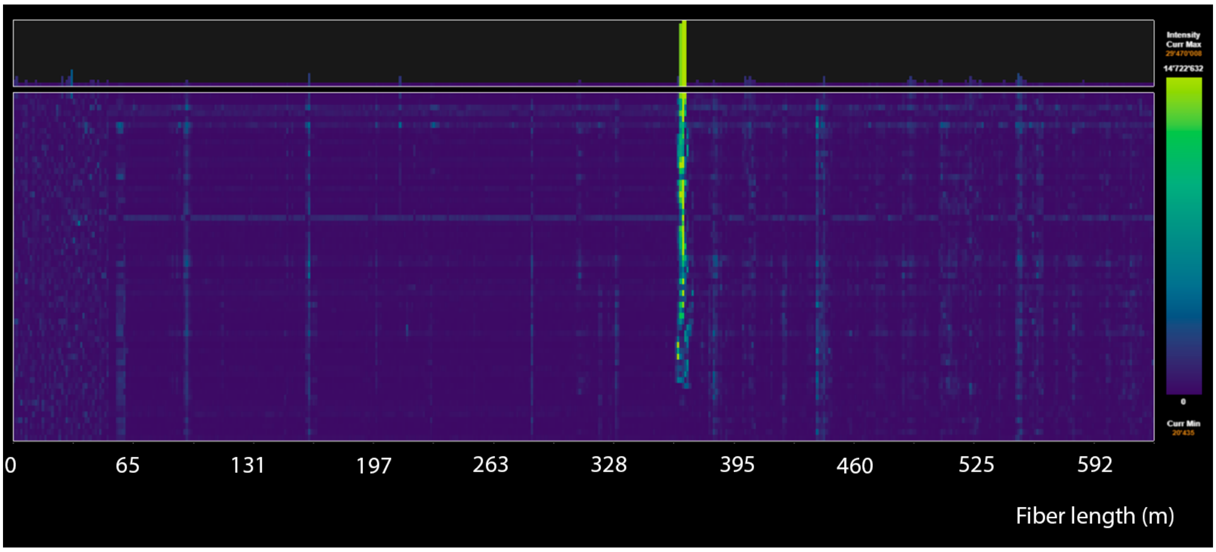

Figure 4.15 – 300 Hz stimulus indicated in the yellow region. The X-axis shows the distance from the fiber (in meters), the Y-axis indicates the time (with resolution in seconds), and the color represents the intensity of the energy.

4.2.4 Interrogator si155 - *Optical Sensing Instrument*

The Micron Optics HIPERION si155 (Figure 4.17) is an interrogator capable of dynamic and absolute measurements of FBGs (Fiber Bragg Grating), LPGs (Long Period Grating and FP (Fabry Perot) sensor. The main features of the HIPERION si155 interrogator are shown in tables 4.6 and 4.7. The core of the X55 Optical Interrogator consists of a laser source capable of scanning a wavelength range from 1460 to 1620 nm at dynamic speeds of up to 1 kHz (or scanning from 80 nm to 5 kHz), the laser also supports scan rates from 2 Hz to 5 kHz. The main function of the si155 core is to make fast, repeatable wavelength measurements on FBGs in a

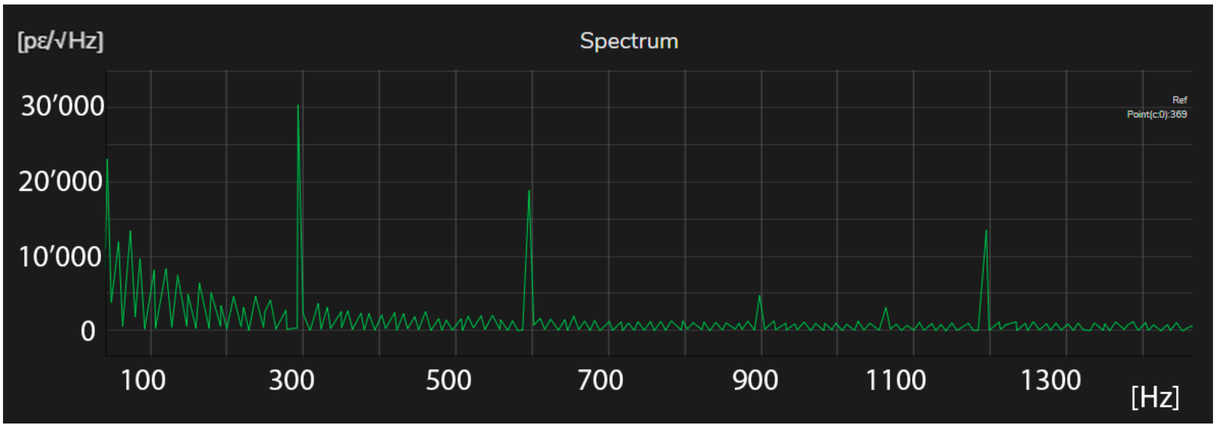

Figure 4.16 – Spectrum with 300 Hz stimulus.

variety of input conditions and with varying sensor signal losses, without the need to manage gain settings or peak detection parameters. And it is the lowest cost equipment compared to the previous ones during the period in which this work was carried out, costing around $25,000.00 USD.

Figure 4.17 – HYPERION si155 interrogator from Micron Optics.

Table 4.6 – HYPERION si155 equipment specifications. Source: (MicronOptics, 2023b)

Features	**Data**
Manufacturer	Micron Optics
Model	HYPERION si155
Dimensions (L x P x A)	206 mm x 274 mm x 79 mm
Pesos	3.0 kg
Operating temperature	-20°C to 60 °C
Optical connectors	LC/APC
Number of channels	4 channels
Compatible sensors	*Fiber Bragg Gratings, Long Period Gratings, Fabry-Perot and Mach-Zehnder Interferometers*

Table 4.7 – Performance properties of the HYPERION si155. Source: (MicronOptics, 2023b)

Features	**10 Hz**	**100 to 1000 Hz**	**5000 Hz**
Wavelength range	1500-1600 or 1460-1620 nm	1520-1580, 1500-1600 or 1460-1620 nm	1500-1580 or 1510-1590 nm
Wavelength accuracy	1 pm / 1pm	1 pm / 1pm	2 pm / 3pm
Wavelength repeatability	1 pm, 0.3 pm a 1 Hz	1 pm, 0.05 pm a 1 Hz	2 pm, 0.05 pm a 1 Hz

To manage the interrogator's functionalities, Micron Optics offers ENLIGHT software. This provides a real-time view of the data from the analyzed sensors. In the "Acquisition" tab, there are four main modes that the user can choose from to view the data collected from the interrogator. The first of these displays (Amplitude View), in which data is collected from the interrogator and displayed in an XY plot of power (dBm) per wavelength (nm). The second mode, "Peaks" changes the display of the Acquisition tab to shows the data from the first mode in tabular form. The third mode, Time Response, provides a graph of the wavelength value of a spectral peak as a function of time. A variable called "Points" determines the resolution of the graph, which is time as a function of wavelength (nm). The fourth mode refers to the FFT (Fast Fourier Transform). It converts a time-domain signal into a frequency spectrum, revealing the different frequencies present in the signal. The resulting graph is presented in FFT magnitude(dB) per frequency (Hz).

With the setup configured, the three sensors that will be interrogated by this device were tested, the FBG sensor model os1100, the FBG-based optical strain gauge model os3200, and the Fabry Perot-based optical accelerometer model os7510. The vibration perception test was carried out using a loudspeaker. The device was used to vibrate the sensors at known, predetermined frequencies to observe the sensor's limits, in similar way as used in the tests with the DAS interrogator. All the sensors were glued to the center of the speaker with adhesive tape and stimulated with frequencies from 31 Hz to 2,500 Hz, which is the interrogator's limit. The FBG sensor model os1100, didn't show a reaction during the frequency analysis in the ENLIGHT software. The hypothesis for this result is the low sensitivity to high frequency signals given the way in which the FBG was coupled to the tubing. The strain gauge, on the other hand, showed a visible peak of vibration at the speaker-stimulated frequency of 200 Hz, as shown in Figure 4.18. The peak is given in dbm to indicate the power in the channel. Finally, the optical accelerometer based on Fabry Perot showed visible peaks from 1,000 Hz to 2,300 Hz as shown in Figure 4.19. These tests provide an initial parameter of the sensitivity of these sensors.

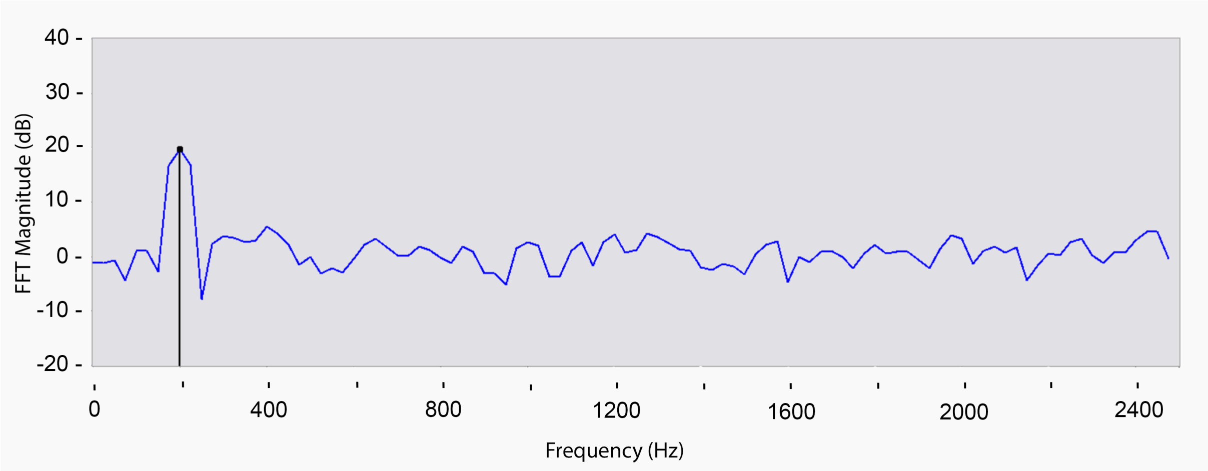

Figure 4.18 – Spectrum obtained by an optical FBG-based *strain gauges* model os3200 during preliminary testing of the sensor.

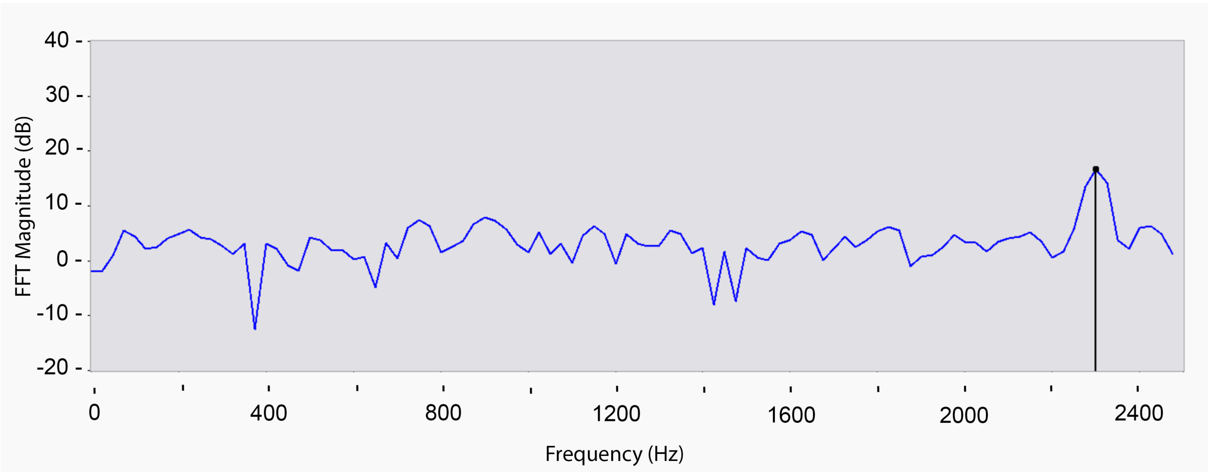

Figure 4.19 – Spectrum obtained by an os7510 optical accelerometer during preliminary testing of the sensor.

4.3 Data processing

This section presents the APIs developed in Python to help to process the data *logs* generated by the equipment (DAS, DTS, si155, and experimental bench) during the experimental tests.

4.3.1 Python API for plotting logs data from DTS and LabVIEW

During the execution of the work, it was necessary to create a program that could help visualize the various logs generated by the DTS and the PT-100 RTD to compare the temperature variations over time at a point of interest in the fiber. The code reads the logs generated by the DTS, synchronizes them temporally with the data generated by the reference thermometers (stores in another log file by the LabVIEW program), and generates graphs similar to the one shown in Figure 4.20. The thermometers data are references for the data obtained with the DTS and this program helps to visualize this data intuitively.

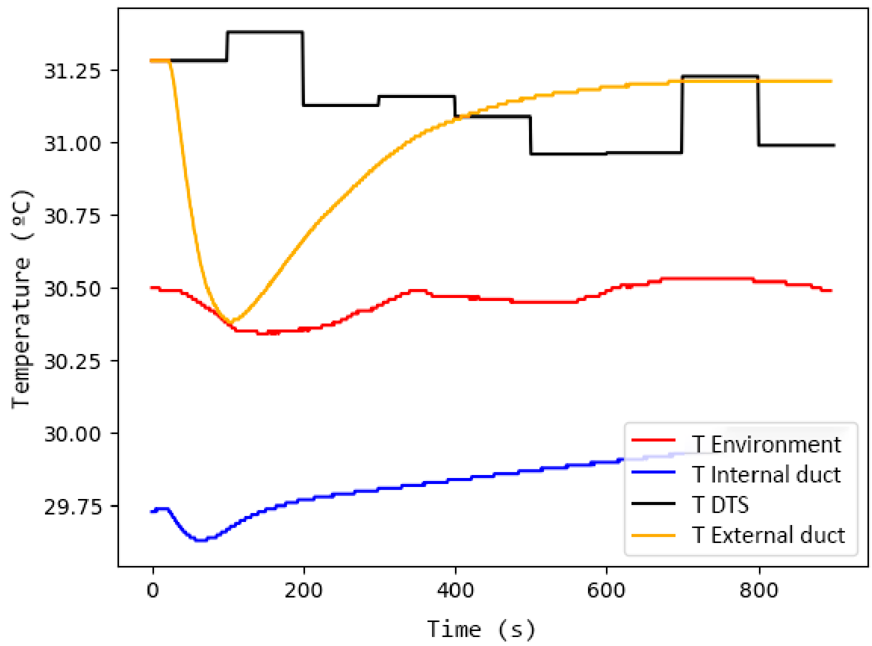

Figure 4.20 – Comparative data from a measurement made with 3 thermometers and a DTS interrogator.

5 RESULTS

This chapter presents the results of tests carried out in the laboratory to identify leaks with the DTS, DAS and, Fabry Perot/FBG sensors.

5.1 Analysis and interpretation of temperature sensors

This subsection deals specifically with the experiments carried out using Omnisens' DTS (Distributed Temperature Sensing) interrogator.

5.1.1 Initial test with DTS

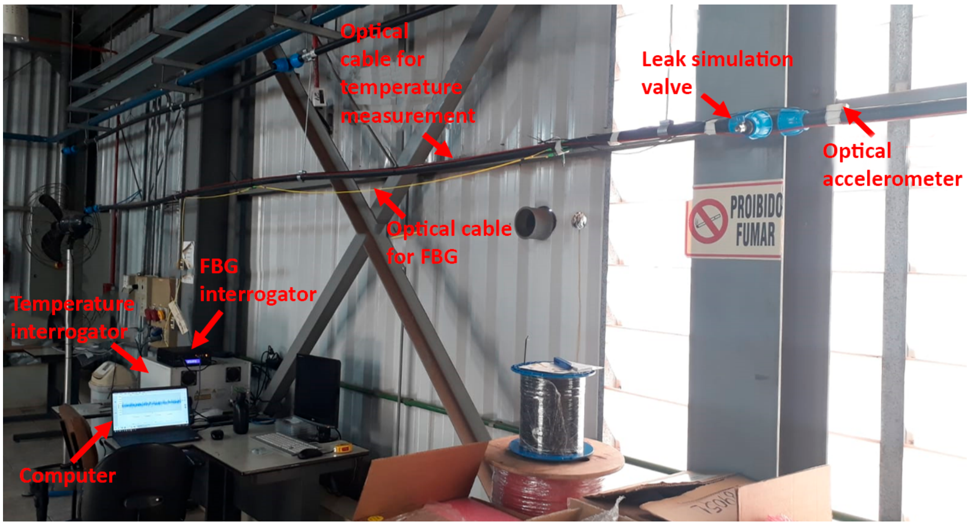

Figure 5.1 – Initial state of the test bench.

Once all the bench equipment was ready and the calibration and configuration of the devices had been carried out, the first leak detection tests were carried out using the DTS interrogator. This was configured to take measurements around ever 5 minutes. To do this, a 50-meter single-mode loose fiber (red cable) was attached to the pipe passing close to the manually operated ball valve that was used at this stage of the experiment to simulate the leak, as illustrated in Figure 5.1. The leakage point is located in the optical fiber 5.5 m from the DTS output. Next, the test line was pressurized to 4 bar and the valve at the end of the line was kept closed, so there would be no airflow from the pipe, the air would only come out through the hole in the "leak" area. This choice was made to maintain a better constancy in the pressure of the pipe, since the laboratory compressor and air line feed is not capable of maintaining a pressure of 4 bar inside the pipe when it is open and with maximum flow at its end. With the preparations made, the valve was then opened and the interrogator began the data acquisition process. Contrary to expectations, the leak did not result in any drop in temperature at the indicated location, as can be seen in Figure 5.2. There was no noticeable reduction in the Brillouin frequency in the region of the optical cable near the leak, since the results did not exceed the noise limits indicated by the red lines. This raise questions about the effectiveness of DTS in detecting leaks in these conditions and the possible factors that may have contributed to this.

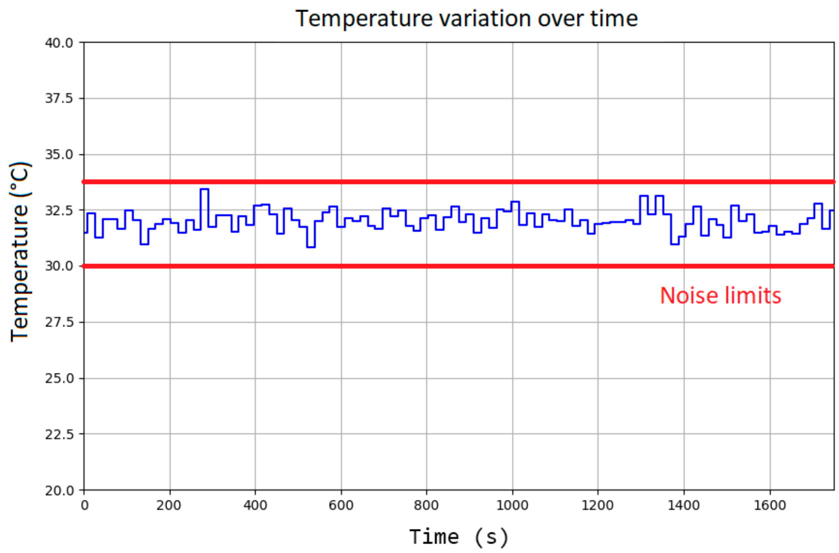

Figure 5.2 – Initial test in which the leak could not be detected using the fiber optic sensor.

5.1.2 Hypotheses for the non-detection of the Joule-Thomson effect

As it was not possible to detect the leak using the DTS in the above ground pipe using a ball valve as a leak emulator, some hypotheses were raised to explain why it was not possible to detect a significant temperature drop by the Joule-Thomson effect, bearing in mind that the technology used by DTS is successfully employed in monitoring underground pipes pressurized with 30 bar (Mishra *et al.*, 2017). Therefore, the next experiment was carried out under the same conditions, but with a thermometer with a resolution of 0.1°C next to the fiber in the area of the leak. The aim was to investigate whether the temperature drop was so small that the fiber couldn't pick it up. With the devices in place, the valve was opened to start the leak, which lasted 15 minutes. When checking the data obtained from the experiment, it was found that even after this time there were no significant variations in the temperature near to the leakage point.

As the Joule-Thomson effect was not detected by a more sensitive sensor, new hypotheses were raised about what was causing it. A hypothesis was the location and nature of the leak. Until then, a ball valve had been used to simulate the leak, which made it easier to control the leak but did not correspond to the phenomenon occurring in the field. The valve outlet is located a few centimeters away from the pipe and is made of a different material, making it difficult to measure. To resolve this issue and bring the experiment closer to reality, a bypass (Figure 5.3) was installed at the outlet of the opening valve to a section of the pipe where a small hole (approximately 2 mm in diameter) was drilled to simulate a leak, as shown in Figure 5.4. A PT-100 RTD temperature sensor and the fiber optic cable connected to the DTS (red cable) were placed next to the hole. With this configuration set up, a new experiment was carried out with the valve completely open and with the same parameters used in the previous experiments. However, after 15 minutes of leakage, no significant drop in temperature was observed in the region of the orifice in either of the two sensors.

Figure 5.3 – Bypassing the pipe to take measurements directly in a hole in the pipe.

So a new hypothesis was drawn up, this time about the pipe material, which is made of PE (polyethylene). This material is a polymer with low thermal conductivity, which means that it has a limited capacity to transfer heat and is considered a thermal insulator (Barbosa *et al.*, 2017). When gas flows through a polyethylene pipe, the expansion or compression of the gas due to the Joule-Thomson effect is less efficient in exchanging heat with the external

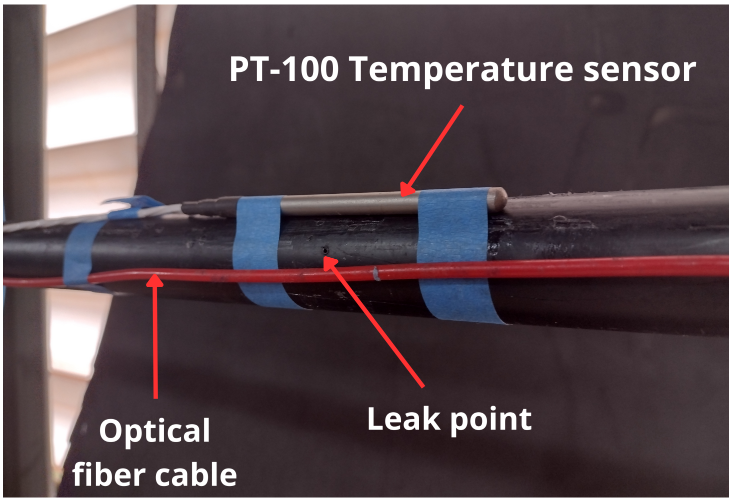

Figure 5.4 – Detail of the leaking area showing 2 sensors in the vicinity of the 2 mm hole in the pipe.

environment, due to this low thermal conductivity. This results in lower temperature cooling of the tube during the expansion or compression process. This leads to the hypothesis that air, which undergoes the Joule-Thomson effect less intensely than natural gas, was not cooling the tube. As the fiber and thermometer are only in contact with the tube and not directly with the air that is expelled, they are unable to detect the temperature variation due to the insulation caused by the polyethylene. To verify this hypothesis, the section of the polyethylene pipe where the leaks were emulated was replaced with a metal one. However, there was still no significant drop in temperature due to the leaks.

5.1.3 Method for detecting the Joule-Thomson effect in polyethylene pipes

Another possible cause was considered to be the fact that there is no material around the pipe in the area, unlike underground pipes, where previous studies have shown that leaks can be identified by the drop in temperature caused by the Joule-Thomson effect (Campanella *et al.*, 2016). This is a relevant factor because in above ground lines the cold gas is expelled away from the point of leakage in the pipe, whereas when the leak is located below ground, even if the pipe doesn't conduct temperature well, the gas is forced through the ground in the vicinity of the pipe, cooling it considerably. Also, consider that the thermal conductivity of dry air at sea level is approximately 0.024 W/m-K, while the thermal conductivity of soil is between 0.15 W/m-K and 2.0 W/m-K, depending on its composition, humidity and density. Therefore, the thermal conductivity of soil is at least an order of magnitude greater than that of dry air.

One solution proposed to test this hypothesis was to wrap the pipe in some material so that the air would be forced to pass close to the pipe for a moment and not be directly dispersed into the environment. To do this, two materials were chosen for the wrapping function: a denim fabric and a polymer conduit. A new test was carried out, this time to compare the use of these two materials with the pipe exposed to the environment. The line was pressurized to 4 bar and the sensors were positioned in the vicinity of the leaking area, but this time three PT-100 RTD thermometers were used. One to measure the ambient temperature, another to measure the internal air temperature at the beginning of the pipe, and a third to measure the temperature on the outside of the pipe, close to the leak point. The configuration of the first experiment was carried out without any type of covering in the leak area, as in previous experiments, just for comparison purposes. In the configuration for the second experiment, denim fabric was used to wrap the hole and the sensors. In the third and final configuration, a polymer conduit was used to cover the leak and the sensors. The three configurations are shown in Figure 5.5.

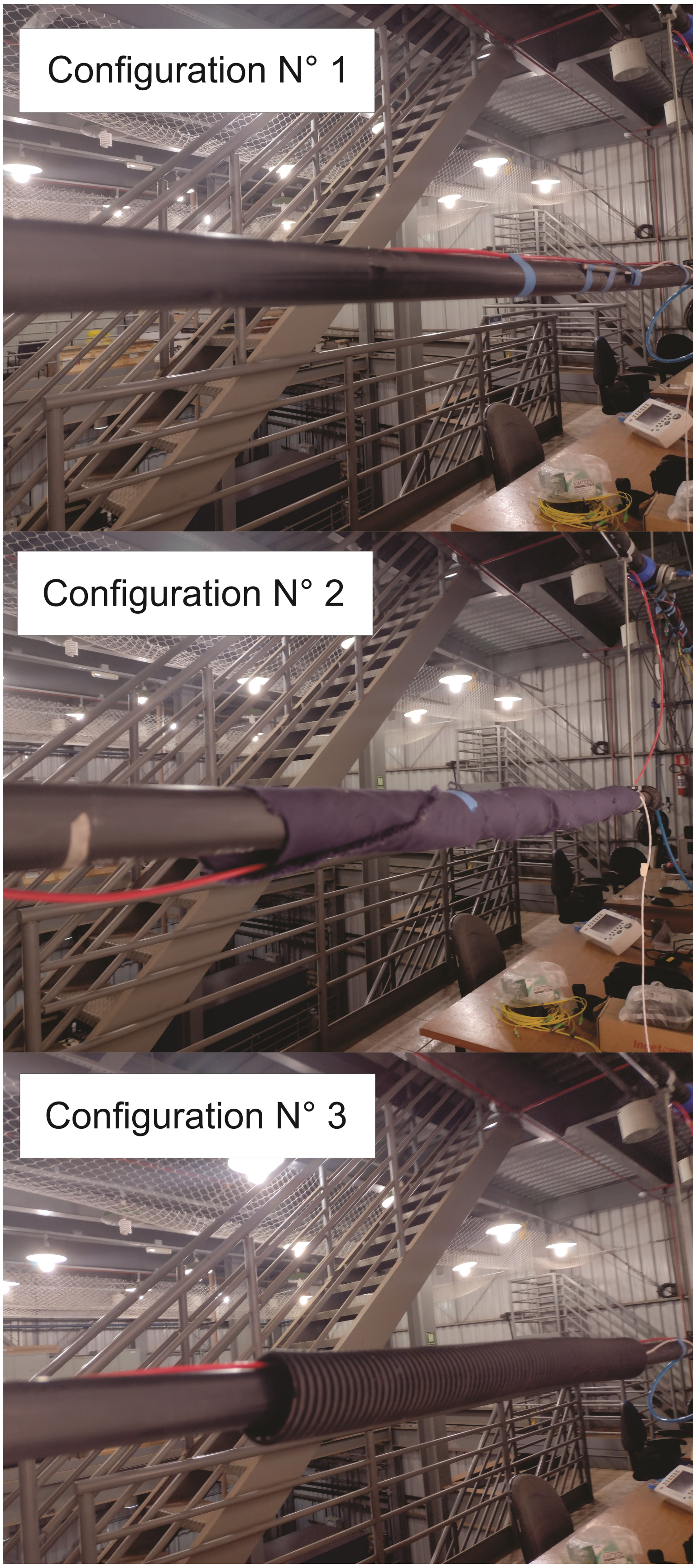

Figure 5.5 – The three configurations used in the experiment to identify leaks using the Joule-Thomson effect: without cover, with fabric and with conduit.

The three leak tests were carried out with the valve kept open for 15 minutes and the results of the first experiment, with the pipe exposed to the environment, generated the data shown in the graph presented in Figure 5.6. In this graph, the yellow curve represents the data obtained by the PT-100 RTD attached to the pipe next to the leak, the blue curve represents another RTD inside the pipe and away from the leak to measuring the internal temperature of the pipe, and a third RTD attached outside the pipe to measure the ambient temperature, shown in the red curve. The results of this first experiment, where there was any cover over the pipe, showed that there was no drop in temperature during the period in which the leak occurred. As expected, over time, the temperature of the air inside the duct remained consistent with the ambient temperature and with the temperature in the area of the leak, the temperature of the three thermometers showed a similar variation, except for the thermometer located inside the pipe (curve in blue) which showed a brief drop and then an increase in temperature which stabilized during the rest of the experiment. This behavior was maintained in the other two experiments. The reason was that the sudden movement of the air reduces the local thermal energy by convection, which quickly rises with the arrival of the air from the compressor, which is warmer than the air previously at rest in the pipe. This effect, however, does not alter the measurements and leakage data.

In the second test, in which the fabric surrounding the leak was used, the drop of about 2.5 °C in temperature due to the leak is noticeable, as shown in the graph in Figure 5.7. The yellow curve, which represents the temperature in the vicinity of the leak on the outside of the pipe, drops by approximately 2.5 °C in relation to the internal temperature of the pipe. This shows that when the gas is forced around the pipe and not dispersed directly into the environment, the drop in temperature becomes noticeable.

In the third test, using the conduit as a wrapping, it was also possible to identify a drop in temperature due to the leak, but a smaller one, as shown in the graph in Figure 5.8. The results obtained remained consistent when the test was repeated. With this result, it can be seen that, in the way it was set up, the fabric wrapping is more effective than the conduit wrapping, i.e. the temperature captured by the thermometer during the fabric-wrapped leak decreases more in relation to the internal temperature of the duct than that captured by the conduit, about 1°C. It is therefore notable that detection is much more noticeable using means of forcing the released gas to pass through the sensors, thus keeping the gas cooled by the Joule-Thomson effect close to the sensing element. All results are briefly summarized in the Table 5.1.

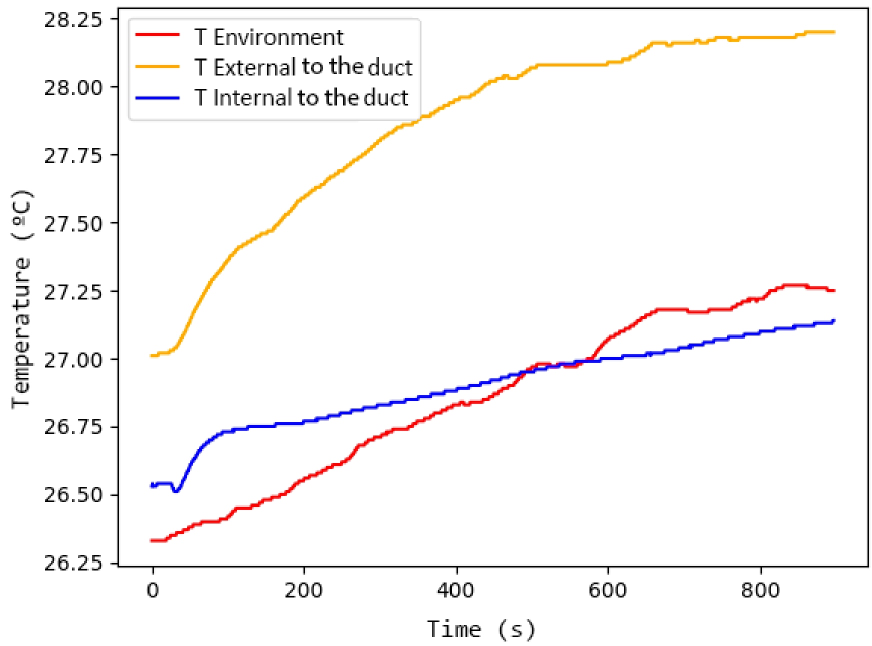

Figure 5.6 – Pipe exposed to the environment.

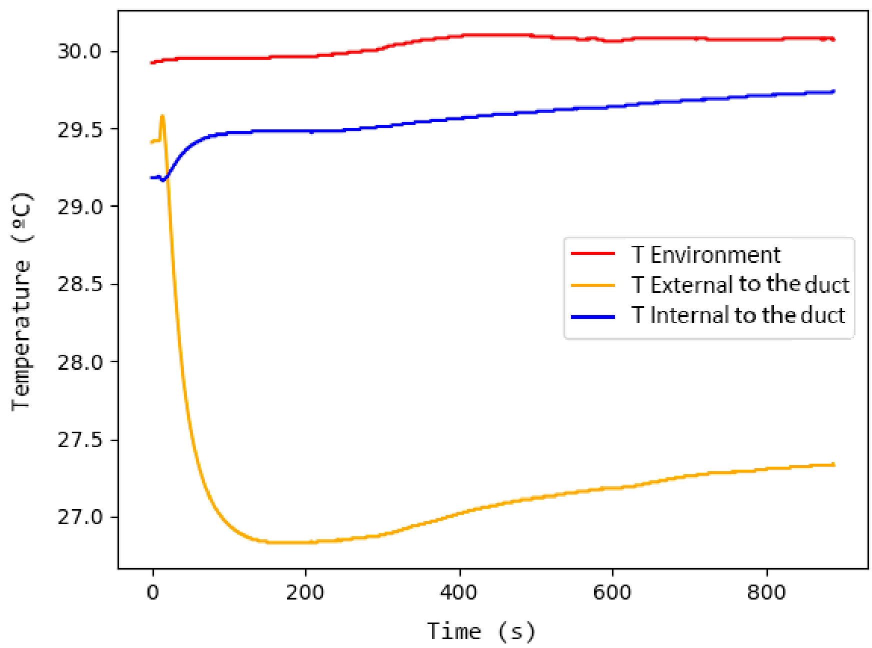

Figure 5.7 – Pipe wrapped in fabric.

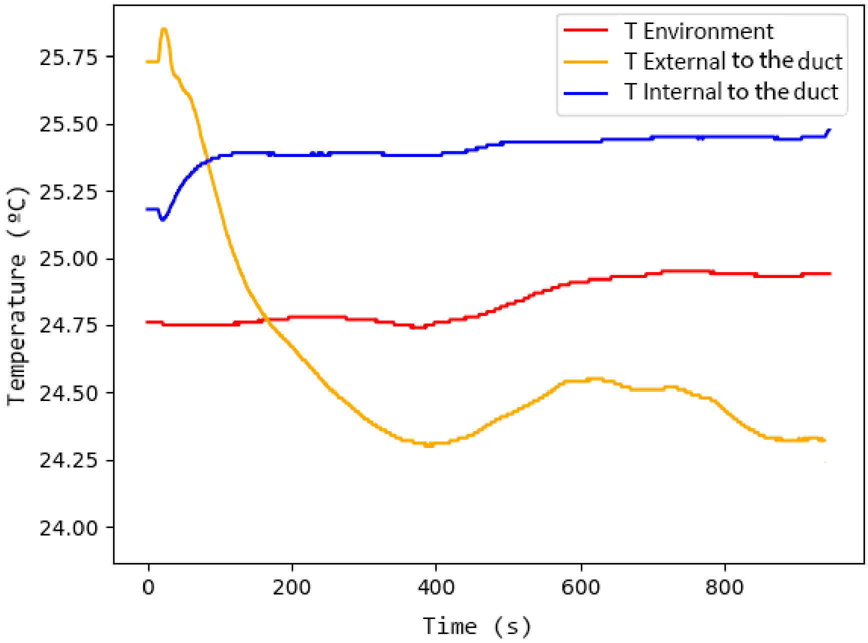

Figure 5.8 – Pipe surrounded by conduit.

Table 5.1 – Results of the three methods

	Method	**Result**
Test 1	Naked Tube	No drop in temperature during the period of the leak
Test 2	Fabric surrounding the tube	Drop of about 2.5 °C in the leakage area
Test 3	Conduit surrounding the tube	Drop of about 1.25 °C near to the leakage area

5.1.4 Minimum detectable leak with DTS

Considering that, leaks were only detectable by thermal sensors when the pipe is wrapped in some kind of material, the tests with the DTS were carried out with the pipe involved in fabric. These tests aimed to identify the minimum leakage detectable with the DTS.

Initially, a test was carried out with the pipe pressurized at 4 bar, with a leakage point at 5.5 meter from the beginning of the tube and with a leak that last 15 minutes. The results of this experiment are shown in Figure 5.9. The yellow curve representing the temperature near the leak area decreases during the event and,it is also possible to observe a drop in the temperature obtained by the DTS, represented by the black curve. The temperature drops recorded by the fiber optic sensor are not as intense as those recorded by the thermometer, given the interrogator's spatial resolution for measure temperature variations in specific regions of the fiber, but the temperature drop during the test is still noticeable. It can also be seen that the temperature drop is slightly delayed compared to that observed by the thermometer, due to the greater thermal inertia of the fiber optic cable, which is made up insulating material. It is also important to remember that the DTS was configured to deliver one sample of temperature at each 5 minutes, which cause this visible discretization in time.

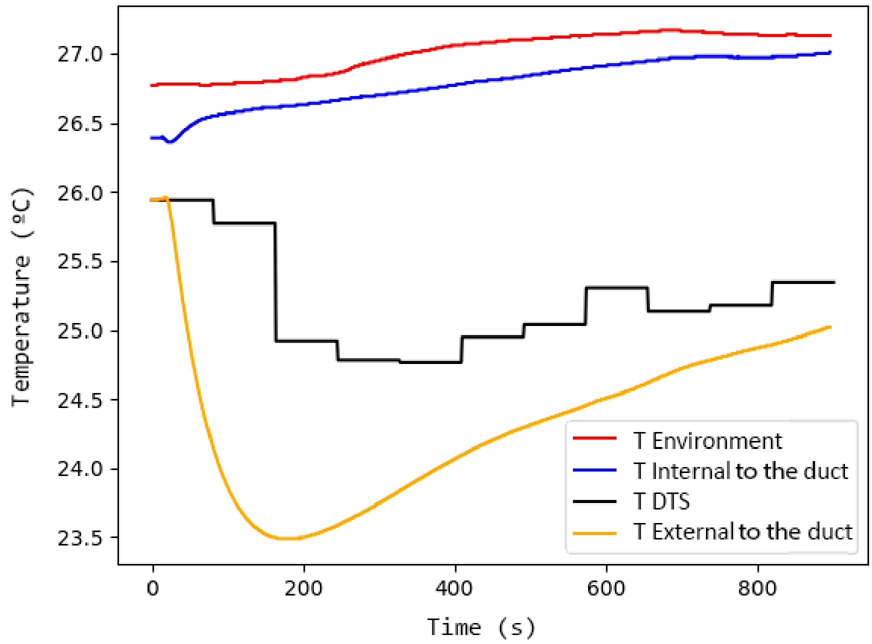

Figure 5.9 – Results of experiments at 4 bar pressure.

Knowing that it was possible to detect the leak with the DTS under the test conditions, the next step was to determine the minimum leak detectable by the device under the same conditions, but varying the pipe pressure and gas flow. To do this, the fabric wrapping and 15-minute leak duration was maintained, as performed previously. However, this time the pressure was gradually reduced over 10 tests, from 4 to 0.2 bar. The pressure data in the pipe and the temperature drop variation obtained by the thermometers are shown in the Table 5.2.

The results of the temperature variations obtained by the PT-100 RTD were according to the expectations, as the pressure increases, so does the temperature drops. As for the results obtained by the DTS interrogator, it is possible to see the same behavior in the graph generated by the data collected during the leak events and the temperature variation along the length of the fiber (Figure 5.10). In this Figure, the arrow shows the point of temperature drop in relation the red line generate by the linear regression of the data. The fiber was placed along the entire length of the test pipe, however, only the leakage region used for the experiment, which is at a point 5.5 m from the beginning of the pipe, was surrounded by the fabric. The

Table 5.2 – Relationship between pressure and temperature drop variation obtained by thermometers in the area of the leak.

Pressure (bar)	RTD Temperature drop (°C)
4,00	-2,2
3,40	-1,8
2,80	-1,4
2,50	-1,2
2,00	-1,3
1,30	-1,1
1,00	-0,8
0,60	-0,5
0,35	-0,4
0,20	-0,3

covered area comprises a space of 1.3 m of the pipe with the leak point in the center. The results show a temperature drop of about 1.7°C in this point. The variation data collected by the RTD thermometer in the same conditions, show a temperature drop of 2,2 °C on this region. For the lower pressures, the negative peak arising from the thermal variation gradually decreased as the tests progressed, but was still noticeable in a visual analysis. During the leak at 1 bar, for example, the variation data collected was about a drop of 0.8°C. Although the cooling in the optical fiber occurred in a region smaller than 1 meter, the temperature drop was still presented in the graph in Figure 5.11 generated by the DTS during the experiment. It was only when the pressure reached 0.6 bar with a variation of 0.5°C that it was no longer possible to separate the signal from the noise, nor to notice any obvious variation in the graphics generated by the interrogator (Figure 5.12).

This experiment indicates that the smallest detectable leak under the conditions of the DTS experiment (hole of 2 mm diameter) is for pressures of 1 bar with 0.8°C of variation. However, as one of the conditions of this experiment was the use of air and not natural gas, it is expected that, in practice, it would be possible to identify leaks as long as the pressure in the natural gas pipe was greater than 0.5 bar. Since the Joule-Thomson coefficient of the natural gas is around two times bigger than the air, it is expected to have the same 0.8 ºC drop in temperature for natural gas pressurized at 0.5 bar.

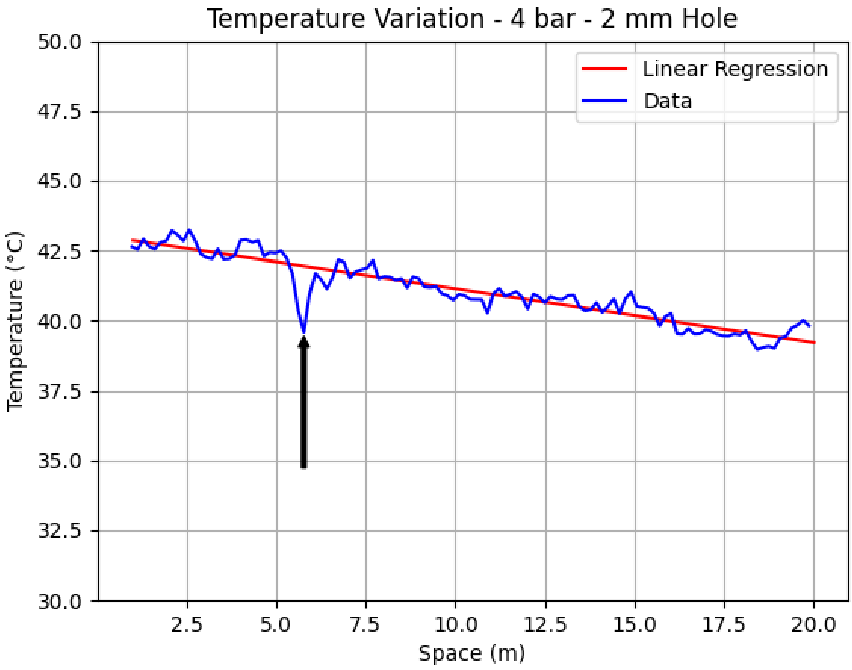

Figure 5.10 – Graphic of the temperature variation generated by the data collected by the DTS with the pipeline pressurized to 4 bar.

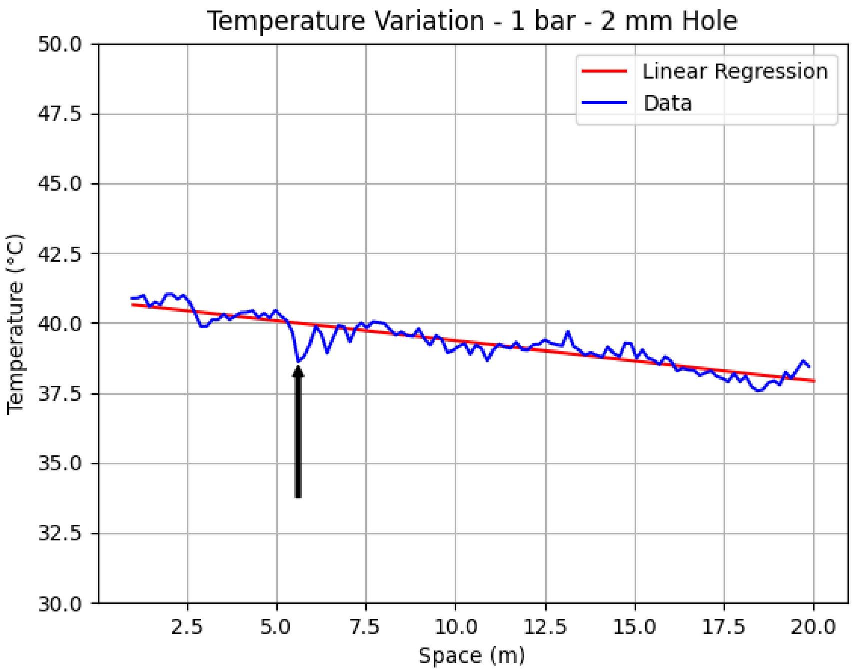

Figure 5.11 – Graphic of the temperature variation generated by the data collected by DTS with the pipeline pressurized to 1 bar.

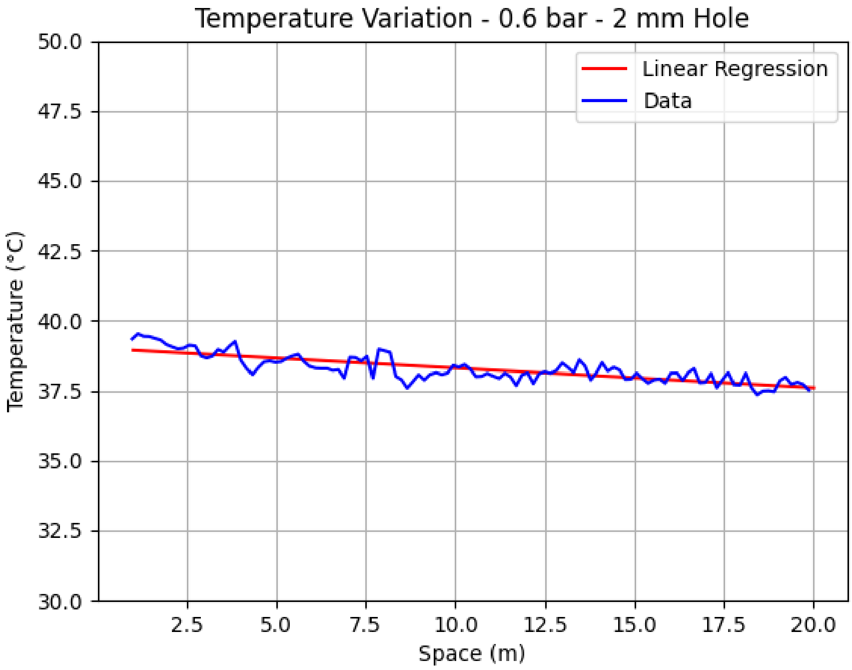

Figure 5.12 – Graphic of the temperature variation generated by the data collected by DTS with the pipeline pressurized to 0.6 bar.

a

5.2 Influence of hole diameter

The Joule-Thomson effect, which describes the change in temperature of a gas when it undergoes adiabatic expansion, is directly affected by the size of the hole. The diameter of the hole determines the flow rate of the gas through the leak, thus impacting the speed with which the gas passes through the detection point. This variation in gas velocity can result in variations in the temperature drops that can be detected by fiber optic sensors. Therefore, understanding how the hole diameter influences the Joule-Thomson effect is important for improving the sensitivity and accuracy of gas leak detection system.

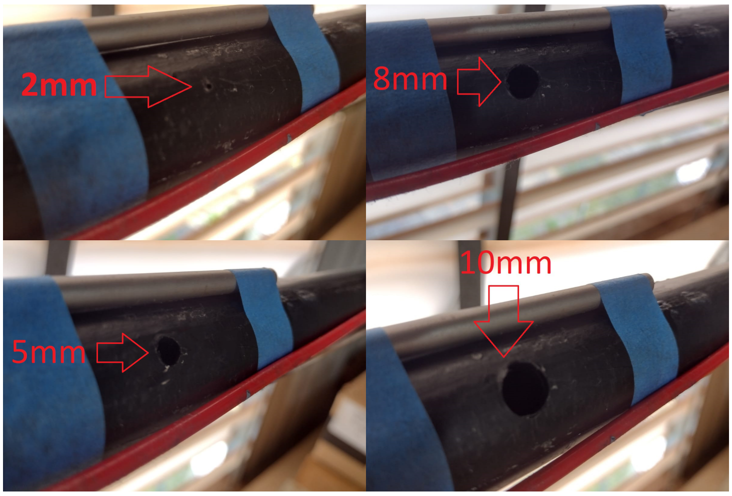

Figure 5.13 – Hole drilled in the pipe.

To better understand the variations obtained, a test was carried out in which increasingly large holes were drilled in the pipe which was pressurized to 4 bar, the holes were 0.2, 0.5, 0.8, and 1.0 cm in diameter, as seen in Figure 5.13. During the tests, that lasted 10 min for each diameter hole, the hole was wrapped by the fabric.

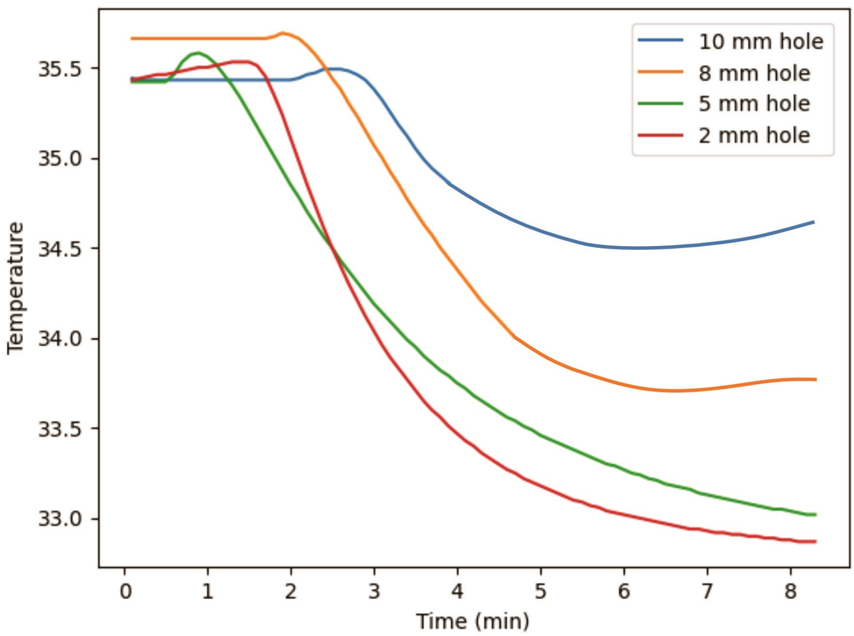

Figure 5.14 – Graph showing the temperature variation obtained in each of the simulated leaks.

Figure 5.14 shows the results of each of the tests compared. It indicates that the average temperature variation decreases as the hole diameter increases for leaks at the same initial pressure. This indicates a drop in the magnitude of the Joule-Thomson effect as the leak increases.. It was found that this is due to the lower velocity of the air leaving the pipe. This shows that the system can really struggle to locate leaks that don't favor a pronounced Joule-Thomson effect due to bigger hole diameters.

5.3 Analysis and interpretation of vibration sensors

This section presents the results of the experiments carried out using the piezoelectric accelerometer, the Omnisens DAS (Distributed Acoustic Sensing) interrogator, and the Micron Optics si155 interrogator with the optical accelerometer and sensors based on fiber Bragg gratings.

5.3.1 Piezoelectric accelerometer

Figure 5.15 – Piezoelectric accelerometer model 352C33 in its box.

Before any vibration tests with the optical sensors, it was necessary to obtain a reference signal for comparison. For the thermal sensor (DTS), PT-100 RTD thermometers were used, and for vibration piezoelectric accelerometer of the brand PCB, model 352C33 was used, as illustrated in Figure 5.15. The sensor, featuring a sensitivity of 100 mV/g (10.2 mV/(m/s^2)) and a measurement range of ±50 g pk (±490 m/s^2 pk), offers a broadband resolution of 0.00015 g rms (0.0015 m/s^2 rms) over a frequency range of 0.5 to 10000 Hz. This sensor's data is acquired by an NI 9234 acquisition module from National Instruments. Just like the data generated by thermometers, the data generated by this sensor can also be obtained via the LabVIEW interface and stored in log files. During all the leak tests for vibration measurement, the ball valve in the middle of the pipe was used as the leak area. The valve is in a continuous area of PE pipe, representing the leak area, which is closer to real conditions. One issue was the length of the accelerometer cable. The original cable is only 5 meters long. An extension cable was tested, but it introduced substantial noise into the measurements and was removed. Due to this limitation, the accelerometer was positioned at the inlet of the airline, about 5 meters from the leak point using cyanoacrylate glue.

With all the parts assembled, a leak test was carried out to determine the spectrum of frequencies present in the pipe during a leak at 4 bar. The acceleration spectrum obtained by the piezoelectric sensor was visualized using graphs presented in the LabVIEW program, as shown in Figure 5.16. This graph shows that the leak in the gas line causes vibrations at various frequencies, with peaks at 2 kHz, 4 kHz, and in the 9 to 12 kHz range. The signal energy in the 0 - 12.8 kHz band increases almost 1,500 times in the presence of a leak. The fact that the vibration frequency is distributed along many frequencies above 1.5 kHz indicates that fiber optic sensors used in this work may have difficulty detecting the leak. The DAS interrogator (Omnisense ODAS)is limited to 1.5 kHz and the the FBG interrogator (Hyperion si155) to 2.5 kHz.

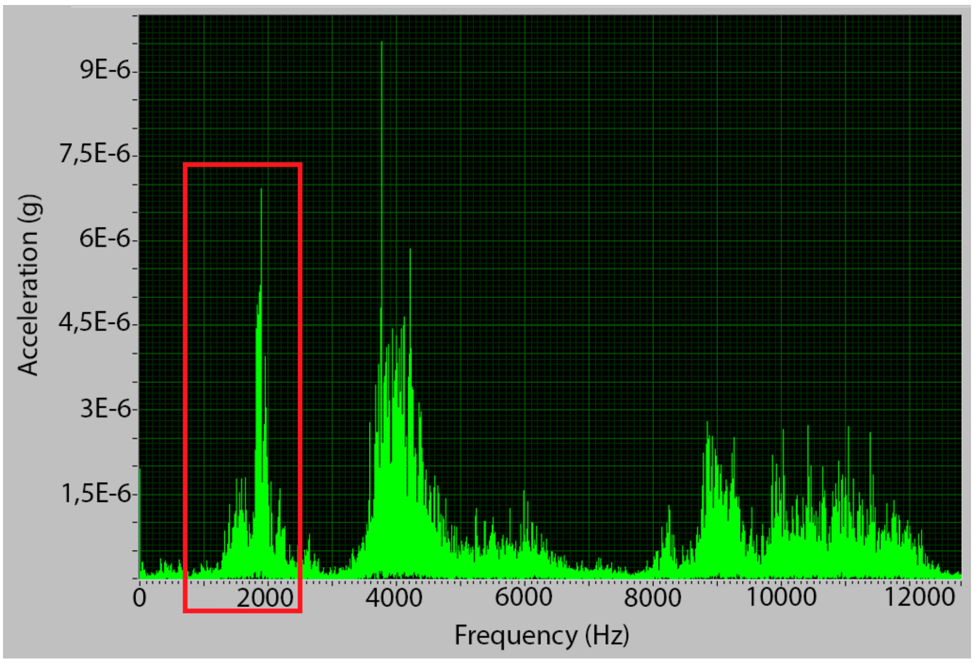

Figure 5.16 – Measurement data from a piezoelectric accelerometer with emphasis on the region marked in red, which is where the first peak of vibrations is located, around 2 kHz.

5.3.2 Tests with the DAS interrogator

To carry out a test using DAS (Distributed Acoustic Sensing), a 500 m coil was used with tight buffer fiber optic cable, ideal for measuring vibration and traction. In the region of interest, which corresponds to the leak near the valve, the cable was glued to the pipe with cyanoacrylate glue for better vibration coupling. In the other areas along the pipeline, it was attached with adhesive tape. Once the acquisition system was set up, the line pressure was adjusted by the system. For this experiment, the pressure was adjusted dynamically by the FESTO proportional pressure valve at a pressure of 4 bar. The function of this valve is to try to stabilize the internal pressure of the pipe at 4 bar even while the leak is happening. When the leak starts, the valve is opened and the air fills the pipe and escapes through the open ball valve. Although this process does not require manual interaction between the operator and the pipe, it does generate initial vibrations that are different from those when the leak is stabilized. It was necessary to wait for the vibrations to stabilize in order to better measure the leak frequencies.

The tests carried out with the piezoelectric accelerometer identifying a vibration peak close to 2 kHz. Although the DAS interrogator does not reach this frequency, being able to obtain signals up to a maximum of 1,5 kHz, it was able to detect vibrations in the transients, when the leak is starting or when it is shutting down, as shown in the figures 5.17 and 5.18. Despite adjustments to the filters to obtain higher frequencies, the interrogator did not identify any significant vibrations from the leaks in the steady-state. These results indicate that Omnisense's DAS interrogator is a promising device for detecting and controlling leaks in air ducts, as it was able to identify vibrations associated with the leak during the initial and final stages when significant changes in pressure and local vibrations occur. However, it is important to note that the interrogator was unable to register the leak after it had stabilized under the conditions of the experiment, even with adjustments to the filters for higher frequencies.

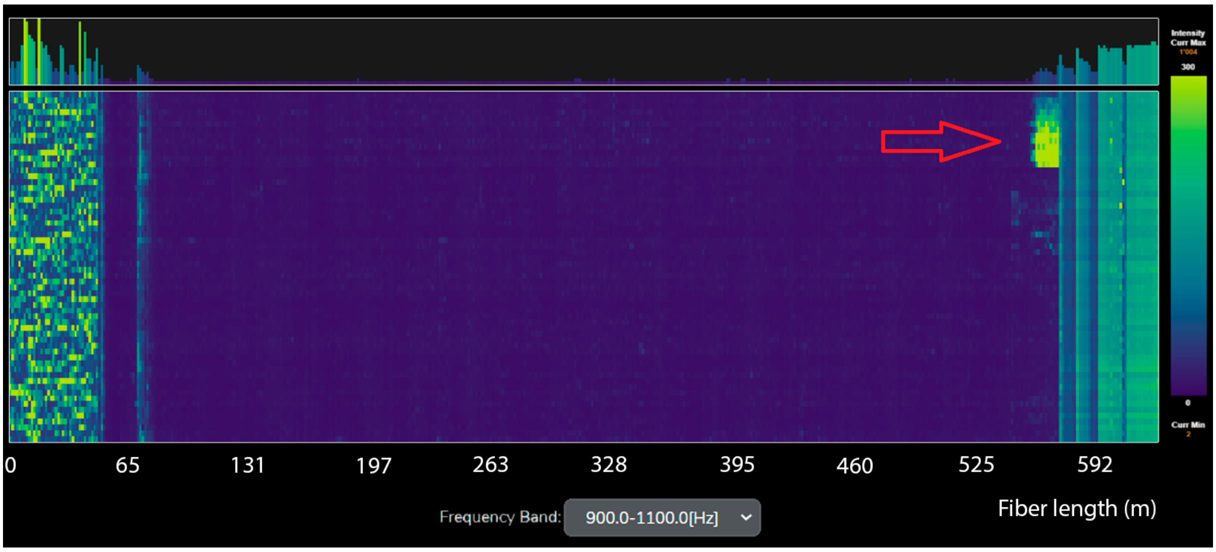

Figure 5.17 – Waterfall graph indicating the vibration in the line length at the start of a leak.

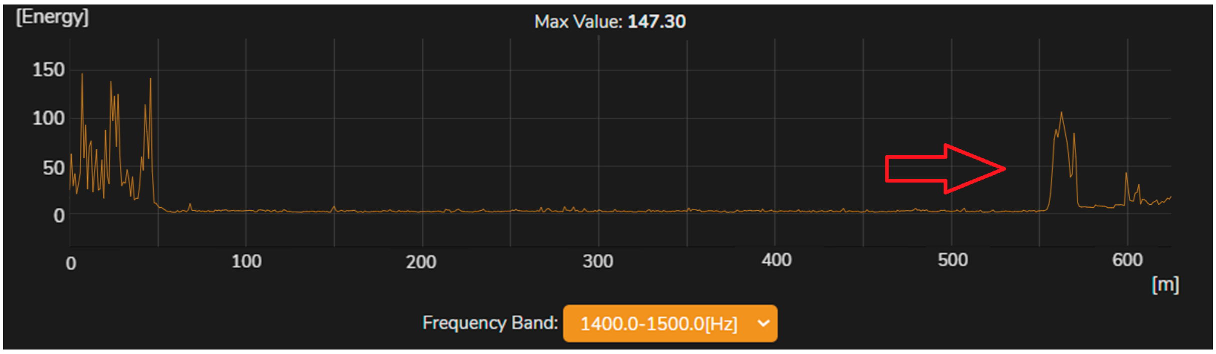

Figure 5.18 – Energy graph indicating a peak at the site during the start of a leak.

5.3.3 Tests with FBG sensors and FBG-based strain gauges

Two of the four channels of the Luna's Hyperion si155 Interrogator were used to interrogate the optical sensors. In channel A, two os1100 model FBGs were connected in series, with wavelengths of 1528 and 1540 nm. In channel B, two optical FBG-based strain gauges model os3200, with wavelengths of 1512 and 1520 nm, were connected in series. In the pipes, the first FBG was positioned next to the ball valve in the pipe. The second FBG was placed at a distance of 2 meters in front of this point, both fixed using adhesive tape. The strain gauges were in the same position as the FBG sensors but glued with the adhesive that came with the product and it was installed as suggested by the manufacturer as seen in the Figure 5.20. For this experiment, once again, the line was pressurized to 4 bar, with the outlet valve at the end of the line closed, but with the valve in the area of the leak opened manually. In these tests, only the moment when the gas flow in the leak is stable was considered. Once this was established, the interrogator's ENLIGHT configuration program set the acquisition rate at 5,000 samples per second and then proceeded to open the leak and start acquiring data.

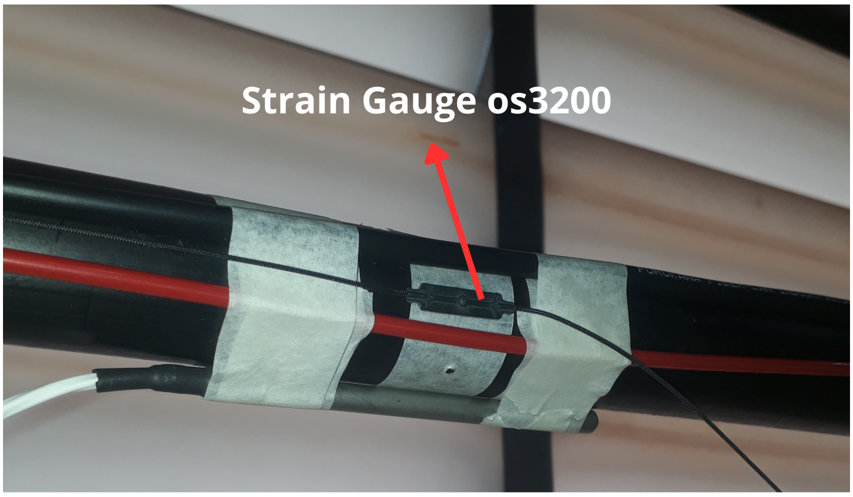

Figure 5.19 – Strain Gauge os3200 installed in the pipe close to the leak region.

The interrogator can analyze sensor data in real time and, as expected, due to preliminary tests with the speaker, the strain gauges only detected low-frequency signals (less than 1 kHz), which is outside the peak frequency range generated by the leaks in the pipelines under the conditions of the experiment, as detected by the piezoelectric accelerometer. The first peak of excitation expected from the leak is close to 2 kHz. However, the frequency response of the strain gauges only allows the identification of low-frequency vibrations, such as those caused by the touch of a finger on the pipes as shown in Figure 5.20. The FBG sensors, on the other hand, as in the preliminary tests, did not detect any vibrations. One of the hypotheses for this is the poor vibration coupling between the sensor and the pipe due to the use of adhesive tape. To eliminate this problem, they were fixed again, this time with cyanoacrylate glue to ensure the maximum possible vibration coupling. In a new leak test, the results obtained were the same as the previous ones, i.e. the sensor did not identify any significant variation in vibration that stands out from natural noise.

5.3.4 Tests with optical accelerometers based on Fabry Perot filters

One optical accelerometers from Micron Optics, model os7510, based on a Fabry-Perot filter, were glued with cyanoacrylate in the pipe of the test bench. One can be seen in the Figure 5.21, with a blue tape that was used to position the sensor until it was completely fixed by the cyanoacrylate. The optical accelerometer was installed close to the leak area, around one meter away from it. As result, the leak test parameters were configured in the same

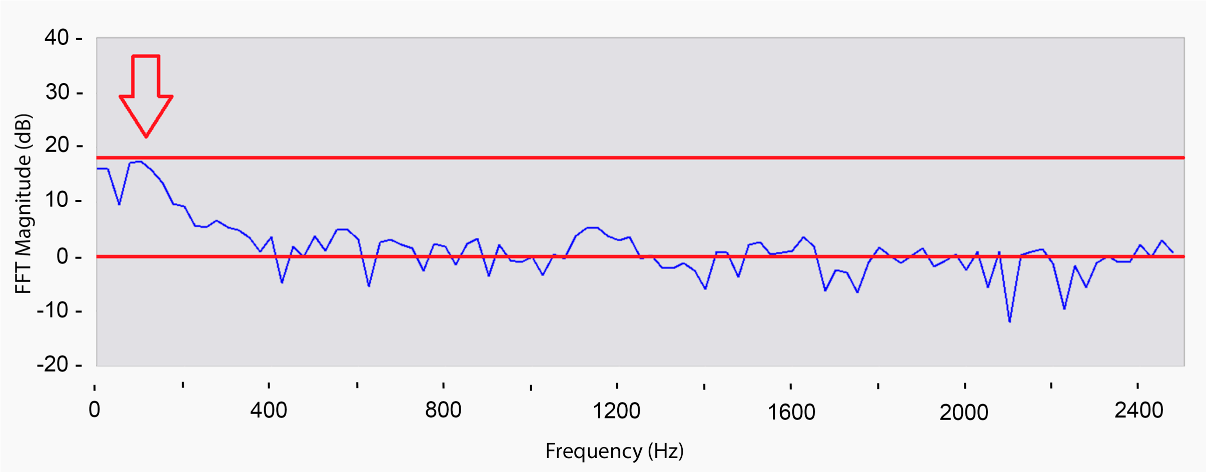

Figure 5.20 – Touching the pipe generates a low-frequency stimulus (indicated by the arrow) picked up by an FBG-based *strain gauges* sensor.

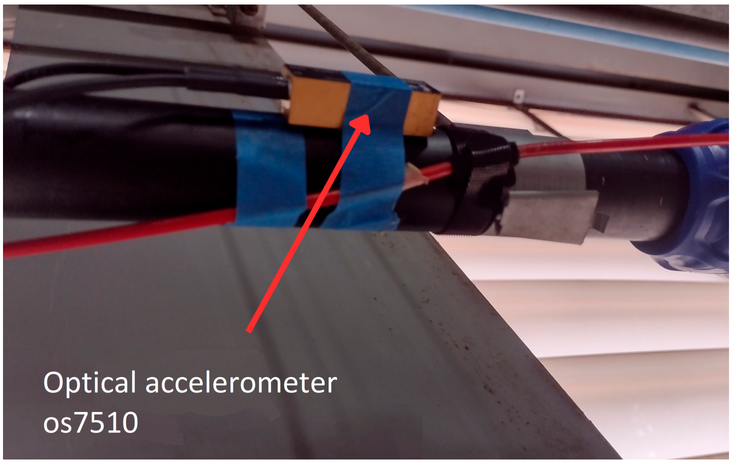

Figure 5.21 – Optical accelerometers attached to the pipe with cyanoacrylate in order to generate the best vibrational coupling.

way as during the experiment with FBGs and strain gauges. The pressure was set at 4 bar, with the outlet valve at the end of the line closed, and with the ENLIGHT software set to an acquisition rate of 5,000 samples per second. With the line properly pressurized, the ball valve that simulates the leak was opened and and after stabilization, the acquisition started.

By the end the acquisition, it was possible to perceive that the accelerometer showed a promising results in detecting leaks. The power peak (dBm) oscillate from 10 dBm (at rest) to around 20 dBm during stimulation, as shown in Figure 5.22 where it is possible to see peaks of signal strength close to 2.2 kHz that was detected by the optical accelerometer close to the leak (around 1 m) during the leak event in relation to the rest state (no leakage) shown in the Figure 5.23. Although this optical accelerometer was designed to detect vibrations of low frequency, it was able to detect a weak signal produced by the leak event. The known frequency of the leak has a first peak around 2 kHz, approximately 6 times higher than the manufacturer's max range with precision (up to 350 Hz) for the optical accelerometer, Due to that, the signal is estimated to be attenuated around 90% in 2 kHz. But even with this attenuation, it is still possible to identify a weak signal of 2.2 kHz during the leak with the sensor close to the leak region.

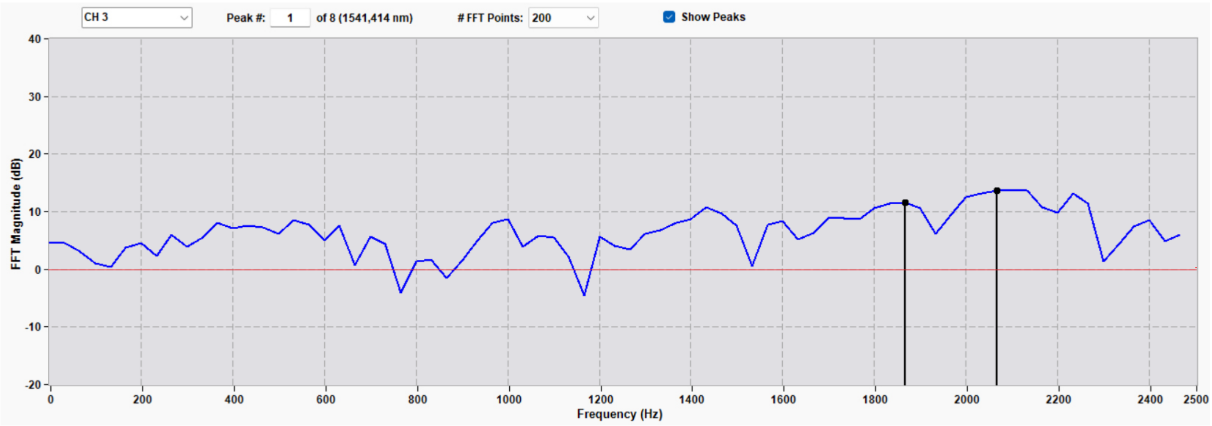

Figure 5.22 – Frequency domain signal captured by the os7510 optical accelerometer during a gas line leak away from the sensor. The red arrow indicates the peak of the signal and its position.

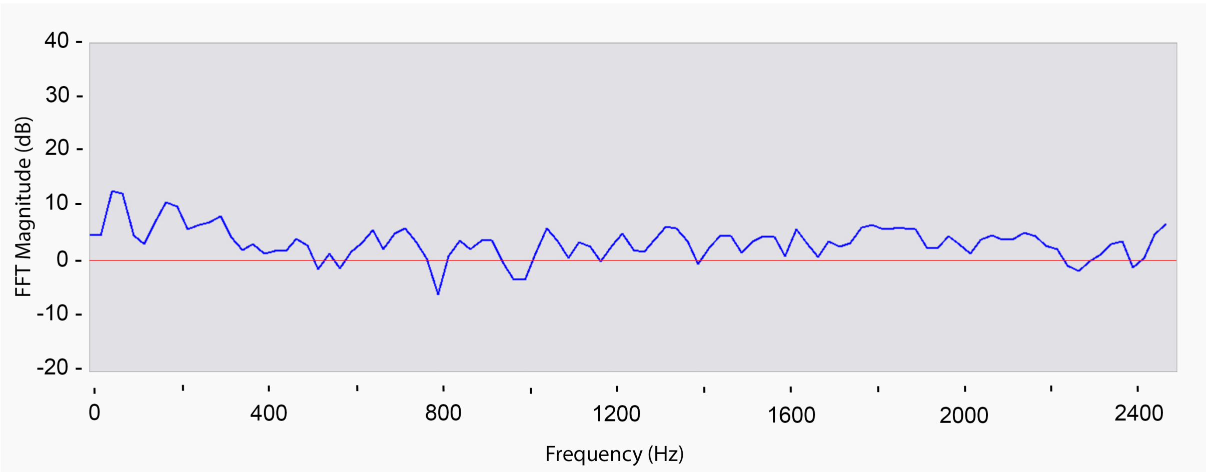

Figure 5.23 – Frequency domain signal captured by the os7510 optical accelerometer while resting one meter away from the sensor.

With the conclusions of this phase of this experiment, a new experiment was carried out to stipulate the smallest detectable leak in a 2 mm hole. The sensor remained positioned one meter from the leak point and the pressure was then gradually reduced, starting at 4 bar until the signal was no longer perceptible. The results of multiple tests show that near the 1 bar of pressure, the signal becomes almost indistinguishable from noise (Figure 5.24). A visible and distinguishable signal was successfully obtained from a 2bar leak event. However, the performance could be significantly improved by using accelerometers with a 2 kHz bandwidth, like the Luna OS7220. This upgrade would enhance the accuracy and reliability of the leak detection system, ensuring more precise monitoring since its frequency range reaches 2000Hz ().

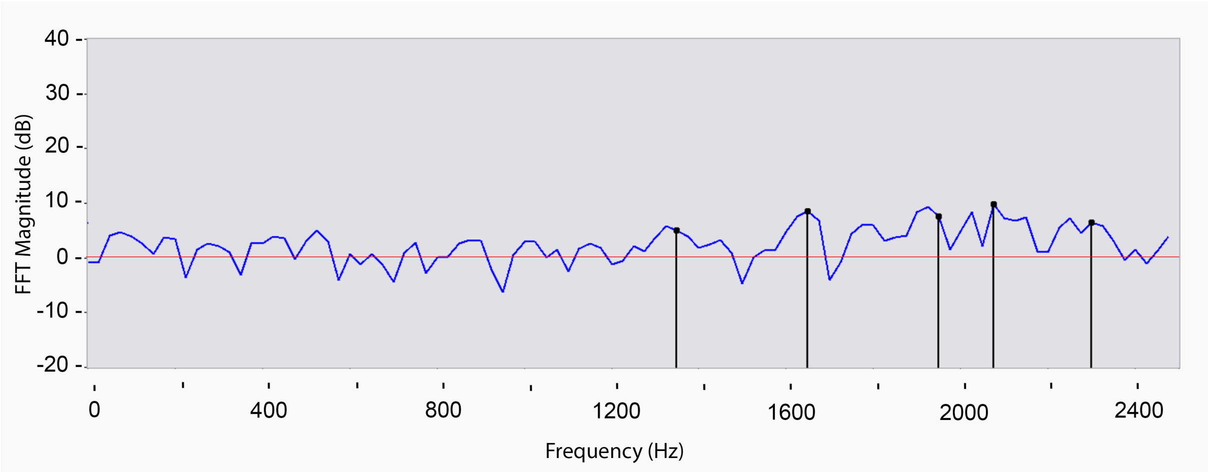

Figure 5.24 – Frequency domain signal captured by the os7510 optical accelerometer one meter away from the leak at 1 bars of pressure and in a 2 mm hole in one of the tests.

5.3.5 Localization of the probable leak region given the signal strength of accelerometers based on Fabry Perot filters

The following experiment aimed to locate the source of the leak given the signal strength to identify the maximum distance between the accelerometers for proper leak detection. The four channels available on the interrogator were used, each for a individual accelerometer. The leak point was a 2 mm hole and the optical accelerometers were placed in the pipe at 1 m, 2 m, 4 m and 7 m from the leak point, with sensors 2 and 4 being 2 m and 7 m to the left respectively and sensors 1 and 3 being 1 m and 4 m to the right of the leak point respectively , as shown in Figure 5.26. The signal of each accelerometer was monitored over a time interval of 5 minutes. The pressure in the line was set to 4 bars and the leak emulation was started one minute after data collection began.

To make it easier to visualize the power peak of the accelerometers, a code that uses the *logs* generated by the interrogator si155 was developed. To reduce the volume of logs, a measurement was taken every 5 seconds for a time interval of 1 minute. This choice allowed for a significant reduction in the amount of raw data generated, making analysis and interpretation of the results more efficient, since there is no need to take measurements at shorter intervals given the constancy of the leak. The interrogator was configured to operate at a rate of 5 kSPS (kilo Samples Per Second), where wavelength values proportional to the acceleration perceived by the accelerometer are obtained. From this data, the program groups 5.000 samples (equivalent to 1 second) to calculate the spectrum of this signal using the FFT (Fast Fourrier Transform). The average magnitude of the vibration is then calculated in the 1.8 kHz to 2.5 kHz band. This procedure was carried out for data obtained at time intervals of 5 seconds, resulting in 12 samples of the spectrum for each accelerometer over 1 minute, which made it possible to calculate the mean and standard deviation. These values were then related to the distance between the leakage points using a polynomial regression. This polynomial makes it possible to estimate, during the operation of the leak identification system, the distance from the leak point to each accelerometer.

The results were organized into graphs that show the average intensity of the vibration signal in relation to the distance from the sensor to the leak region. The results of the first phase of the proposed methodology are presented in the graphic shown in the Figure 5.25. The abscissa axis indicates the distances (in meters) between each sensor in relation to the leak area (defined as 0) and the ordinate axis the average power in dBm like as the graph of the Figure 5.24. Each sensor are represented by a vertical bar which corresponds to the standard deviation of a series of data obtained over 12 measurements for each of the four sensors and, in the middle of each bar, a point that represent the average values of intensity obtained during the acquisitions. The interpolation of this data was calculation using a second order polynomial curve represented by the red line. This interpolation is essential for the next step, which aims to find the likely location of the leak.

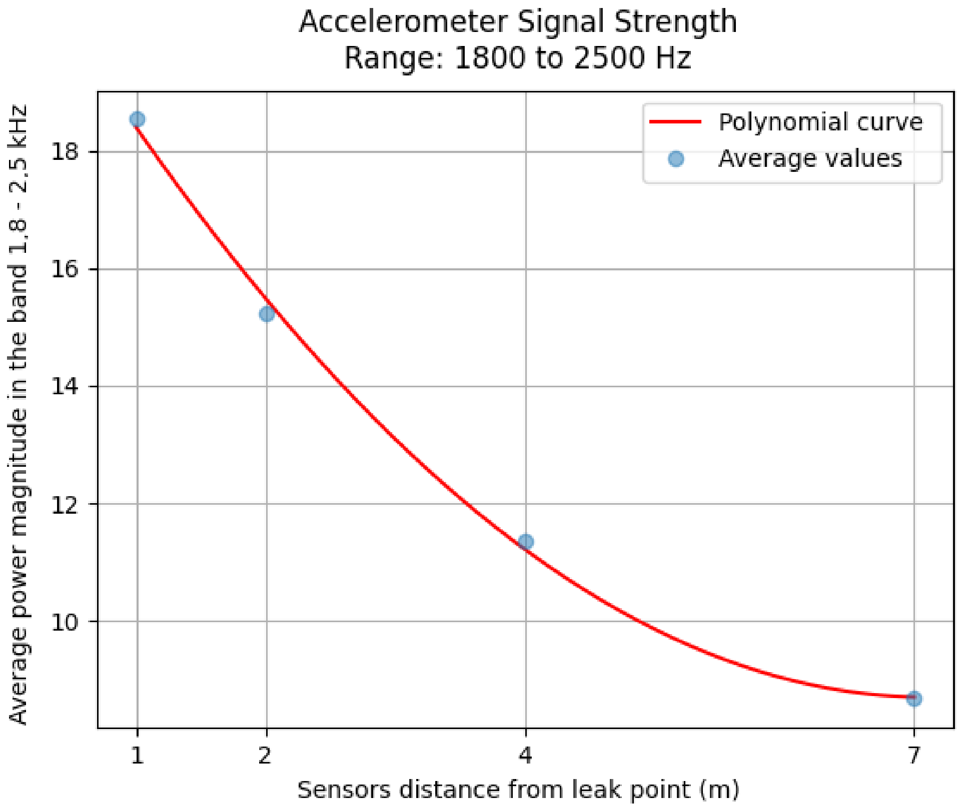

Figure 5.25 – Average power magnitude for each optical accelerometer (band from 1,800 Hz to 2,v500 Hz) and polynomial curve.

The next step, illustrated by the graph in Figure 5.26, show the estimated distance of a leak provided by each sensor for one measurement (5,000 samples of the accelerometer). These distance estimation, represented by the radius of the circles, are based on the polynomial equation obtained in the previous phase, allowing us to determine the likely position of the leak using the collected vibration data. In a gas distribution line where the sensors are placed at a known point, the data will indicates the probable position of the leak. However, it does not specify if the position is to the right or left of the sensor, resulting in two potential points. To visualize this in Figure 5.26, the abscissa represents the pipe and the circles corresponds to the estimated distance from the leak to their respective sensor. The points where the radius intersects the abscissa denote the two possible positions of the leak.

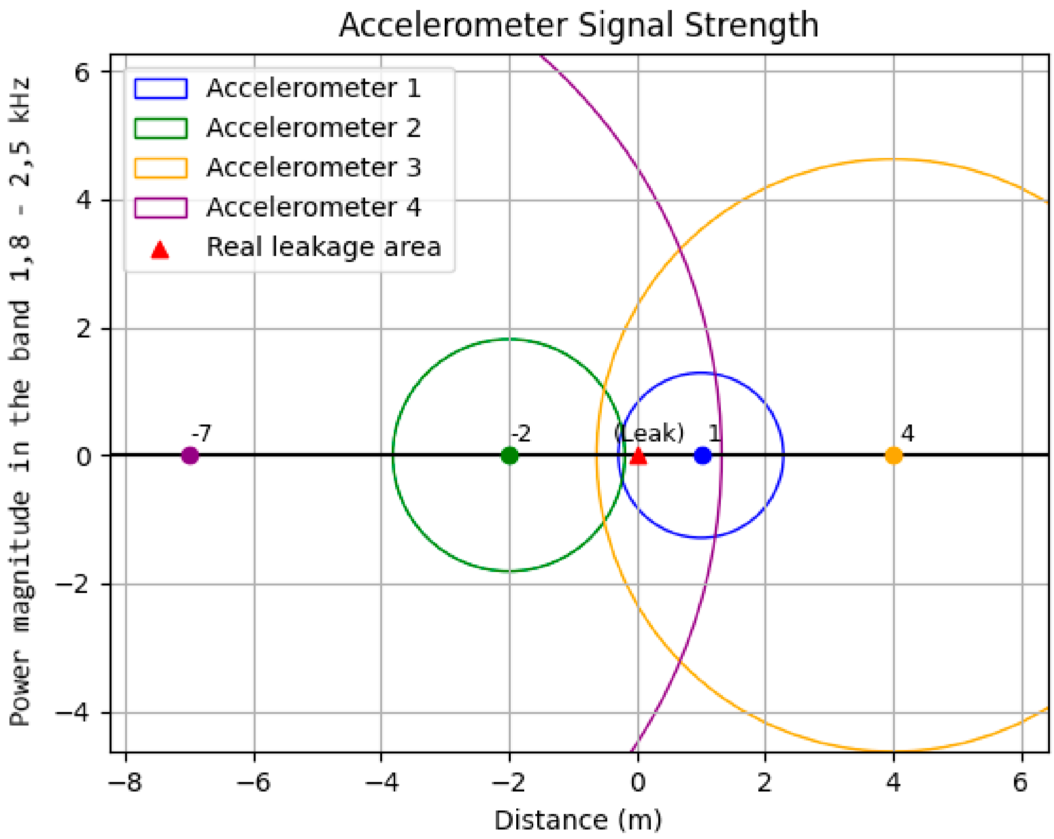

Figure 5.26 – Relative position of the accelerometers and their respective signal intensity strengths represented by the circles radius.

These distances estimates result in a cluster of circles in which the smaller the radius, closer the sensor is to the leak. However, the actual leakage location is undetermined, as seen in Figure 5.27 which shows a close-up view of the leakage region. The radius of the circles tends to approach the region where the leak is (red triangle in the graph), the region where they approach or intersect is the probable leak region, but the radius of the circles does not touch the leak point since the radius are approximations and estimations of the actual leak region. And even if a radius did touch the point of leakage, it would not be possible to determine whether or not this event had actually occurred. So far, only the probable region of the leak has been revealed, not the probable point of leakage.

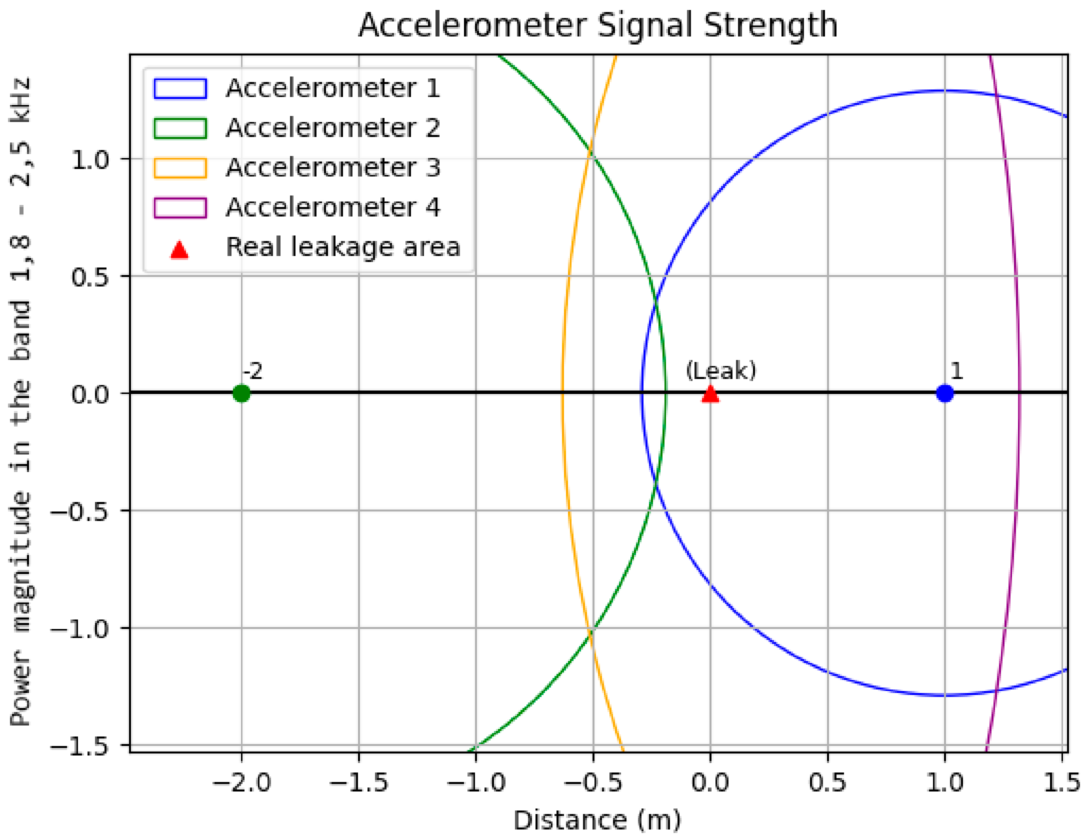

Figure 5.27 – Close-up view of the actual leakage region.

5.3.6 Localization of the probable leak point given the signal strength of accelerometers based on Fabry Perot filters

To identify the probable leak point, an algorithm was developed based on the previously obtained data. The first step in this process is to set a threshold for vibration intensity, which helps distinguish between potential leaks and non-leak events. For this experiment, a threshold of 10 dBm was determined based on previous results with the accelerometers, though this value can be adjusted to suit different line conditions and sensor characteristics. When the intensity surpasses this threshold, the corresponding accelerometer and its position are factored into the calculation to predict the leak's location. The algorithm requires activation of at least two sensors to begin the calculation.

The second step involves determining whether the leak is to the right or left of each activated accelerometer. This is achieved using the method of intersecting intervals, which considers the two probable leakage points identified by each accelerometer to form these intervals. By assuming that the leak point lies within the intersection of these intervals, the algorithm can classify the points provided by the accelerometers as either before or after the interval containing the leak.

In the third step, an even number of accelerometers is selected—specifically, two to the right and two to the left of the leak location indicated by the earlier interval. From these, the four probable leak points (one from each accelerometer) that are closest to the interval containing the leakage region are chosen. This selection process helps balance the triangulation of the leak position. The implementation of this algorithm begins by sorting the estimated leak positions for all the activated sensors (two positions per sensor). It then searches for the smallest distance interval in which there is a sample from each activated sensor. These estimated leak positions are selected for the next stage of the algorithm.

The fourth and final step is to accurately determine the probable leak point. This is accomplished by calculating the modulus of the derivative of the polynomial that relates the acquired vibration power with the distance to the leak point (Figure 5.25) for the selected sensors. The value of this derivative for each sensor is then used as a weighting factor to calculate the leak point - the weighted average of the leak points of the selected sensors. This method enhances the accuracy of leak prediction compared to a simple average, as it incorporates the sensitivity of each sensor in the given scenario. Following these steps led to the result depicted in Figure 5.28, where the estimated leak point (marked in green) closely aligns with the actual leak location at ground zero.

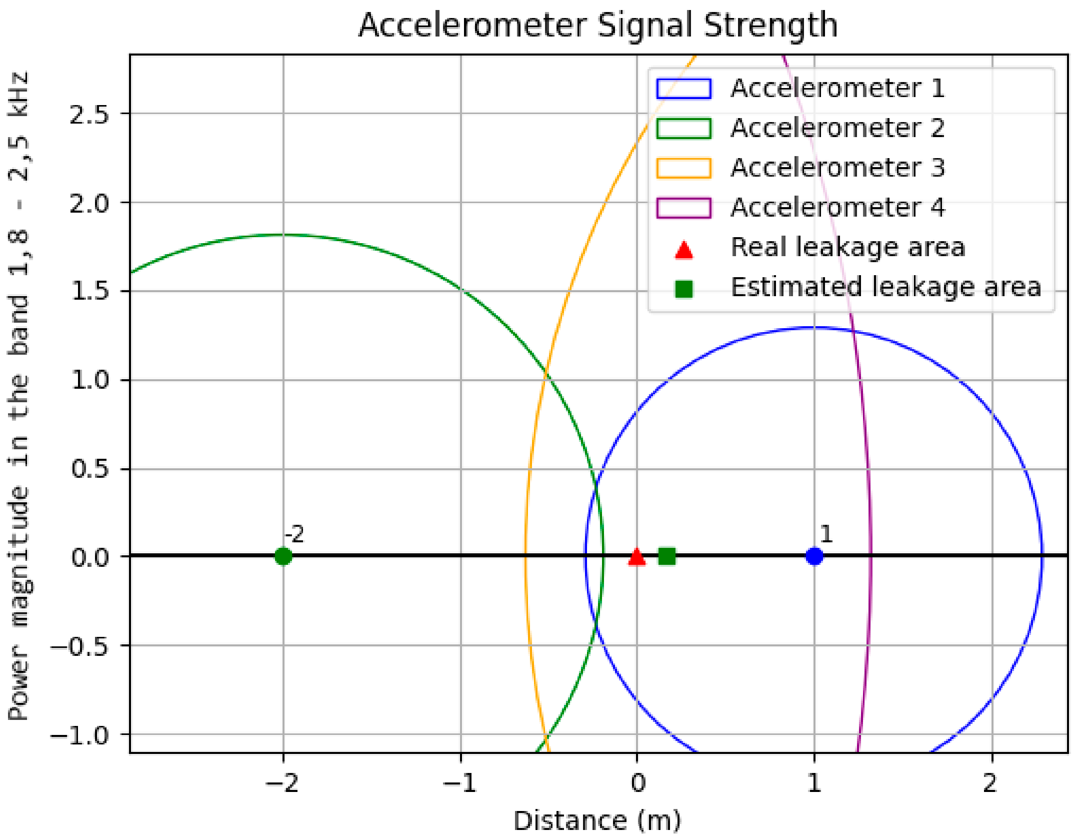

Figure 5.28 – Actual point of leak compared to estimated location.

This method demonstrates approach for localizing leak points by leveraging the signal strength and spatial distribution of accelerometers. Its adaptability, through the adjustment of thresholds and the selection of sensors based on sensors sensitivity, ensures that it can probably be applied in various pipeline conditions. However, further refinement could be achieved by creating procedures to adjust the polynomial curve that relates the acquired vibration power vs. the distance to the leak point (Figure 5.25) during the leakages. Future work may explore these approaches to optimize the algorithm's performance in real-world applications.

In the tests carried out, it was observed that the maximum distance from the sensor to the point of leakage in order to obtain vibration signals is a maximum of 7 meters, indicating that the sensors should be located a maximum of 14 meters from each other. However, it is important to note that the optical accelerometers used in this project were designed to obtain signals in the frequency range of up to 350 Hz, and in this application they are being used to obtain signals in the 1,800 Hz to 2,500 Hz band, which results in great attenuation. By using more sensitive accelerometers in the band of interest, it will be possible to obtain leakage signals over greater distances. Future work will include a study to verify the impact of leak diameter and pipe pressure on leak identification using optical accelerometers.

5.3.7 Results summarization

Table 5.3 summarizes the various results obtained from the optical devices used. The comparative analysis provide a objective view of the variations and similarities between the results under the condition of a low-pressure leak in an urban environment.

Table 5.3 – Results summary.

Interrogator DTS DITEST-12 Omnisens	**Techniques**	Distributed Temperature Sensing, Brillouin scattering
	Advantages	Indicates to be able to detect leakages of natural gas lines pressurized with at least 0.5 bar.
	Disadvantages	Requires covers to be able to detect leakages in aerial pipes. May be influenced by ambient temperature changes. Is expensive. Is not capable to identify excavations.
Interogator DAS ODAS Omnisens	**Techniques**	Distributed Acoustic Sensing, Rayleigh scattering
	Advantages	Can be used to detect when the leak starts, before the flow stabilizes. Is not strongly sensitive to temperature changes. Is capable to identify excavations. Is expensive.
	Disadvantages	The model used is not capable of detecting the frequency ranges reached during the stable phase of the leak under the test conditions.
Strain Gauge os3200	**Techniques**	Reflectivity Modulation Principle
	Advantages	It can be used to identify low-frequency pipe movements, such as those caused by soil movements.
	Disadvantages	It was unable to detect the high-frequency vibrations caused by leakages. It is capable to monitor short distances compared with distributes systems, is more difficult to install.
FBG os1100	**Techniques**	Reflectivity Modulation Principle
	Advantages	It can be used to identify low-frequency pipe movements, such as those caused by soil movements. Is cheap.
	Disadvantages	It was unable to detect the high-frequency vibrations caused by leakages. It is capable to monitor short distances compared with distributes systems, is more difficult to install.
Optical accelerometer os7510	**Techniques**	Fabry-Perot interferometery
	Advantages	Capable of detecting leakage by vibration during the stable phase of the leak when in 7 m or less.
	Disadvantages	Expensive, shorter distance than distributed systems, more difficult to install, highly attenuated signal

6 FINAL CONSIDERATIONS

In the gas infrastructure scenario, where safety and integrity are imperative, the challenges of ensuring reliability and safety have fostered the development of solutions employing fiber optic sensors for leak monitoring. Identifying leaks in gas lines can be done by monitoring temperature and/or vibration along the pipe, using distributed sensors based on Brillouin, Ramam, and Rayleigh scattering and/or interferometry; or by point measurement using sensors based on FBGs (Fiber Bragg Gratings) or Perot Fabry filters. Although fiber optic sensor technologies are being used in some pilot systems for monitoring leaks in transmission lines, there is still uncertainty about which techniques and sensors are the most suitable for this application, specifically in low-pressure gas distribution lines.

In this context, this work was carried out with the aim of experimentally investigating the potential, performance and limitations of the main optical technologies for monitoring leaks in gas lines. The following sensors/interrogation systems were analyzed: DAS (Distributed Acoustic Sensing), DTS (Distributed Temperature Sensing), FBGs and, and optical accelerometers based on Fabry Perot filters. The focus of this work was on identifying technologies capable of identifying leaks in low-pressure (up to 4 bar) polyethylene (PE) above ground distribution gas lines in urban environments.

The experimental results obtained during this research showed that sensors based on various optical fibers sensor techniques can be used to identify leaks in gas lines. Starting with the distributed sensors, it was concluded that the DTS is capable of theoretically identifying natural gas leaks as long as the pipe is pressurized to at least 0.5 bar and covered by some material (soil, fabric, or conduit). However, it does have some limitations, such as not being able to detect leaks in uncovered above ground pipes. The size of the leakage area also influences the measurement, since it has been observed that the larger the hole in the pipe, the lower the intensity of the Joule-Thomson effect and the smaller the temperature variation.

Experimental measurements on the emulated gas line showed that leaks in gas lines generate vibrations at various frequencies, especially in the 2 kHz, 4 kHz, and 9 to 12 kHz range. The DAS model used in the experiment was limited to detect frequencies up to 1,500 Hz, despite not obtaining the vibration generated during the stable phase of leakage events, since the first peak is in the 2 kHz frequency area. However, it was able to obtain the vibrations generated at the start of the leaks (transients) for pressures above 1 bar. The DAS can also be sensitive to noise and interference in the vibration, which can compromise the quality of the data. This sensitivity to noise can limit its applicability in environments with a high level of acoustic interference, such as busy urban areas or close to intense noise sources, which will require signal processing techniques to separate the interference from the signals of interest. However, this also creates the opportunity to identify events such as excavations in the vicinity of pipelines, which may pose risks to them.

Concerning the point sensors, it was concluded that the bare FBGs are not able to identify the vibrations generated due to leaks in the gas line at any of the test pressures. The strain gauges, although able to detect low-frequency vibrations, like touch the pipe line, were unable to identify the leak at high frequencies under the test conditions. The accelerometers based on the Fabry-Perot filter, on the other hand, proved capable of identifying leaks at frequencies above 2 kHz, even with high signal strength attenuation in the model used, as long as the pipe was pressurized to at least 2 bar. It was also able to be used to find the likely leak location using the intensity of the vibration and estimating the distance in relation to the sensor. However, the test was carried out at short distances (up to 7m) from the leak point and at this point the signal is already very close to the noise. For the spacing between accelerometers to be greater in a real application, models more sensitive to high vibration frequencies would be necessary. With this accelerometer it was also possible to sketch a model to multilaterate the location of a possible leak. Given that the accelerometers used in this experiment has a high cost per unit (1,500.00 dollars on the date of publication of this work). This cost could be a barrier to large-scale applications, especially in long-distance monitoring, where it is necessary to use multiple sensors along the line. Finally, none of the techniques mentioned proved capable of identifying leaks in pipes above ground pressurized to 350 mbar.

The results of experiments with point sensors can be improved by using optical accelerometers with a higher frequency response, such as the Luna os7220, capable of obtaining accelerations of up to 4 kHz without attenuation. It should be noted that this method of identifying leaks in gas lines is considerably less expensive than using DTS and DAS for short distance monitoring. While a DTS or DAS device costs from 80 to 200 thousand dollars on the date of publication of this work the high frequency FBGs interrogators start at 10 thousand dollars. Therefore, for monitoring leaks in critical sections of the gas distribution line in urban areas, such as bridges, the use of optical accelerometers in conjunction with FBG interrogators seems to be the most appropriate solution.

Future work should be carried out to to validating the findings in real application scenarios. Especially the detection capabilities using the DTS and a pipe wrap in fabric; and the capability of optical accelerometers in a real gas line. Also, new tests with holes of different sizes in the pipe and their influence on the triangulation of the leak point and minimum thresholds in different environments with the accelerometer must be performed. Signal processing and sensor fusion techniques could also be developed to increase the system's robustness to false positives and negatives due to external interference.

The UNICAMP research group has been working on developing new techniques and equipment for interrogating FBGs at a lower cost. Together with partners from other Brazilian institutions, accelerometers based on FBGs are also being developed that can be used to identify leaks in gas lines. In this way, there is potential for future projects to create low-cost national technologies that allow gas leaks to be identified with fiber optic sensors.

This work is an important step towards ensuring greater safety in the transportation and distribution of natural gas and reducing operating costs and consumer costs due to gas losses. Through a comparative analysis, it was possible to identify the potential and limitations of various techniques and fiber optic sensors for identifying leaks in gas lines.

BIBLIOGRAPHY

Agrawal, G. P. **Fiber-optic Communication Systems**. [S.l.]: John Wiley & Sons, 2010. ISBN 978-0470505119.

Albert, J.; Shao, L.-Y.; Caucheteur, C. Tilted fiber bragg grating sensors. **Laser and Photonics Reviews**, v. 7, n. 1, p. 83–108, 2013, first published: 27 February 2012.

Arpaci, V. S.; Smith, J. M. **Introduction to Heat Transfer**. [S.l.]: Pearson, 2001. ISBN 978-0201890424.

Barbosa, L. A.; Dreger, A. A.; Schneider, E. L.; Morisso, F. D. P.; Santana, R. M. C. Low density polyethylene (ldpe): market, production, properties, and applications. **Espacios**, v. 38, n. 17, p. 10, 2017.

Bell, C.; Contributors. **Thermo: Chemical properties component of Chemical Engineering Design Library (ChEDL)**. 2016–2024. <https://github.com/CalebBell/thermo>.

Bohren, C. F.; Huffman, D. R. **Absorption and Scattering of Light by Small Particles**. [S.l.]: Wiley, 1983. ISBN 978-0471293408.

Campanella, C. E.; Ai, G.; Ukil, A. Distributed fiber optics techniques for gas network monitoring. In: **2016 IEEE International Conference on Industrial Technology (ICIT)**. [S.l.: s.n.], 2016. p. 646–651.

Cengel, Y. A.; Boles, M. A. **Thermodynamics: An Engineering Approach**. [S.l.]: McGraw-Hill Education, 2014. ISBN 978-0073398174.

Daley, T. M.; Freifeld, B. M.; Ajo-Franklin, J.; Dou, S.; Pevzner, R.; Shulakova, V.; Kashikar, S.; Miller, D. E.; Goetz, J.; Henninges, J.; Lueth, S. Field testing of fiber-optic distributed acoustic sensing (das) for subsurface seismic monitoring. **The Leading Edge**, 2013.

Gannon, M. **Fiber optic cabling solutions for sensing applications**. 2018. <https://www.wireandcabletips.com/fiber-optic-cabling-solutions-sensing-applications/>.

Gigih, P.; Ghazali, M. S. M. Leak detection in pipelines using wavelet transform and cepstrum analysis methods. **International Journal of Electrical, Energy and Power System Engineering**, v. 4, p. 159–162, 2021.

Gouveia, C. A. J.; Batista, J. M.; Jorge, A. S. P. Refractometric optical fiber platforms for label-free sensing. **Current Developments in Optical Fiber Technology**, v. 1st ed., p. 30, 2013.

Hao, W.; Zhong, Z.; Gao, Q.; Bai, Y.; Dong, H. Research on positioning and monitoring method of pipeline abnormal state based on sliding window outlier analysis. **Scientific Programming**, p. 1755375, 10 pages, 2022.

He, Z.; Liu, Q. Optical fiber distributed acoustic sensors: A review. **Journal of Lightwave Technology**, v. 39, p. 3671–3686, 2021.

Hou, Q.; Ren, L.; Jiao, W.; Zou, P.; Song, G. An improved negative pressure wave method for natural gas pipeline leak location using fbg based strain sensor and wavelet transform. **Mathematical Problems in Engineering**, v. 2013, p. 1–8, 2013.

Jia, Z.; Ren, L.; Li, H.; Sun, W. Pipeline leak localization based on fbg hoop strain sensors combined with bp neural network. **Applied Sciences**, v. 8, p. 146, 2018.

Jiang, T.; Ren, L.; Jia, Z.; Li, D.; Li, H. Application of fbg based sensor in pipeline safety monitoring. **Applied Sciences**, v. 7, p. 540, 2017.

Johnson, B. R. Theory and experiment in rayleigh scattering. **American Journal of Physics**, v. 40, n. 12, p. 1690–1694, 1972.

Kashyap, R. **Fiber Bragg Gratings**. San Diego, CA: Academic Press, 1999.

Keck, D. B.; Maurer, R. D.; Schultz, P. D. Evolution of optical fiber fabrication techniques for low loss and single-mode transmission. **Applied Optics**, v. 12, n. 3, p. 514–523, 1973.

Kersey, A. D.; Davis, M. A.; Patrick, H. J.; LeBlanc, M.; Koo, K. P.; Askins, C. G.; Friebele, E. J. Fiber grating sensors. **Journal of Lightwave Technology**, v. 15, n. 8, p. 1442–1463, 1997.

Lu, Q.; Wang, Y.; Wang, X.; Yao, Y.; Wang, X.; Huang, W. Review of micromachined optical accelerometer. **Opto-Electronic Advances**, v. 4, p. 200045–200045, 2021.

Maurer, R.; Keck, D.; Schultz, P. Ultralow loss optical fiber. **Applied Physics Letters**, v. 19, n. 4, p. 130–132, 1971.

Miah, K.; Potter, D. A review of hybrid fiber-optic distributed simultaneous vibration and temperature sensing technology and its geophysical applications. **Sensors**, v. 17, n. 11, p. 1–25, 2017.

MicronOptics. **Distributed Vibration Monitoring using FO Accelerometers**. 2023. <lunainc.com/product/os7500>.

MicronOptics. **User Guide**. 2023. <www.omnisens.com>.

Mikucki, D.; Opoka, S. Application of platinum resistance thermometers (prts) in temperature measurements. **Measurement Science Review**, v. 11, n. 3, p. 91–96, 2011.

Mishra, A.; Gabani, S. H. A.; Hosany, A. J. A. Pipeline leakage detection using fiber optics distributed temperature sensing (dts). In: **Abu Dhabi International Petroleum Exhibition & Conference**. [S.l.: s.n.], 2017. SPE-188407-MS.

Motil, A.; Bergman, A.; Tur, M. State of the art of brillouin fiber-optic distributed sensing. **Optics & Laser Technology**, v. 103, p. 78–81, 2016.

Mulugeta, C. F.; S, J. Fibre optic methods of prospecting: A comprehensive and modern branch of geophysics. **Surveys in Geophysics**, 2021.

Omnisens. **User Manual DAS INTERROGATOR - Fiber Optic Distributed acoustic and vibration Analyzer**. Www.omnisens.com.

Omnisens. **User Manual DITEST INTERROGATOR - Fiber Optic Distributed Temperature and Strain Analyzer**. Www.omnisens.com.

Onoufriou, A.; Kalli, K.; Kohnke, G. E. Fiber bragg gratings: fundamentals and applications in telecommunications and sensing. **Physics Today**, v. 53, n. 5, 2000.

Optasense. **OptaSense Secures The Delivery Of Energy Supplies To Europe**. 2021. <https://www.optasense.com/optasense-monitors-key-european-pipeline/>.

PHMSA. **Pacific Gas & Electric Pipeline Rupture in San Bruno, CA**. 2017. <https://www.phmsa.dot.gov/safety-awareness/pipeline/pacific-gas-electric-pipeline-rupture-san-bruno-ca>.

PIRG. **Methane Gas Leaks**. 2022. <https://pirg.org/resources/methane-gas-leaks/>.

Qiao, X.; Shao, Z.; Bao, W.; Rong, Q. Fiber bragg grating sensors for the oil industry. **Sensors**, v. 17, p. 429, 2017.

Rao, Y. J. Recent progress in fiber-optic bragg grating sensors. **Journal of Lightwave Technology**, v. 17, n. 11, p. 2070–2088, 1999.

Roebuck, J. R. The joule-thomson effect in air. **Proceedings of the American Academy of Arts and Sciences**, v. 60, n. 13, p. 537–596, 1925.

Rong, Q.; Qiao, X. Fbg for oil and gas exploration. **Journal of Lightwave Technology**, v. 37, n. 11, p. 2502–2515, 2019.

Schawlow, A.; Townes, C. Infrared and optical masers. **Physical Review**, v. 112, n. 6, p. 1940–1949, 1958.

Sebok, B. Joule-thomson effect in case of mixtures of natural gas and hydrogen. **Note**, October 2022, q/A: Torben Kvist.

Senior, J. M. **Optical Fiber Communications: Principles and Practice**. [S.l.]: Pearson, 2008. ISBN 978-0130326812.

Smith, R. G. **Optical Sensors: Industrial Environmental and Diagnostic Applications**. [S.l.]: Springer Science & Business Media, 2004. ISBN 978-1402023987.

Soni, N.; Shaikh, A.; Nandwalkar, J. R.; Pete, D. J. Improvement in performance of ofc & fusion splice loss. In: **2020 6th International Conference on Advanced Computing and Communication Systems (ICACCS)**. [S.l.: s.n.], 2020.

Stajanca, P.; Chruscicki, S.; Homann, T.; Seifert, S.; Schmidt, D.; Habib, A. K. Detection of leak-induced pipeline vibrations using fiber-optic distributed acoustic sensing. **Sensors**, v. 18, p. 2841, 2018.

Sun, M.; Yuquan, T.; Yang, S.; Sigrist, M.; Dong, F. Fire source localization based on distributed temperature sensing by a dual-line optical fiber system. **Sensors**, v. 16, p. 829, 2016.

Tarcea, N.; Frosch, T.; Hilchenbach, M. Raman spectroscopy: A powerful tool for in situ planetary science. In: **Space Science Reviews**. [S.l.]: Springer, 2008, (Space Sciences Series of ISSI, v. 25).

Tejedor, J.; Macias-Guarasa, J.; Martins, H. F.; Pastor-Graells, J.; Corredera, P.; Martin-Lopez, S. Machine learning methods for pipeline surveillance systems based on distributed acoustic sensing: A review. **Applied Sciences**, v. 7, p. 841, 2017.

Thévenaz, L.; Robert, P.; Niklès, M. Simple distributed fiber sensor based on brillouin gain spectrum analysis. **Optics Letters**, v. 21, n. 18, p. 1545–1547, 1996.

Tur, M. Optical scattering: Measurement and analysis. **Measurement Science and Technology**, v. 10, n. 4, p. R15–R32, 1999.

Ukil, A.; Braendle, H.; Krippner, P. Distributed temperature sensing: Review of technology and applications. **IEEE Sensors Journal**, v. 12, p. 885–892, 2012.

Vogel, B.; Cassens, C.; Graupner, A.; Trostel, A. Leakage detection systems by using distributed fiber optical temperature measurement. In: Udd, E.; Inaudi, D. (Ed.). **Smart Structures and Materials 2001: Sensory Phenomena and Measurement Instrumentation for Smart Structures and Materials**. SPIE, 2001. v. 4328, p. 23–34. Disponível em: <https://doi.org/10.1117/12.435546>.

Wang, Y.; Yuan, H.; Liu, X.; Bai, Q.; Zhang, H.; Gao, Y.; Jin, B. A comprehensive study of optical fiber acoustic sensing. **IEEE Access**, v. 7, p. 85821–85837, 2019.

Yoffe, G.; Krug, P.; Ouellette, F.; Thorncraft, D. Passive temperature-compensating package for optical fiber gratings. **Applied Optics**, v. 34, p. 6859, 1995.

Zemansky, M. W.; Dittman, R. H. **Heat and Thermodynamics: An Intermediate Textbook**. [S.l.]: McGraw-Hill Education, 1981. ISBN 978-0070170592.

Zhang, P.; Wang, S.; Liu, T.; Li, Z.; Yang, H. A fiber-optic accelerometer based on extrinsic fabry-perot interference for low frequency micro-vibration measurement. **IEEE Photonics Journal**, v. 14, p. 1–6, 2022.

Zhang, S.; Xie, S.; Li, Y.; Yuan, M.; Qian, X. Detection of gas pipeline leakage using distributed optical fiber sensors: Multi-physics analysis of leakage-fiber coupling mechanism in soil environment. **Sensors**, v. 23, p. 5430, 2023.

Zuo, J.; Zhang, Y.; Xu, H.; Zhu, X.; Zhao, Z.; Wei, X.; Wang, X. Pipeline leak detection technology based on distributed optical fiber acoustic sensing system. **IEEE Access**, v. 8, p. 30789–30796, 2020.